Universidade de Aveiro Departamento de Engenharia Civil
2013

João Mário
Dias de Oliveira

Avaliação sísmica de edifícios existentes em betão armado

Seismic assessment of existing reinforced concrete buildings

Universidade de Aveiro Departamento de Engenharia Civil
2013

João Mário
Dias de Oliveira

Avaliação sísmica de edifícios existentes em betão armado

Seismic assessment of existing reinforced concrete buildings

Dissertação apresentada à Universidade de Aveiro para cumprimento dos requisitos necessários à obtenção do grau de Mestre em Engenharia Civil, realizada sob orientação científica de Humberto Salazar Amorim Varum, Professor Associado com Agregação do Departamento de Engenharia Civil da Universidade de Aveiro, de Hugo Filipe Pinheiro Rodrigues, Investigador do Departamento de Engenharia Civil da Universidade de Aveiro e de Gerardo Mario Verderame, Investigador do Departamento de Análise e Projeto Estrutural da Universidade de Nápoles Federico II.

o júri / the jury

presidente / president

Prof. Doutor Carlos Daniel Borges Coelho
Professor Auxiliar da Universidade de Aveiro

Doutor Vitor Emanuel Marta da Silva
Investigador da GEM Foundation

Prof. Doutor Humberto Salazar Amorim Varum
Professor Associado com Agregação da Universidade de Aveiro (orientador)

Prof. Doutor Hugo Filipe Pinheiro Rodrigues
Investigador da Universidade de Aveiro (co-orientador)

Prof. Doutor Gerardo Mario Verderame
Investigador da Università Degli Studi di Napoli Federico II (co-orientador)

agradecimentos / acknowledgements

Esta dissertação é apenas 14% do meu percurso na Universidade de Aveiro e quero utilizar este pequeno espaço para estender a gratidão pela formação técnica e cívica que me foi dada. Encontrei nas universidades por onde passei, na Falculdade de Arquitectura da Universidade Técnica de Lisboa, no Departamento de Análise e Projecto Estrutural da Universidade de Nápoles Federico II, e em vários departamentos da Universidade de Aveiro, uma verdadeira paixão pela passagem de conhecimento. Acredito ser um factor ponderante que distingue diferentes graus de formação.

Tive o prazer ser orientado pelo Professor Humberto Varum, um investigador com uma paixão e conhecimento enormes, um professor talentoso e preocupado em transmitir os fundamentos em vez de receitas, e um homem que genuinamente se interessa pelo carácter pessoal das pessoas.

Foi o Professor Hugo Rodrigues que me ensinou as bases do cálculo estrutural, e foram as suas aulas que mais prazer me deram. Obrigado pela simpatia, descontracção e preocupação.

To Paolo Ricci, I want to thank the kind and friendly orientation on the short period I stayed in Naples, and to Gerardo Verderame for opening me the doors to start my dissertation in Naples.

I thank to Professor Giorgio Serino and to Professor Marco Di Ludovico for introducing me to the seismic field. Acknowledgements to my special classmates Ravi and Chandra.

Gostava de reconhecer em particular alguns bons professores que me transmitiram boas lições por via técnica e pessoal, ao Professor Carlos Coelho pela organização e rigor sempre com boa-disposição, à Professora Margarida Lopes pelo apelo para se fazer o que se gosta, ao Professor Miguel Morais para ver o todo em detrimento do superficial, e ao Professor Romeu Vicente pela frontalidade e humor ácido.

Obrigado aos colegas e amigos mais próximos que viveram comigo a saga dos cinco anos de curso, em especial ao Diogo Limas, Rui Gamelas, Rui Maio e Susana Ferreira.

Não particularizando ninguém, obrigado a todos os seres que tornaram e tornarão a minha vida mais especial. Thank you. Grazie.

⋮ :

Aos meus pais, João Mário e Maria de Fátima, obrigado pela educação e amor. É com muito carinho que termino este passo, também por vós.

Aos meus irmãos, João Alexandre e Rui Pedro. Os maiores, os mais bonitos e os melhores exemplos. Obrigado pela vida, amor e pela eterna amizade.

keywords R.C. buildings, Modelling, Dynamic and non-linear analysis, Seismic assessment, Plain steel

abstract

This dissertation aims to the discussion and application of tools and processes which allows to assess the non-linear behaviour of a reinforced concrete structure.

When a numerous amount of buildings was built in concrete, in a period when the regulations did not have the design philosophy for the occurrence of earthquakes, it is important to carry out full and effective structural assessments.

Among several possibilities to make the evaluation as, simplified, linear analysis and static non-linear analysis, the non-linear dynamic can provide the most approximate numerical behaviour compared to the real one. With the potentialities of the computers, it is possible to run the analysis with this complex simulation using dynamic excitations of real earthquakes.

It is made a historical reference of numerical models which simulates the behaviour of materials, and the ones integrated on the analysis are further explored. Is presented the study cases, its assumptions and some procedures that should be applied in structural modelling. The discussion is divided in two groups. On the first the global analysis is discussed in terms of global behaviour, deformations and progression of forces, and on the second group is referred to the local assessment of structural elements. The local analysis has some comparisons between different interpretations of the code and also regarding the Italian code. Is analysed the bond-slip mechanism due to the smooth bars in some elements, which better simulates the global response of the structures.

palavras-chave

Edifícios em betão armado, Modelação, Análise dinânima e não-linear, Avaliação sísmica, Armadura lisa

resumo

A presente dissertação visa a discussão e aplicação de ferramentas e processos de verificação que permitam analisar o comportamento não linear de estruturas em betão armado.

Existem actualmente inúmeros edifícios em betão armado, construídos num período em que os regulamentos não previam a ocorrência de sismos, é importante proceder a avaliações estruturais completas e eficazes.

Entre várias possibilidades para fazer a avaliação, como simplificadas, análises lineares, análises estátiocas não-lineares, é a análise dinâmica não-linear que mais aproxima o comportamento numérico ao real. Com as potencialidades numéricas permitidas pelos computadores, é possível prever esse complexo comportamento onde podem ser simuladas excitações dinâmicas de sismos reais.

É feita uma referência histórica de modelos numéricos que simulam o comportamento dos materiais, aprofundando os que são integrados na análise. São apresentados os casos de estudo, os pressupostos e alguns procedimentos que devem ser aplicados na modelação estrutural. A discussão dos resultados é separada em dois grupos. No primeiro é feita uma análise global onde se discute o comportamento global, deformações e progressão de forças, e no segundo uma análise local dos elementos estruturais. A análise local é acompanhada de algumas comparações entre diferentes interpretações do código europeu e entre o código italiano. São analisados alguns elementos em relação ao deslize da armadura lisa, representando melhor a resposta das estruturas.

Contents

List of Tables

Intentionally blank page.

List of Figures

Intentionally blank page.

Part I

Introduction and Background

Chapter 1

Introduction

1.1 Overview

Accounting for seismic action in the design and construction of buildings has always been a delicate matter in engineering. The unpredictable nature of these natural phenomena, both in terms of occurrence and intensity, has always posed tough challenges. In countries like Italy, in particular, this is a serious requisite in design and planning. There are several large scale earthquakes reported along the history of numerous regions of the country. In Portugal, earthquakes as the one in Lisbon, in 1755, raise particular concern. Even if seismic activity in this country is not that much constant or intense, there are alerts for the possibility of another one soon. Therefore it is of the most importance to perform assessments to the existing buildings, protecting human life in the first place, as well as the loss of beautiful cities, such as, for example, Cuzco - Chile (1950), Trujillo - Chile (1971), Burma (1975), Friuli - Italy (1976), Popayán - Colombia (1983), Loma Prieta - USA (1989), Kobe - Japan (1994) [Varum 2003]. Several earthquakes took place in Europe in the last years, alerting that this continent may also be vulnerable to an earthquake [Varum 2003], with a fresh example of massive destruction on L'Aquila, Italy, in 2009.

From a Civil Engineering perspective, this field of research is of great importance. It is essential to better understand the behaviour of the different types of building when subjected to seismic loads. This is of the foremost relevance, since it allows engineers to improve current buildings and to plan for its recovery, as well as to learn for future projects.

In spite of some areas of the world being more exposed to these actions, there is still a lot of research on the development of procedures to protect human lives and material goods. With the elaboration of recent technical codes for this purpose, like the European Design Codes, the Eurocode 2 and 8, approved in 2004, the Italian code NTC08, the American ACI codes, or, for example, older codes as the Portuguese Design Code RSA of 1983, a lot of research has been made to design new efficient structures towards seismic actions. This research field studies more of new materials, demands and technologies to answer these new requisites. Nowadays, all over Europe, a large part of the building stock was not designed according to modern seismic engineering principles. There is still a lack of relevant research for those existing structures when compared to the new designed structures, which harms the performance of better structural assessments and the applicability of better interventions.

With the changing of philosophy towards seismic actions, structures became successively more ductile [Ricci 2010], compared to the old ones which have a clear different behaviour. In the meanwhile, the old plain round bars used in Portugal and Italy until the early 70's were gradually changed to deformed bars, strong-beam-weak-column design has changed to have failures prior failures on beams instead of on the columns, among others, but come of these deficiencies are still present in a lot of existing buildings. This important issue needs the contribution of further work so that these old reinforced concrete structures can be assessed in a close future, preventing potential accidents and failures.

1.2 Motivation

After the boom of construction in Europe, and in particular in Portugal, because of the massive use of fast construction provided by the recent use of concrete material (compared to ancient materials commonly applied), it is evident the application on the construction field on civil engineering. Linked with the accelerated building process, a lot of structures were constructed, without seismic provisions, but more importantly with materials and designs not so well studied and applied. Thus, some buildings now require interventions to delay the rapidly ageing after presenting some degradation signals. Therefore, the most important focus must be on the improvement of the research on old buildings, so that the vulnerability assessment and then the rehabilitation can be performed in a more accurate fashion. For this, the specialization should start to redirect itself to these kinds of studies, improving the quality and quantity of engineers.

The present dissertation, integrated in the final project of the Integrated Master degree on Civil Engineering, is intended to deepen the study on rehabilitation issues. With this in mind, this work still aims to provide a general introduction to the subject, providing organized steps which are necessary to assess an existing building. Understanding and proving the most common deficiencies on the assessment phase provides a better understand on how the approach to rehabilitation should be performed. Moreover, this work aims to introduce some effects of rotation localised at critical regions. While very important in old buildings, the study of this specific mechanism could have a big global impact on the health and behaviour of old Reinforced Concrete (R.C.) buildings when subjected to some lateral excitation or suffering the effects from the ageing of materials. In the meanwhile, it also aims to contribute with practical work on existing examples of structures.

1.3 Main Objectives

The main objective of this work is the improvement of the assessment of old R.C. structures with plain round bars, taking into account the influence of the mechanism of fixed-end rotation. This aims to provide further developments to the knowledge of the estimation of structural response, energy dissipation and accuracy of displacements for a better assessment of existing buildings. Within this framework, several specific objectives must be addressed, as seen in the following topics:

- Modelling and calibration of existing structures;

- Characterization of dynamic response of buildings without seismic provisions;
- Global and local assessment, based on Eurocode and other approaches available on literature;
- Evaluation of the influence of infill panels on framed R.C. structures;
- Evaluation of fixed-end rotation influence on seismic assessment of existing R.C. frames.

1.4 Document Structure

In the following chapters, this document provides a further framing of the work, divided in nine chapters, distributed on three parts.

The two first chapters are integrated in a global part entitled "Introduction and Background". On this first one, is presented the introduction, framework and objectives proposed for the dissertation. The second chapter has a review of the state of the art, featuring some of the models which compute stress-strain behaviour of materials, which are integrated on the used finite-element program, and also the slip-bond mechanism approaches, previously completed with a brief historical overview. The topics are separated in four main sections for the concrete, steel and masonry infills models, and another dedicated to the fixed-end rotation mechanism.

The next three chapters are integrated in a part named "Modelling". On the third chapter, the buildings used as study cases are introduced from an architectural point of view, explained the period of construction in terms of techniques and design approaches, general dimensions of elements and location of the infill panels. The fourth chapter is divided in various sections. It begins with a short introduction to the program used to model the structures, followed by an explanation of the adopted proprieties, assumptions and made modifications to better represent the structure without causing much convergence difficulties. In the final section, is presented experimental data useful to calibrate the modelling. The fifth chapter is dedicated to show the used earthquakes on the modelling, and deepens more details about them, as also the possibility of comparison to the spectrums available on the Eurocode 8.

The final part contains the last four chapters, where are developed the results from the models, named "Discussion". The sixth chapter has a preliminary discussion towards seismic assessments, exploring some of the existing approaches, as on the European Code and also some particularities of others. The seventh chapter is dedicated to global analysis/assessment, in which some conclusions are presented, at the beginning, in terms of modal behaviour of the building, the various frequencies and modal shapes, with and without infill panels, with the respective analysis on its influence. The chapter is completed by some brief results (without an exhaustive amount of all the plotted graphs and calculation sheets on the analysis) presenting global assessment topics, with the respective conclusions. The global assessments are mainly addressed to the progression of deformations, drifts, base and storey shear demands, comparing it to recommended limits available on literature. The eighth chapter is about the local assessments, addressed to ductile mechanisms, as chord-rotation control, and brittle mechanisms, as shear failure on the elements and joints strength. It concludes with a study of the influence of the fixed-end rotation mechanism related to the moment-curvature behaviour of the elements

and its implications on the seismic response. All these results and its conclusions are made for both buildings, also with a comparison of its response with and without the infill panels. On the ninth and final chapter is made a summarized conclusion which covers latter chapters and some of the future possibilities of development.

The work has five annexed groups which is supporting the dissertation body, since is not presented along with the text for organization matters. On the first four appendixes are presented some architecture drawings of the buildings, some information about the modelling, and a collection of data results organized through graphs and tables. The last appendix is a list of adopted nomenclature and acronyms.

The bibliography is located on the last pages, with all the references made on the dissertation.

Chapter 2

Previous Research and Background

The goal of this study is to analyse the behaviour of structures when excited by an earthquake. To perform the analysis is of the utmost importance to incorporate accurate models which predict the real response of the structure in respect to cyclic and nonlinear behaviour of the materials. Therefore the state of the art review firstly focus in some detail on the research regarding the integrated formulations to model the structures on software programs regarding a better correlation of the stress-strain proprieties of materials. The chapter also reviews some aspects related with local assessment of the Fixed-End Rotation (FER) mechanism. These are essential aspects that must be considered when working with the problems featured in this document.

2.1 Review of Concrete Material Models

The use of an accurate model for both concrete and steel are of the most importance in order to get the better data on this type of complex analysis. The difficulties which are inherent to the dynamic/cyclic behaviour are challenging, and with the use computer potentialities like the power on iterative calculation speed, which wasn't available to vast researchers, has started to get more attention.

On a actual paper, Penelis and Kappos [Penelis and Kappos 1997] exalts the importance of describing the envelope curve on the concrete modelling as much accurately as possible compared to cyclic behaviour, limiting errors from the initial analysis of monotonic loading. As an exemplification of experimental results, figure 2.1 shows the big correlation between monotonic and cyclic loadings, supporting the Penelis conclusion. Hereupon, the rest of the cyclic behaviour also needs to be explained.

One of the first known researchers to work on the modelling of concrete cyclic behaviour, Karsan and Jirsa [Karsan and Jirsa 1969], specified through experimental work the concrete behaviour through a point where two different curved branches of unloading and loading intersects, linking these specific points through second degree parabolas. One limitation of the model is the fact of not taking into account the confinement given to concrete by the stirrups.

Later, Blakeley [Blakeley and Park 1973] developed a simplified model which had the capacity of computing the envelope curve of the concrete. For the unloading behaviour, the model is made through a straight line with simplified assumptions of non energy dissipation or stiffness deterioration for strains equal or smaller compared to the peak

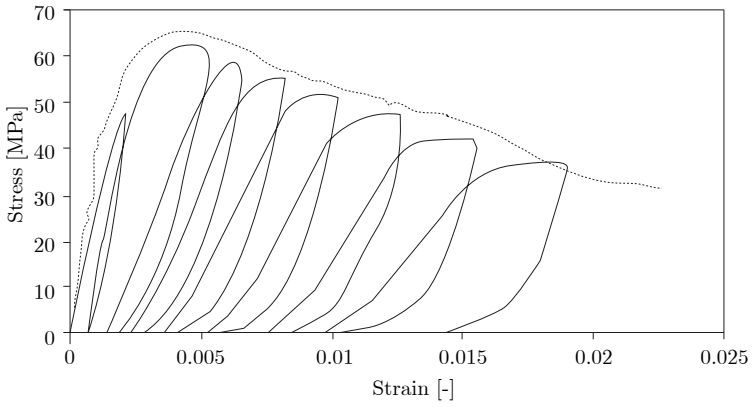

Figure 2.1: Raw experimental results plot from repeated uniaxial compression, for cyclic and monotonic loadings.

stress. The reduction of stiffness is calculated through a processed parameter. The loading is made through another two straight lines, the first one 50% stiffer than the calculated for unloading until the maximum past strain and then a vertical line until the last achieved stress.

Yankelevsky and Reinhardt [Yankelevsky and Reinhardt 1987] proposed a model dedicated to explaining unloading and reloading behaviour, considering that the envelope curve is already given, prior defined. The model considers a linear shape for the cyclic branches with different stiffness according to assumptions at different strain ranges.

Mander [Mander *et al.* 1988] presented a simplified version of the Karsan model and included the tensile stress-strain relationships. It also uses equations proposed by Popovic [Popovic 1973] for the envelope curve, accounting for the confinement influence. The model predicts the updating of inelastic strain each time that the maximum strain is achieved, allowing the prediction of its behaviour over repeated cyclic excitations for even greater strains. Martinez [Martínez-Rueda and Elnashai 1997] modified the model, correcting the lack of numerical stability which was increased for large displacements. It was modified mainly though the creation of three different phases in the calculation of inelastic strains, instead of the single parameter of Mander, accounting for softening of concrete, and the shape of reconnecting to the envelope curve on reloading. These models, envelope curves of Mander and cyclic rules of Martinez, are the ones used on later modelling.

An efficient definition of the concrete model is very important to compute the formation of plastic hinges during the seismic excitation and also consider the ductility of the material to guarantee that moment redistribution occurs on the element frames. The distinction of confined concrete on the core section, if good stirrups are applied, is important since it can deal with much higher stresses at bigger strains compared with the not confined cover concrete, needed to be modelled to achieve better results. In the case of old R.C. buildings, it is necessary to be careful on the definition of the confinement factor because of the way the stirrups were applied, with no clamping provisions which are predicted on the new codes. If the stirrups are not clamped in a good manner, when the element is submitted to a stress, it can open wide and not give conditions to increase

its response.

2.1.1 Mander and Martinez Model Formulation

The Mander model compared numerical results to 40 experimental concentric axial compression tests, which consisted on full sized sections of reinforced concrete columns, tested for slow and fast dynamic rates of strain, with or without cyclic loadings [Mander *et al.* 1988].

Early researchers represented the confined concrete behaviour through confined concrete by a hydrostatic fluid pressure. To compute it, the following two expressions of stress and strain relationships were used,

$$f'_{cc} = f'_{co} + k_1 f_l \text{ and} \tag{2.1}$$

$$\varepsilon_{cc} = \varepsilon_{co}(1 + k_2 \frac{f_l}{f'_{co}}) , \tag{2.2}$$

where f'_{cc} and ε_{cc} are the maximum values for either stress and strain, respectively. f'_{co} and ε_{co} are the maximum values for unconfined elements, values which are increased by factors of f_l, fluid pressure, and k_1 and k_2, coefficients to calibrate the formulation, with different proposed values according to different researchers. This approach had its limitation due to the difficulties of calibration for different confinements and sections shapes.

In order to surpass that limitation, Mander [Mander *et al.* 1988] developed Popovic's [Popovic 1973] equations and suggested an unified stress-strain approach with monotonic loading at slow strain rates, which predicts the envelope for the next presented cyclic loading stress-strain response, f_c, longitudinal compressive stress, through

$$f_c = \frac{f'_{cc} x r}{r - 1 + x^r} , \tag{2.3}$$

where, f'_{cc} is the compressive strength of confined concrete, later defined on equation 2.13. To compute completely f_c, are need two factors, factor r,

$$r = \frac{E_c}{E_c - E_{sec}} , \tag{2.4}$$

$$\tag{2.5}$$

with $E_c = 5.0\sqrt{f'_{co}}$ [MPa] and $E_{sec} = f'_{cc}/\varepsilon_{cc}$, and factor

$$x = \frac{\varepsilon_c}{\varepsilon_{cc}} , \tag{2.6}$$

$$\tag{2.7}$$

which depends of ε_c, the longitudinal compressive strain of the concrete, and ε_{cc}, strain of maximum compressive stress,

$$\varepsilon_{cc} = \varepsilon_{co}\left[1 + 5\left(\frac{f'_{cc}}{f'_{co}} - 1\right)\right] , \tag{2.8}$$

where f'_{co} and ε_{co} are the unconfined values.

To take into account the confinement (see Fig. 2.2), it is necessary to consider the effectiveness of the hoops on the response of the section. The pressure of the transversal reinforcement,

$$f_{\mathrm{l}}' = f_{\mathrm{l}} k_{\mathrm{e}} \ , \tag{2.9}$$

which represents the level of confinement, is assumed to be uniform on Mander's formulation, and needs to be multiplied by,

$$k_{\mathrm{e}} = \frac{A_{\mathrm{e}}}{A_{\mathrm{cc}}} \ , \text{ with} \tag{2.10}$$

$$A_{\mathrm{cc}} = A_{\mathrm{c}} \left(1 - \rho_{\mathrm{cc}}\right) \ , \tag{2.11}$$

where A_{e} is the effectiveness of the confinement, A_{c}, the area of hoops and ρ_{cc} the ratio of longitudinal reinforcement. For both sectional directions (i), f_{l} is dependent on $A_{\mathrm{s}i}$, the total transversal steel area running on the element, by

$$f_{\mathrm{l}i} = \frac{A_{\mathrm{l}i}}{s d_{\mathrm{c}}} f_{\mathrm{yh}} \ . \tag{2.12}$$

For both rectangular and circular hoops, there are ways to calculate the effectiveness of the confinement, A_{e} and k_{e}, presented on [Mander *et al.* 1988].

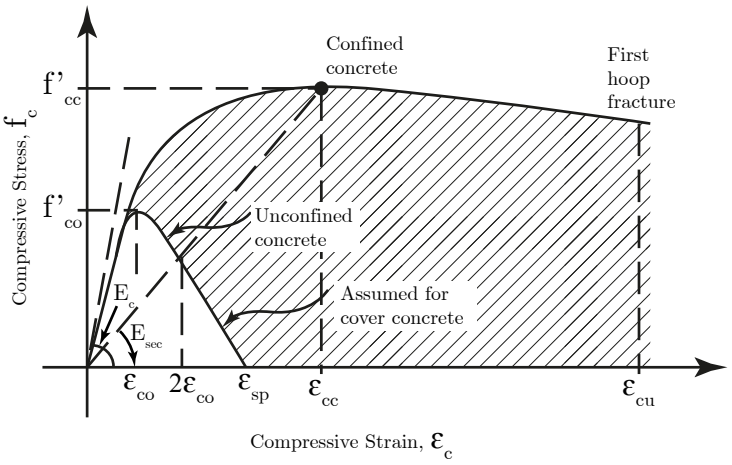

Figure 2.2: Representation of the Mander model (adapted from [Mander *et al.* 1988]).

Now is possible to compute the compressive stress of confined, referred on equation 2.3, of confined elements, through a procedure formulated by parameters calibrated with experimental data, expressed by

$$f_{\mathrm{cc}}' = f_{\mathrm{co}}' \left(-1.254 + 2.254 \sqrt{1 + \frac{7.94 f_{\mathrm{l}}'}{f_{\mathrm{co}}'}} - 2 \frac{f_{\mathrm{l}}'}{f_{\mathrm{co}}'} \right) \ . \tag{2.13}$$

The model, regarding tensile behaviour on monotonic analysis, is assumed to have a linear behaviour.

$$f_{\mathrm{c}} = E_{\mathrm{c}} \varepsilon_{\mathrm{c}} \text{ for } f_{\mathrm{c}} < f_{\mathrm{t}}' \tag{2.14a}$$

$$f_{\mathrm{c}} = 0 \text{ for } f_{\mathrm{c}} \geq f_{\mathrm{t}}' \tag{2.14b}$$

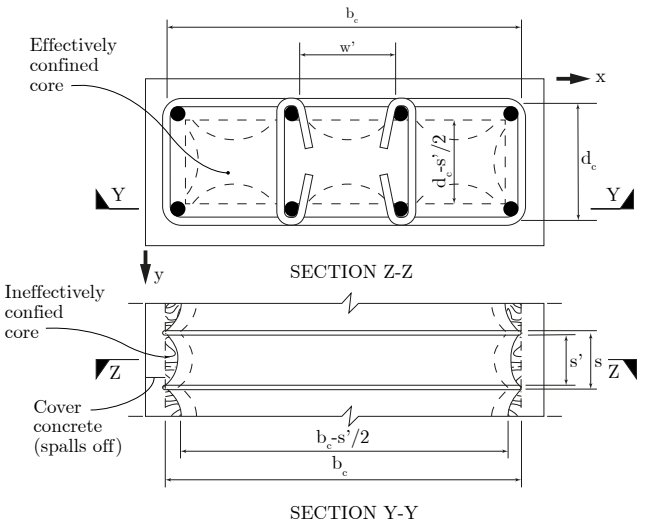

Figure 2.3: Confinement of stirrups (adapted from [Mander *et al.* 1988]).

As already referred, Martinez proposed a different model for cyclic behaviour, solving some difficulties in respect to stiffness calculation, which could lead to convergence problems on implementations with a fibre element approach, in non-linear programs. His work proposed an improvement regarding the increasing degradation of strength and stiffness due to cyclic effects. The procedure is capable of calculating the unloading either for confined or unconfined elements.

For the cyclic behaviour, the stress-strain is determined on the coordinates $\varepsilon_{\mathrm{un}}$ and f_{un}, for unloading, $\varepsilon_{\mathrm{re}}$ and f_{re}, for reloading, $\varepsilon_{\mathrm{pl}}$, residual/plastic strain with no stress, and f_{new}, for the new stress on reloading at strain $\varepsilon_{\mathrm{un}}$, visualized on figure 2.4.

The inelastic strain is calculated differently for different steps and should be updated every time the maximum strain is achieved, separating the different rates of strain range with the following equations,

$$\varepsilon_{\mathrm{pl}} = \varepsilon_{\mathrm{un}} - \frac{f_{\mathrm{un}}}{E_{\mathrm{c}}} \ , \ 0 \leq \varepsilon_{\mathrm{un}} \leq \varepsilon_{35} \ , \tag{2.15a}$$

$$\varepsilon_{\mathrm{pl}} = \varepsilon_{\mathrm{un}} - \frac{\varepsilon_{\mathrm{un}} + \varepsilon_{\mathrm{a}}}{f_{\mathrm{un}} + E_{\mathrm{c}}\varepsilon_{\mathrm{a}}} \ , \ \varepsilon_{35} \leq \varepsilon_{\mathrm{un}} \leq 2.5\varepsilon_{\mathrm{cc}} \quad \text{and} \tag{2.15b}$$

$$\varepsilon_{\mathrm{pl}} = \frac{f_{\mathrm{cr}}\varepsilon_{\mathrm{un}} - |\varepsilon_{\mathrm{f}}|}{f_{\mathrm{cr}} + f_{\mathrm{un}}} \ , \ 2.5\varepsilon_{\mathrm{cc}} \leq \varepsilon_{\mathrm{un}} \ . \tag{2.15c}$$

The concrete behaviour on the first step is essentially elastoplastic, where ε_{35} is the strain corresponding to $0.35f'_{\mathrm{c}}$. On the second step the same formula defined by Mander is used [Mander *et al.* 1988]. The plastic strain is dependent on both the initial slope of the stress-strain behaviour and the "common strain" ε_{a}, where

$$\varepsilon_{\mathrm{a}} = a\sqrt{\varepsilon_{\mathrm{un}}\varepsilon_{\mathrm{cc}}} \ , \tag{2.16}$$

$$a = \frac{\varepsilon_{\mathrm{cc}}}{\varepsilon_{\mathrm{cc}} + \varepsilon_{\mathrm{un}}} \ . \tag{2.17}$$

The last step is the numerical approximation made in Martinez's experimental work, an adaptation of the Yankelevsky and Reinhardt [Yankelevsky and Reinhardt 1987] for-

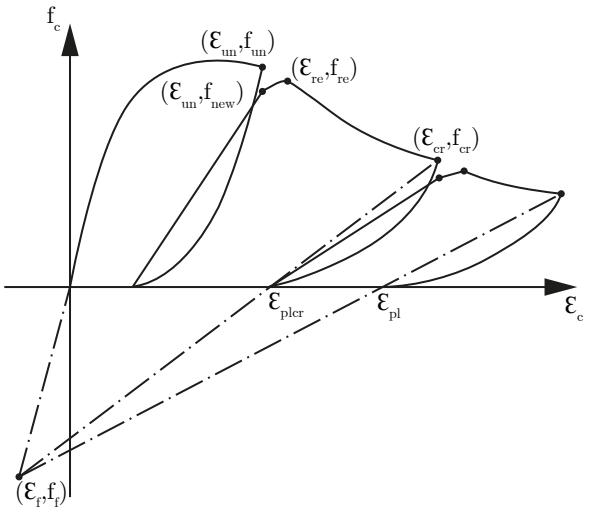

Figure 2.4: Loading and reloading model of Martinez (adapted from [Martínez-Rueda and Elnashai 1997]).

mulation. To compute the transition to high strain range it is necessary to define the coordinates of the "focal" (f) point. In this sense, $\varepsilon_{\mathrm{plcr}}$ on the next equations corresponds to the upper limit of the intermediate strain range $\varepsilon_{\mathrm{cr}}$, according to

$$|\varepsilon_{\mathrm{f}}| = \frac{f_{\mathrm{cr}}\varepsilon_{\mathrm{plcr}}}{E_{\mathrm{c}}(\varepsilon_{\mathrm{cr}}\varepsilon_{\mathrm{plcr}}) - f_{\mathrm{cr}}} \ , \tag{2.18}$$

$$|f_{\mathrm{f}}| = E_{\mathrm{c}}|\varepsilon_{\mathrm{f}}| \quad \text{and} \tag{2.19}$$

$$\varepsilon_{\mathrm{cr}} = 2.5\varepsilon_{\mathrm{cc}} \ . \tag{2.20}$$

This formulation can predict a continuous behaviour of the material as it computes the damage on the concrete.

To compute the unloading curves (*vd.* Fig. 2.4) equation 2.21 is used, joining reversal $(\varepsilon_{\mathrm{un}}, f_{\mathrm{un}})$ to $(\varepsilon_{\mathrm{pl}}, 0)$, as

$$f_{\mathrm{c}} = f_{\mathrm{un}} \left(\frac{\varepsilon_{\mathrm{c}} - \varepsilon_{\mathrm{pl}}}{\varepsilon_{\mathrm{un}} - \varepsilon_{\mathrm{pl}}} \right)^2 \ . \tag{2.21}$$

The reloading branch between the strain $\varepsilon_{\mathrm{un}}$, the maximum strain achieved by the element, and the degrading strength point $\varepsilon_{\mathrm{ro}}$ (vd. fig. 2.5) is made by a straight line. The correspondent stress is calculated using

$$f_{\mathrm{new}} = \frac{0.9f'_{\mathrm{cc}}\frac{\varepsilon_{\mathrm{c}}}{0.9\varepsilon_{\mathrm{cc}}}r}{r - 1 + (\frac{\varepsilon_{\mathrm{c}}}{0.9\varepsilon_{\mathrm{cc}}})^r} \ . \tag{2.22}$$

When the element reaches the unloading strain $(\varepsilon_{\mathrm{un}}, f_{\mathrm{new}})$ and is stressed to rejoin the monotonic envelope curve $(\varepsilon_{\mathrm{re}}, f_{\mathrm{re}})$, it is calculated as an average between $\varepsilon_{\mathrm{un}}$ and $\varepsilon'_{\mathrm{re}}$, the latter calculated thought a calibrated empirical equation, as

$$\varepsilon_{\text{ret}} = \frac{\varepsilon'_{\text{ret}} + \varepsilon_{\text{un}}}{2} \quad \text{where ,} \tag{2.23}$$

$$\varepsilon'_{\text{re}} = (0.00273 + 1.2651\frac{\varepsilon_{\text{un}}}{\varepsilon_{\text{cc}}})\varepsilon_{\text{un}} \ . \tag{2.24}$$

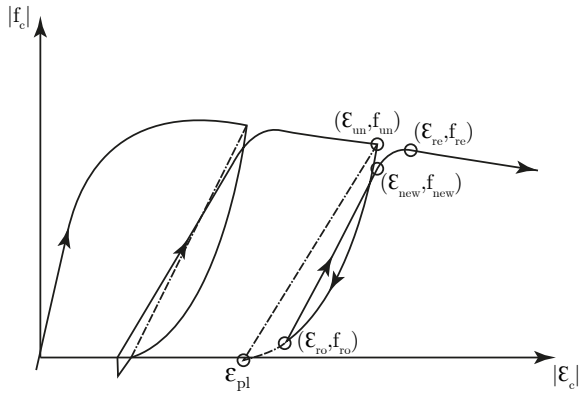

Figure 2.5: Reloading (adapted from [Mander *et al.* 1988]).

Mander [Mander *et al.* 1988] considered an increase of both strength and stiffness for higher strain rates. He proposed a correction of the values through dynamic magnification factors which were calibrated for both strain rates and different unconfined concrete strengths, to correspond to numeric and experimental results with lower errors. To overcome this difference between high strain rate (dynamic) and low strain rate (quasi-static), some researchers advise to consider 25% of the peak stress, of the strain at the peak stress and the slope of the post-yield falling branch. [SeismoSoft 2012]

2.2 Review of Steel Material Models

The steel takes a massive impact on the cyclic response of structures, depending on the amount of reinforcement. Due to the micro-proprieties of the material, its behaviour, compared to concrete, is more predictable but has some characteristics which changes on cyclic excitations. Both materials have its important and individual role maintaining the safety of a structure, but an incorrect amount of steel can lead to weak capacity of the elements on the highly demand of bending moments during an earthquake.

Yu [Yu 2006] points out, from past research, that macroscopic models for materials are the best numerical approach to predict steel response. It is also referred that the use of recent models can already be accurate enough for engineering regarding strains and stresses results.

In terms of non-linear analyses, some models were developed and can be grouped in different approaches, as Linear Elastic-perfectly plastic, Linear Elastic with strain hardening, Linear elastic with non-linear hardening and Ramberg-Osgood model [Ramberg and Osgood 1943].

In terms of cyclic behaviour, several investigators developed and discussed modelling and several models were developed throughout history. Some of these models are summarized in the following section and afterwards discussed in comparison to the one used in this work. One of the first researchers was Dafalias [Dafalias and Popov 1976] which started to discuss different models of purely kinematic and purely isotropic hardening. From the two approaches some disadvantages were pointed out, as inaccuracy regarding the modelling of stress after post yielding effect of isotropic models, and, despite of simple computational application, kinematics models could not take into account the quick reduction of elastic stress after plasticity due to negligence of isotropic hardening. Therefore, Popov [Popov and Petersson 1978] developed another model, solving some limitations using a "multi-surface" model capable of creating a real transition between monotonic and cyclic behaviour of the material. Santhanam [Santhanam 1979] presented a simplified linear model accounting for the effects of cyclic stiffness degradation and the fact that yield stress growth was not accurate enough to predict its behaviour in loading and unloading demands without considerable plastic flow. Tseng [Tseng and Lee 1983] used a two surface model which used an isotropic hardening approach to a bounding surface calculated to a monotonic response, coupled with reduction of a yield surface. Despite representing cyclic softening and hardening and stress relaxation well enough, it could not also compute an accurate behaviour in loading and unloading demands without considerable plastic flow. Cofie [Cofie and Krawinkler 1985] used some past relationships to support a model and still could not predict the best results because it did not updated enough parameters related with the cyclic strain amplitude.

The next two models were a modification of Ramberg-Osgood model, a non-linear equation able to compute the stress-strain relationship transition at yielding and the strain hardening of materials like steel. In Ma's work [Ma *et al.* 1976] the model was modified to achieve a cyclic response, but according to Elnashai [Elnashai and Izzuddin 1993], it developed an overestimated response and good results for monotonic response. Menegotto [Menegotto and Pinto 1973] presented a stress-strain relationship which would be later modified by Filippou [Filippou *et al.* 1983] and which included some isotropic hardening rules. This set is the used formulation to model the structure on this work, as is a more stable formulation and with accurate results.

2.2.1 Menegotto-Pinto Model Formulation

In the model proposed by Menegotto-Pinto [Menegotto and Pinto 1973], an explicit algebraic stress-strain formulation is used, which is better to implement and less computationally demanding when compared to implicit methods, as the Ramberg-Osgood model. The model computes the stress-strain relationships, $f(\sigma, \varepsilon) = 0$, between loading branches, and updates its parameters with each strain reversal, as

$$\sigma^* = b\varepsilon^* + \frac{(1+b)\varepsilon^*}{(1+\varepsilon^{*R})^{1/R}} \quad \text{where ,} \tag{2.25}$$

$$\varepsilon^* = \frac{\varepsilon - \varepsilon_\mathrm{r}}{\varepsilon_0 - \varepsilon_\mathrm{r}} \quad \text{and} \tag{2.26}$$

$$\sigma^* = \frac{\sigma - \sigma_\mathrm{r}}{\sigma_0 - \sigma_\mathrm{r}} \, . \tag{2.27}$$

These equations define the curve of a first asymptote, limiting the curve through an envelope of initial slope line, corresponding to Young modulus, E_{s0}, and with another line, "hardening" modulus E_{sp}. This latter modulus is bE_{s0}, where b is the strain hardening ratio, a propriety of the material. R is a parameter which changes the shape of the transient curve, making it more or less tight and allowing to adjust the curve to predict the Bauschinger effect [1]. The stress-strain values "0" and "r" are initial and final coordinates which are changed in each strain reversal, as identified on figure 2.6.

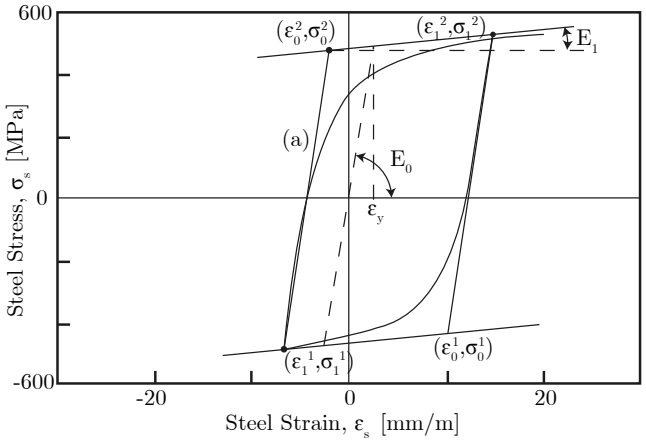

Figure 2.6: Menegotto-Pinto steel model (adapted from [Yu 2006]).

The shape of the curvature, controlled by the parameter R, is dependent on the two asymptote intersection points, calculated for the target strains. The parameter can be calculated as

$$R^n = R_0 - \frac{a_1 \zeta_{\mathrm{p}}^n}{a_2 + \zeta_{\mathrm{p}}^n}\,, \tag{2.28}$$

where the plastic parameter ζ_{p}^n is being updated by

$$\varepsilon_0^n = \varepsilon_{\mathrm{r}}^{n-1} + \frac{\sigma_0^n - \sigma_{\mathrm{r}}^{n-1}}{E}\,, \tag{2.29}$$

with

$$\zeta_{\mathrm{p}}^n = \varepsilon_{\mathrm{r}}^n \varepsilon_0^n\,. \tag{2.30}$$

Parameters R_0, a_1 and a_2 can be experimentally determined. The definition of ζ remains valid for cases where reloading occurs after partial unloading [Yu 2006].

In order to overcome some difficulties on the computational integration, Filippou [Filippou *et al.* 1983], using the Menegotto model, proposed a limitation of past stress-strain history on each iteration, which makes a small and acceptable discrepancy between model and real behaviour, but still keeps it more conservative. The proposal can be

[1] The Bauschinger effect can be defined as changes of the material microscopic stress distribution, changing its characteristics, as an increase of tensile yield strength with a reduction of compressive yield strength

observed on figure 2.7, were the real behaviour is represented in line (a) and the proposed one in line (b). This is due to how the model calculates ζ with limitation of past memory, which tightens the curve on the two formed asymptotes.

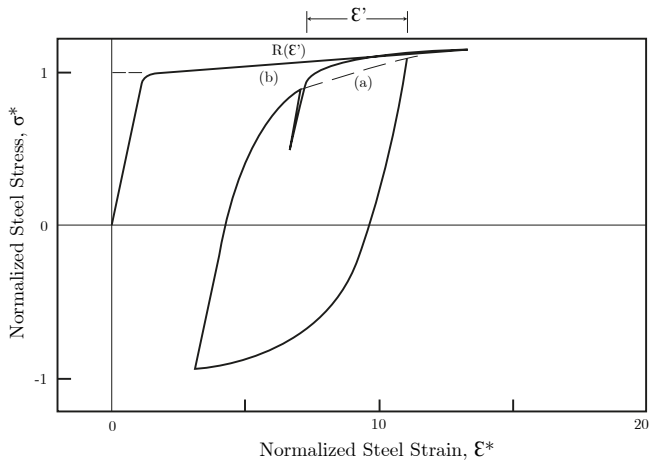

Figure 2.7: Partial unloading curve with reloading (adapted from [Yu 2006]).

Filippou also proposed an upgrade for the model taking into account hardening rules, allowing isotropic hardening on cyclic behaviour by

$$\sigma_{\text{shift}} = \sigma_{\text{y}} a_3 \left(\frac{|\varepsilon_{\max}|}{\varepsilon_{\text{y}}} - a_4 \right) > 0 \, . \tag{2.31}$$

σ_{shift} is the shift of yield stress after a load reversal and $\varepsilon_{\max}$ the maximum strain at the beginning of reversal. The parameters a_i can be determined experimentally, linked to isotropic hardening and strain of verification of the phenomenon. The parameters R_0 and a_{1-4} have already proposed values, which can be consulted if is not possible to determined it experimentally. One set of proposed values were R_0=20, a_1=18.5, a_2=0.15, a_3=0.02 and a_4=2.

2.3 Review of Infill Models

The calibration of the infill panels is explained later on. It is not in the scope of the dissertation to go into much detail about infills. The main concern is to model it as well as possible to get the best results regarding its influence in the global behaviour of the building. See section 4.5.2 for further details.

As a superficial overview on the evolution of models regarding the infills on structures, is presented a brief summary which can be important for further studies. Polyakov [Polyakov 1956] started the modelling of the shear stresses on infills which was later improved by Holmes [Holmes 1961], with a equivalent diagonal struts formulation. The method and calculations of the struts were more developed by Stafford-Smith [Stafford-Smith 1966] and by Carter and Stafford-Smith [Carter and Stafford-Smith 1969]. The earliest non-linear formulation for struts was presented by Klingner and Bertero [Klingner and Bertero 1976], while Liauw and Lee [Liauw and Lee 1977] presented another

development introducing the capability of modelling infills with openings. Later on Thiruvengadam [Thiruvengadam 1985] tested the integration of several diagonal struts on the same model, which has initiated some other complex tendencies. A new proposal for strength deterioration was presented by Doudoumis and Mitsopoulou [Doudoumis and Mitsopoulou 1986]. In 1997, Crisafulli [Crisafulli 1997] presented a integration of several struts computing independently shear and struts together. This last model is used on the modelling of the structures.

2.4 Fixed-End Rotation

Local behaviours in a structure have a big impact in the global performance. To perform the assessment of existing buildings it is absolutely necessary to take into account particularities such as cracking and bond capacity on the extremities sections, where the stress levels become higher, making such a important role the interactions between materials, concrete and steel. With the cracking of concrete on the member extremities, the member deforms, changing the level of stress which leads to a rearrangement of stresses on the section and reinforcement bars, developing higher bond demands [Fabbrocino *et al.* 2004]. The mechanism called Fixed-End Rotation (FER) can be defined as the slippage of the reinforcing bars, which can be exalted by the deterioration of bond capacity in the anchorage, located at the end section of the element, when the concrete cracks. This provokes a local rotation of the fixed-end element [Kwak *et al.* 2004]. The FER mechanism can be visualised in figure 2.8. In a simple way, this rotation is often evaluated as

$$\theta_{\mathrm{FE}} = \frac{u^{\mathrm{t}} - u^{\mathrm{b}}}{d'}\,, \tag{2.32}$$

where u^{t} and u^{b} are the displacements of the top and bottom reinforced bars, respectively, and d' is the distance between them.

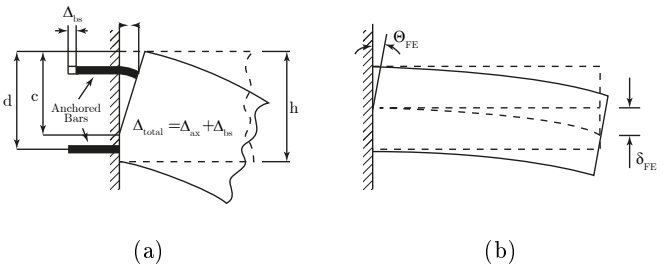

Figure 2.8: Rigid body deformation at the beam-column joint: (a) anchorage slip and (b) fixed-end rotation (adapted from [Kwak *et al.* 2004]).

2.4.1 FER in Structural Behaviour

To accurately simulate the structural behaviour it is important to take into account the FER mechanism because of the increase of concentration of displacement phenomena

(rotation) on fixed-end sections due to lateral loads. This is the case in events like earthquakes. This type of actions, together with gravity loads, can create demands on the joints that were not well designed with the old philosophy, which did not take horizontal loads into account. The mechanism is even more important when we analyse the little regard usually given to this effect together with the application of plain reinforcing bars, with low bond capacities that influence the three main deformation mechanisms: bending, shear and fixed-end rotation [Verderame *et al.* 2010]. These are illustrated in figure 2.9, in a global point of view of the member.

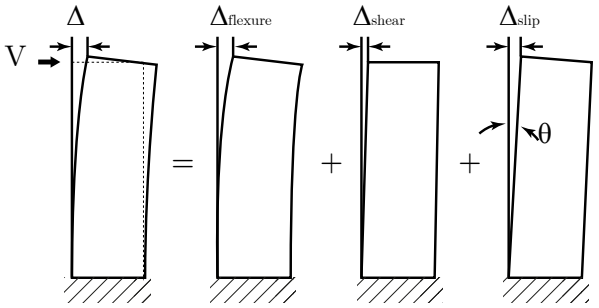

Figure 2.9: Main deformation mechanisms (adapted from [Cho and Pincheira 2006]).

The weak bond between the surrounding concrete and the longitudinal plain bars allows a bigger crack development which influences shear and bending deformation contributions, reducing shear deformability and increasing bending deformability, following the material strength principles. Poor bond capacity of the reinforcement has a particular influence on the deformation of the member. The FER of the member, due to this slippage, can represent values of 80% to 90% of all the overall deformation contributions [Verderame *et al.* 2008a, Verderame *et al.* 2008b]. Since the rotation of members is verified, it means an increase of flexibility and an overestimation of ductility that can lead to a wrong analysis and bad assessments [Varum 2003].

It is noteworthy that some experimental work showed some direct impact of the FER and slippage of plain reinforced bars to substantiate the importance of this mechanism. The work of both Verderame *et al.* [Verderame *et al.* 2008a, Verderame *et al.* 2008b] and Melo *et al.* [Melo *et al.* 2012b] provide useful results. In [Verderame *et al.* 2008a, Verderame *et al.* 2008b], the experimental results show a clear difference in terms of response between deformed bars and smooth bars in the rotation of the members, due to a large crack opening in the interface of the column-foundation. In the monotonic field, this work points to an increase of flexural strength of about 50% when the axial load on the column increases from 12% to 24% of the ultimate axial load. A larger chord rotation capacity of 25% is observed on columns with continuous bars on foundation interface compared with lap-spliced columns, while presenting lower density crack patterns, i.e. larger but in lower number. Also the rotation of the fixed-end on columns represents 90% of predominance at conventional collapse. In the cyclic field, aspects of monotonic behaviour were confirmed and pointed to a big influence of the FER together with yielding spreading along in column length. It also showed that cyclic loading leads to an average reduction of chord rotation capacity compared to monotonic. In [Melo *et al.* 2012b], the main conclusions are a decrease of the dissipated energy and increase of damage

in the fixed-end, due to lap-splice on cyclic behaviour, less energy dissipated and less equivalent damping when compared to deformed bars. However, the conclusions of this work present some differences when compared to the results by Verderame. Melo obtained in monotonic behaviour a 9% drift at the ultimate point compared with 6% of two specimens in the work of Verderame, as well as a small strength degradation and, in cyclic behaviour, a higher drift of 40% and 85%, with and without lap-splice, respectively, for the maximum strength in the columns.

To analyse the FER, it is important to characterize the bond in plain bars with high detail. The existing literature on bond mechanisms dates back to the first half of the last century but it is not very detailed when it comes to cyclic or post-elastic behaviours. As Verderame [Verderame *et al.* 2008a] states in his work, "experimental data relative to conditions of cyclic load and post-elastic deformation are almost totally absent (...) however, the characterization of the bond performance of plain bars is of fundamental importance for purposes of the assessment of the effective deformation capacity in existing R.C. elements."

To characterize the bond capacity it is needed to look at the problem with a more experimental approach, making the experimental tests and then trying to approximate the results with analytical models that lead to the same behaviour curves. The other possibility is to develop numerical modelling, with physical principles which explain the phenomena, and then compare it to the results obtained in experimental prospects.

Two of the first works on the bond-slip relationship with plain bars is presented on the work of Abrams [Abrams 1913], who performed a series of 1500 pull-out tests in a displacement control, and Bach [Bach 1911] who tried to also evaluate the effectiveness of end details on plain bars. The main consideration made by this author was that there are two different types of mechanisms of transferring load between bars and concrete: adhesive resistance, which develops before the movement between the materials begins; sliding resistance, after the movement starts. When the movements do not happen, the chemical bonds and the static friction contribute to the bond capacity. After this capacity is overcome, the sliding resistance, as a frictional mechanism, takes place. From his results, the author concluded that adhesive resistance has a contribution of up to 50% to 60% of the maximum resistance and has a slip of 0.25 mm. Saliger [Saliger 1913] got similar results to Bach, performing a wide number of tests on evaluating the performance on anchorages without considering the deformation.

After the work of Abrams, other researchers further developed the explanation of these mechanisms. One of them was Fishburn [Fishburn 1947], on the 1940's, who compared the force-slip response of plain straight or anchored bars. Rehm [Rehm 1961,Abrams 1913] gathered experimental data to improve the understanding of bonding capacity. Stoker and Sozen [Stoker and Sozen 1970] also explained the bond relation with two slightly different phases, the micro-interlocking phase and frictional resistance. On the first phase it is due to shear strength developed with the penetration on the rigid cement particles on the surface roughness of the bars added to the chemical bonds between the materials. When the movement starts it is followed by the slip of the bars, leading to the crushing of the adhesion of the cement along with the bars surface, which in turn leads progressively to a reduction of the bond capacity. In another research, Tassios [Tassios 1979] found a conclusion close to the work of Stoker and Sozen, explaining that with a pull-out test the low slip is controlled by adhesion and then, when the load starts to increase, the micro-interlocking mechanism begins between the materials. Continuing with

the load, the interlocking mechanisms start to crush the concrete linked to the bars and with the reductions of bond stiffness the frictional behaviour starts to take effect. These results show a reduction of frictional resistance with the increasing of slip to around 30% of the maximum resistance verified.

Recent experimental work from Kankam [Kankam 1997], who performed a series of double pullout tests on concrete specimens reinforced with plain round steel, showed plots of the distribution of steel stress, bond stress and slip, and represented the results with empirical formulas. Also Fabbrocino *et al.* [Fabbrocino *et al.* 2005], performed a series of experimental tests on plain bars describing the force-slip relation on bond mechanisms of anchored end (hook) and straight detail bars, comparing the two behaviours. Felman and Barlett [Feldman and Bartlett 2005,Feldman and Bartlett 2007], performed pullout tests on square plain bars, comparing the effect on the bond capacity changing the concrete strength, roughness and diameter of the bar.

In the work of Verderame *et al.* [Verderame *et al.* 2008a], a series of experimental pull out tests were performed on plain round bars. This work filled a gap on the research on this field, analysing specimens submitted to monotonic and different cyclic demands. This topic is well addressed with an accompanying paper [Verderame *et al.* 2008b] that describes the results on an analytical approach, which is addressed further ahead.

There are only a few tests on bond behaviour of plain bars in cyclic field, concerning the influence of corrosion on bond performances [Fang *et al.* 2006].

In Portugal, in particular in the University of Aveiro, some recent work is being done to better understand the behaviour of old R.C. buildings. For this purpose Varum [Varum 2003] performed further analyses on a pseudo-dynamic in two full-scale four-storey frame of concrete, analysing them with and without infill walls, and also the answer to seismic actions after the rehabilitation. This work is aimed to better understand the global capacity of an old building without specific design in terms of seismic action, therefore, bond-slip of plain bars is one of the main issues to better calibrate the non-linear models developed.

Fernandes *et al.* [Fernandes *et al.* 2011b] subjected a two-span beam, collected from an ancient structure, to a unidirectional cyclic load until it collapsed. The data served to calibrate the numerical model and to analyse force-deflection diagrams, deformed shape and damage evolution, energy dissipation and chord-rotation on beams, and behaviour of the slippage of the plain bars. Fernandes *et al.* [Fernandes *et al.* 2011a] also performed cyclic excitations on two full-scale beam-column joints, built with plain bars and another with deformed bars to extract information valuable to compare the influence of the bond-slip effect on a joint. In another paper, Fernandes *et al.* [Fernandes *et al.* 2012] performed a series of cyclic tests on four full-scale joint, beam-column, built without any seismic detail and another with deformed bars for comparison. These topics are also explained on the author's PhD thesis [Fernandes 2012].

Melo *et al.* [Melo *et al.* 2012a] performed experimental cyclic tests on five interior and five exterior full-scale beam-column joints with different characteristics in terms of deformed and plain bars. In another paper, the authors [Melo *et al.* 2012b] tested seven full-scale columns built with different types of plain bars and cross sections, on cyclic excitation, and a monotonic test for one of the specimens, and, for comparison, another specimen built with deformed bars was tested in the same way. In this last work, the influence of the reinforcement amount in the displacement history of the column was investigated.

2.4.2 Modelling of Reinforcement Slip and FER

Addressing the modelling of this mechanism, some researchers had different approaches to approximate the formulas to the true behaviour of the bond connection. Since the seismic action is the more influential on making the bond-slip an important issue, the cyclic loading models give the more accurate response. Many analytical approaches were developed [FIB 2000], but only a few of more importance are addressed.

One of the earliest models developed taking in account cyclic behaviour on bond slip was presented by Morita and Kaku [Morita and Kaku 1974], who proposed a model with different monotonic envelope depending the load direction, in compression or in tension, and for confined or unconfined concrete [Verderame *et al.* 2009b]. In his model, for cyclic loading there is no bond degradation, just taking into account a bigger slip at the end of the cyclic but reaching the monotonic values. The model is still accurate for a low number of cycles and slippage bellow than 80%.

Tassios [Tassios 1979] improved the model when compared to Morita, accounting for the different mechanisms while performing the monotonic and rendering a more accurate approximation to the real behaviour of the bars. In terms of cyclic loading it was taken into account the reduction of the bond capacity, reducing on one third of the monotonic capacity. Quoting the paper [Verderame *et al.* 2009b], "the cyclic model applies only to slip values lower than the one corresponding to the maximum monotonic strength".

Viwathanatepa *et al.* [Viwathanatepa *et al.* 1979] proposed a quadri-linear monotonic envelope model differencing the tension or compression state of the member. The monotonic envelope presents degradation during the cyclic load which provokes bigger slippage values. Hawkins *et al.* [Hawkins *et al.* 1982] developed a tri-linear monotonic envelope model that corresponded to an approximation of statistical values that allow the determination of the slip and envelope behaviour. Solving three linear equations, the bond can be applied to a value of slippage. The model predicts a degradation of the monotonic envelope in cyclic behaviour for values of slip higher than the corresponding maximum monotonic strength.

Eligehausen *et al.* [Eligehausen *et al.* 1983] developed a bond-slip model which approximated several experiments to verify the reduction of bond capacity. This model was used with several additions and modifications by many researchers [Filippou *et al.* 1983, Lowes *et al.* 2004, Soroushian and Choi 1991].

Filippou *et al.* [Filippou *et al.* 1983] improved the last model and nowadays it is one of the most accurate models to evaluate cyclic bond performance of deformed bars, in the absence of splitting failure [Verderame *et al.* 2008b]. Literature does not present a lot of experimental results on plain bars compared with deformed bars to calibrate better the models.

More specifically concerning fixed-end rotation, Filippou [Filippou *et al.* 1983] performed a comparison between analytical and experimental data. For this propose, the author took data from joint frame experiments, which are well defined in his paper. The analytical model describes the hysteretic behaviour due taking in account the cyclic bond deterioration between bars and concrete, and divide the region of the member which performs inelastic in sub-regions depending on where the cracks are expected to be formed when the concrete tensile strength is exceeded (vd. Fig. 2.10). To simplify the model, the cracks should be considered parallels along with the member. Each sub-region should satisfy the equilibrium of horizontal forces and bending moments, and with the bond de-

terioration is associated a relative rotation between the crack surfaces. The equilibrium of the steel force-slip relations are complemented by non-linear equations which results can describe the hysteretic behaviour of each and all sub-regions, assembling the response of the member.

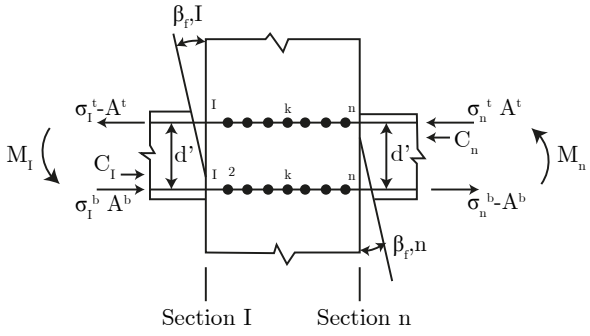

Figure 2.10: Analytical model for interior beam-column joint (adapted from [Filippou *et al.* 1983]).

To compute the fixed-end rotation, the results take only into account the end slip of the reinforced bars, due to deterioration of bond capacity inside the joint. In this study the slip between the bars and the beam is not considered, but is accounted for later on the inelastic rotations. The fixed-end rotation in this case is expressed as shown in equation 1. In the report it is possible to understand that this equation does not give good results when the bond is completely damaged because it does not take into account the relative slip between the bars and the surrounding concrete on the beam end region. This leads to an underestimation of the real rotation which in turn leads to an overestimation of the strength. For this reason, the model is only valid until the anchorage failure.

In the work of Alsiwat and Saatcioglu [Alsiwat and Saatcioglu 1992], an analytical procedure was developed to establish the monotonic force-deformation between bars and concrete, for the useful anchorage of plain bars. The modelling was performed together with experimental works which consisted in the pull and push of the reinforcement of interior joints and pullout of the reinforcement on exterior joints. The first paper treats the monotonic loading behaviour and has a companion paper [Saatcioglu *et al.* 1992] which deals with the hysteretic behaviour. In the monotonic paper [Alsiwat and Saatcioglu 1992] adopted the Ciampi *et al.* [Ciampi *et al.* 1981] and Eligehausen *et al.* [Eligehausen *et al.* 1983] models and developed a calibration for his experimental data. In his work, he also predicts a use of another similar model to compute the force-deformation to be applied to the resistance provided by the hook. In terms of bond-stress, the authors proposed a model in which the slip is calculated as the area of the integration of the strains along the bar length.

In the work of Saatcioglu *et al.* [Saatcioglu *et al.* 1992] full scale reinforced columns were built to investigate the hysteretic behaviour of the columns due to slippage, subjecting them to axial forces and lateral-deformations at the same time. A model was developed to express the hysteretic response of the anchorage, which performed very well. This model is a set of rules that consist on moment-slip rotation describing the load and unloading during the cyclic action. The first curve, the envelope of the mono-

tonic loading, was developed on the first accompanying paper [Alsiwat and Saatcioglu 1992]. This model uses some rules to explain the hysteresis which can be consulted on the following reference [Saatcioglu *et al.* 1992]. The author's experiments demonstrate, among other things, that the tension on beam-column interface has bigger strain on bars, generating significant contribution to fixed-end rotations.

Cho and Pinchera [Cho and Pincheira 2006] developed a useful model which consists on a two-dimensional and non-linear analysis to estimate the response columns with short lap-splice. It is based on local bond stress-slip calibrated with experimental results of cyclic loading tests. In spite of dealing with different kind of mechanism, his work is also well addressed in this paper.

In the work of Zhao and Sritharan [Zhao and Sritharan 2007], it is introduced a new concept of approach to develop the model, the author uses a fibre-based analysis (distributed system) which has differences when compared to the ones that use lumped system. Shortening the comparison, a lumped system uses dependent variables that work independently in time, $y.k(t)$, meaning a set of ordinary equations to explain a given behaviour. On a distributed system, all the dependent variables are functions of time and space, $y(x,t)$, and should be solved with differential equations. It is clear that the fibre-based analysis is much more complex and has higher computational costs.

The basic idea behind this approach consists of evaluating the fixed-end rotation as the curvature in a zero-length section element placed at the end section of the element. To this aim, the stress-strain relationship of the steel material used in this section is assumed equal to the corresponding stress-slip relationship. The rotation is then obtained as the curvature multiplied by the (fictitious) unitary length attributed to the zero-length section element [Taucer *et al.* 1991]. The model was verified for a column and a T-joint with specific formulas to account for the slope K, ductility and normalized bar stress and slip.

To apply the model to cyclic cases some rules need to be applied as shown in the paper [Zhao and Sritharan 2007], using similar equations for the hysteretic behaviour with some different particularities.

Sezen and Setzler [Sezen and Setzler 2008] studied the rotation slip of columns to get the contribution to the total lateral displacement of structures. To get it, the author developed a model to predict the lateral deformation of a column due to slip of anchorages on joints with load and unload demands. In the same work, the model is compared with five other models, currently used in literature, and concludes that for a simple and computed model, it performs very well. One important conclusion of his paper is the verification of a contribution of 25% to 40% of total deformation on experimental results from four double-curvature columns tested by the author [Sezen 2002]. The model consists of a macro approach which is appropriate to use later on the analysis of entire structures. It separates the u_{b} and u'_{b}, steel stress until yielding and, after that, on the respective l_{b} or l'_{b} length. The slip can be calculated as the integration of strain along the bar, considering l_{d} and l'_{d} the development lengths for elastic and inelastic portions of the bar. The slip equation can be separated in two different values, depending on the yielding deformation of the bar (ε_{y}), which allows calculating l'_{d} in the inelastic field.

After the first approach to bond capacity it is possible to calculate the slip rotation, taking into account only the slippage on the tensile bar and movement of the neutral axis of the system when a crack opens on concrete, as shown on figure 2.11. The author proposes the simple equation 2.32, consisting on the quotient of relative slip by distance

between bars, which can be developed to compute the rotation due to inelastic and elastic behaviour of the bar. On his work, this is referred to as embedment length. For further information, it is necessary to check the equations for modelling the $l_{d,min}$ which are presented on his document, as well the maximum strain in elastic portion, slip at unload end bar and the slip to which is verified the failure of the pullout. The author concluded that five of the compared models get approximate values including his own model [Alsiwat and Saatcioglu 1992,Eligehausen *et al.* 1983,Hawkins *et al.* 1982,Lehman and Moehle 2000,Sezen and Setzler 2008].

Fabbrocino *et al.* [Fabbrocino *et al.* 2004] developed models to deal with plain bars anchored through circular hooks, using results from experimental tests previously performed by the author. The models are addressed to the critical regions of the structures as interior and exterior beam to column or base column.

Verderame *et al.* [Verderame *et al.* 2008c], along with additional work by the author [Verderame *et al.* 2009a, Verderame *et al.* 2009b], developed an implementation model of element through fibre and distributed plasticity analysis. The global deformation capacity is calculated summing that the displacement of flexural bending and the rotation in the end of the element. The model is different from the other literature because of the way how it evaluates the deformation capacity, through the study of behaviour of anchoring element characteristics. The envelope of concrete model is in accordance with model of Mander and co-authors [Mander *et al.* 1988], the stress-strain of steel of Chang and Mander [Chang and Mander 1994], and hysteresis rules of Yassin [Yassin 1994]. For the rigid rotation of the element it is used exactly the same formula as Filippou [Filippou *et al.* 1983].

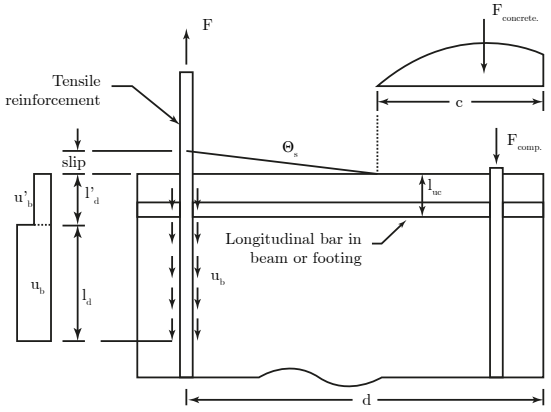

Figure 2.11: Slip rotation on proposed model (adapted from [Sezen and Setzler 2008]).

Varum [Varum 2003] proposed a simplified method to include the bond-slip in the numerical analysis of RC frame pseudo-dynamically tested. The bond-slip modelling includes a correction to the concrete-steel bond reduction through a factor, in accordance with the maximum deformation observed during the experiments. The model, as said by the author, is yet to be improved.

One of the goals of Fernandes [Fernandes 2012] was to apply a numerical model, non-linear fibre-based, to experimental specimens, in order to perform an evaluation more

focused on the beam bond-slip behaviour. To achieve it, the author used a slippage model from OpenSees program which was developed and calibrated with Zhao's results [Zhao and Sritharan 2007], for cyclic tests with deformed bars. To adapt the model to this field of studies, paying special attention to bond-slip mechanism of plain bars, some changes were performed: redefinition of a parameter alpha which defines the non-linear branch of the monotonic envelope; reducing the value of ultimate capacity for slippage; definition of a minimum value for stiffness reduction. The field of work was more focused on the beam behaviour. To validate the numerical modelling was extracted experimental data which was acquired on real scale beam-column joints, representing joints found on the interior of the buildings, without any seismic provision, and with plain bars. For comparison, it was performed another test on a real old joint and a joint with deformed bars [Fernandes 2012, Fernandes *et al.* 2010, Fernandes *et al.* 2012].

Melo *et al.* [Melo *et al.* 2010] applied models based on OpenSees program to analyse the deformation on a cyclic excitation of the experiments on the two-span beam which were later published by Fernandes *et al.* [Fernandes *et al.* 2011b]. The obtained data served to calibrate the model, with special attention to the bond-slip mechanism, important to approximate accurately the numerical results to the experimental data.

For further reading about the topics studied in this work, consult the following references [Banon 1980, Lowes *et al.* 2003, Manfredi and Pecce 1998, Verderame *et al.* 2010].

Intentionally blank page.

Part II

Modelling

Chapter 3

Study Case Description

Two buildings built on the fifties, in Portugal, are used as a study case to perform the analysis. Both are representative of the type of construction in concrete, made in Portugal, until the later design codes had been applied as [RSCCS 1958], [RSEP 1961,REBA 1967] or [RSA 1983,REBAP 1984], predicting the reinforcement of structures to respond an occurrence of an earthquake. In the next two sections is made a brief overview of the buildings in terms of architecture and engineering. On the appendix part, are presented some drawings to support the descriptions (see appendix A). Further descriptions about geometrical proprieties and materials of the buildings is available on the next chapter 4.

3.1 Costa Cabral Building

3.1.1 Description

The Costa Cabral building is located in the Street Costa Cabral, city of Oporto, which makes the connection between the Marquês de Pombal Square and the street of Circunvalação, in the centre of the city. It was designed by a Portuguese architect, Viana de Lima, and built in 1953, exclusively for habitation purposes. The building design is influenced by a architectural modern movement which gives this specific construction an special interest about its assessment. As Fonseca [Fonseca 2005] said, it is an admirable example of progress, innovation and technical and formal experiences from that period applied in our buildings, also with a not usual monumental volumetric shape that triggered its use some decades later.

3.1.2 Architecture

This building has a rectangular implantation of 37.22 front per 16.35 square meters and 24.80 meters of height. The block is formed by a cellar beginning below the soil level, a ground floor and other six storeys, the last one indented. The cellar is reserved for parking spots for the dwellers and the rest of the storeys, from the ground floor to the sixth, are used entirely for habitation, with different typologies.

The two first floors are indented relatively to the first five storeys, creating an irregular shape on the building and making it develop an extension of the interior space on the front and back direction/façade of the building, south-west and north-east. Some of its

portion works as a cantilever, besides the balconies which also (and just) exist in the same levels. On the last floor, the indented block recovers a perimeter shape similar to the bottom floors. On the two main façades a series of pilotis (columns) stand out from the vertical alignment, linking the ground to the slab of the first storey, and are presented not just as a structural concept but also integrated in a modern architecture approach. See figures on the appendix section A.1.1.

3.1.3 Structure

The structural design of the Costa Cabral Building was performed by the engineers Vercingetorix Abelha and Napoleão Amorim in a straight collaboration with the architect, providing a good correlation between the aesthetics and function towards the structural design. The structure is formed by frames of reinforced concrete in all its height development, with a lot of specific frames, orientations and cross sections of beams and columns. From the first until the fifth storey it is possible to verify a short repetition of the design. See figures on the appendix section A.1.2.

On the cellar, the adopted structural solution was an integration of ten longitudinal frames crossed by four transversal frames. This solution is adopted also for the ground floor, but is not repeated for the rest of the floors, creating the distinction of the habitation typologies upper ground floors. So, on the other floors, the scheme of beams is symmetric but reorganized in a slightly different way, integrating differences in terms of slab design. This change between typologies of floors forces some adaptations on the structural design, changing the disposition of beams and floors to avoid interference with the architecture purposes. With this in mind, it is important to consult white prints for a better understanding of the designs.

Between the ground floor and the top floors, there is a service floor of 1.3 meters which has beams with about one meter height to sustain the top floor columns, which have no continuity to the foundations, transferring the load from the two different structural solutions. The slabs are of waffle reinforced concrete type, with hollow brick, on all the floors, and thick R.C. slabs on the balconies, stairs and ground floor slab. All the waffle slabs are reinforced one way except on the ceiling of the cellar, that is two-way reinforced. The vertical accesses are done by two escalators and stairs which have an independent behaviour related to the structure.

The building has infill in all the height and perimeter, with exception to the two entrances for the garage and on the centre frames on the back of the building. The interior walls are double or simple hollow brickwork, depending on the necessity of hiding columns or beams, and are 5 centimetres thick. The exterior walls are built of solid brickwork doubled walls, glazed on the outer face. From the first to the fifth floor, the exterior walls of the front and rear façade are not confined from columns but from slabs, which contributes to the global stiffness. Only the totally confined walls are considered on the modelling. The location of the infills are represented on the respective drawings located on the appendix (see section B.1.1).

3.2 Parnaso Building

3.2.1 Description

The Parnaso building is located in Cedofeita, city of Oporto, on the crossroads of Street Oliveira Monteiro and Street Nossa Senhora de Fátima, in the west zone of the city. It was designed by José Carlos Loureiro in 1954, and built in 1955. The building has three different blocks with a garden in the interior. The first is exclusively for habitation, the second is mixed between habitation and commercial space, and a third is used for a ballet school. Note that, in the context of the present work, only the main block, the mixed one, is modelled. This building is also an example of modern architecture in Portugal, which is classified as a monument of public interest. It was built with some of the Athens Charter principles: constructions over pilotis, rooftop with terrace/garden, white-print and façade free from structure.

3.2.2 Architecture

The building has a rectangular implantation of 26.20 per 9.90 square meters and 18 meters of height. It has different kinds of typologies. The ground floor is dedicated to a cultural place for children activities and the house of the building security. The first to the third storeys are used for different private houses, and the two last storeys are a duplex house belonging to the building owners, which makes a different habitation typology. On these last floors, a stairs is used inside the block and house and it has also an exterior connection through stairs to a gardened zone on the roof. See figures on the appendix section A.2.1.

3.2.3 Structure

The structural design was done by the engineer Alcino José Salvador Paixão. The middle block is formed of three longitudinal frames separated by 4 and 4.4 meters, and an extension cantilever balcony of 1.40 meters length. The ground floor has 4 meters and the other five have 2.8 meters of height, creating an open and big space on the first floor. This may also create problems in terms of soft storey because half of the columns have no continuity to the foundations of the building. Generally, in one set of frames of the main longitudinal façade, the beams length span are 3.25 meters excepting on the ground level which has 6.5 meters of span, which are typically repeated on the parallel frames. See figures on the appendix section A.2.2.

The slabs of the storeys are waffle R.C. slabs of hollow bricks with 0.17 meters height, and a compression depth of R.C. of 5 centimetres. On cantilevers, inside zones, the slabs are thick R.C. slabs of 0.14 meters, and the balcony ones have 0.16 meters.

The vertical access of the building is made by exterior stairs, located on a separated framed structure from the building but linked through some beams which do not unlink it from the structure. This extra block is formed by a concrete wall in all its height on one of the side, linked by beams and columns to the structure. Although this support structure has its role in increasing the stiffness of the system, the stairs themselves have an independent behaviour from the whole structure because they are unlinked by some release systems. It has also an interior escalator unlinked from the structure, which had an old function where it was pulled up, therefore it is supported directly on the ground.

Just the confined infill walls were considered for the model. Because the project does not provide the information about its characteristics, the infills are considered with similar proprieties compared with the Costa Cabral building. It has an exterior wall almost in its entire perimeter and another two interior walls from the second to the forth storey. The location of the infills are represented on the respective drawings located on the appendix (see section B.1.2).

Chapter 4

Modelling and Assumptions

4.1 Modelling

The chosen tool to perform the seismic assessments was an award-winning program, Seismostruct® [SeismoSoft 2012], capable of achieving a high level of accuracy for the results. SeismoStruct® is a Finite Element Method package capable of computing large displacement response of framed structures under static or dynamic loadings, considering both material and geometric non-linearities. The program works in three different phases. The pre-processor is where the modelling and all the geometries and characteristics, masses and loads to the structure are defined. The processor is where the analysis is performed, in a black-box configuration, according to the defined types of processing. On this dissertation it is used the "eigenvalue" mode, where the global stiffness and weight (self weight and loads converted to masses) of the structure are used to calculate the natural modes of vibration of the structure. And also the "dynamic time-history analysis" mode is used, in which the program computes the behaviour of the structure according to the defined accelerogram. The third phase is the post-processor, where the analysis of the results are performed, such as modal quantities, step by step results of deformations, elements stress-strain, nodal forces and global response parameters, among others, with instant plotting capabilities and excel value export options for different analyses.

To perform the modelling of the structures it is necessary to understand the various modelling implementations, so in this regard, the next subsections develops the integrated assumptions and how the program performs the main analyses. It is important to refer that the program SeismoStruct® has no current integrated model to compute the effect of steel slippage. To overcome it, is necessary to have a good definition of the proprieties of the materials and the plastic hinges, making a prior step to achieve a good assessment.

4.1.1 Finite Element Formulation

The cross-sections, on the program, are represented through a fibre modelling approach. The response models are implemented at each individual fibre, using the uniaxial stress-strain behaviour already referred. The discretization of the sections is made automatically according to a finite number of fibres defined by the user (see figure 4.1). A number of 150 to 200 fibres are usually enough to model accurately the non-linearity distribution along the section area. To avoid some difficulties on the convergence process, on elements like the wall and beams with big dimensions, the number of fibers has been increased to

500 and 300 respectively. The distribution along the elements may be done through two different finite element formulations (FE): (the classical) displacement-based (DB) and a more recent force-based (FB) approach [SeismoSoft 2012].

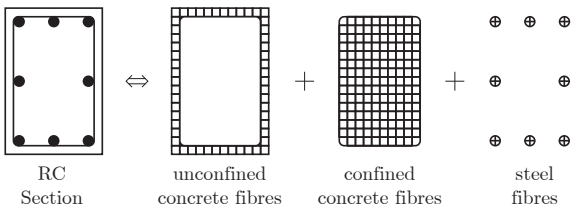

Figure 4.1: Discretization of a R.C. section (adapted from [SeismoSoft 2012]).

4.1.2 Element Connections

The elements are defined through a "infrmFBPH" which is a FB formulation, distributed inelasticity force-based formulation and concentrating the inelasticity in the fixed length of the element, where the non-linear behaviour is formulated as plastic hinge. This formulation has its advantages on the amount of time consumption since it performs the fibre integration on the two fixed-end parts of the element, providing more control of the plastic hinge length ("spread of inelasticity"). The plastic hinges on the program are defined as the percentage of plastic length on the total length of the element.

4.1.3 Numerical Convergence

Throughout the learning process along with the modelling, the convergence of the structures can be challenging, since all the error should be tracked and corrected. After the definition of all the elements, it is very important to analyse the modelling to see if some of the elements are not correctly linked to each other. It seems obvious but, on a model with almost 2000 elements and 700 structural nodes, one bad link can create unsolved errors on the matrix definitions. The masses can be defined as self-weight but, as different materials and geometric sections are defined, the introduction of masses would not be accurate. Therefore, the masses should be automatically calculated for structural materials, and defined as lumped or distributed masses for the slabs, non-structural materials and other permanent and live loads. Almost all masses on the model are distributed and they need to be defined on all individual elements, without jumping some nodes on one divided element. The importance is to attribute the masses and its influence correctly, since the program deals with the mass loads on the extremities and not along the elements.

While searching for errors, it is necessary to overview if all the proprieties of the materials and elements and correspondent units are well defined. If a model is not running, for example for higher loads, it is necessary to assess if it can happen due to numerical difficulties or by the formation of normal mechanisms or high drifts which leads to unstable models. For drifts higher than 5%, the models may become unstable. On a dynamic analysis, it is important to have an increasing step of not less than the step on the accelerogram. A increment of 0.01 seconds should be enough. For the constraints,

to model the influence of slabs as rigid diaphragms, the Penalty Functions exponent, needed to be applied on large models instead Lagrange Multipliers due to extremely slow analysis, should be carefully accounted to achieve the real behaviour. As previously mentioned, it is important to increase the number of fibres for large sections. For short elements, may be recommendable the use of displacement-based elements, since they are controlled by shear, increasing the stresses which may induce numerical instability.

To track possible errors, the best procedure is to proceed to a systematic simplification, backing up all files, and running at each step. Normally, if from one iteration to another, the convergence difficulties are surpass, then the problems are from the deleted or simplified parts. Some of the simplifications can be the removal of masses, removal of rigid diaphragms, decrease of elements, gradually removing columns and beams, and storeys, change the force-based elements to displacement-based ones, which are more simple and stable, change subdivisions of elements, trying what is expected to create the problem on some simple and small modellings. Finally, changing the program definitions, like convergence tolerances and steps, may help to to track deficiencies.

4.2 General Properties

The existing materials on both buildings, according to the design project, are the same. Therefore, concrete of class C16/20 and smooth steel of A235NL were used, with model formulation of Mander and Martinez, and Menegotto and Filippou, respectively, as referred before.

The main concrete properties are weight of 24 kN/m^3, characteristic strength, f_{ck}, of 16 MPa. The used strength on seismic analysis is a calibration of the values measured on the actual building through tests. The expected strength of the building, calculated by Eurocode 2 [CEN 2004] is $f_{\mathrm{cm}} = f_{\mathrm{ck}} + 6 = 22$ MPa. Eurocode 8 [CEN 2005] gives specific factors, named knowledge levels, to reduce the used values depending on how well the material properties, geometry and details are known. The values goes are 1.00, 1.20 and 1.35, the latter level of confidence should not be used on non-linear analysis because is not reasonable to perform non-linear analysis on structures without a knowledge level to accurately define the material proprieties. Despite of none in-situ tests having been performed and no full information regarding the details being available, that would lead to a normal level of knowledge. Even so, the current work is academic and intends to analyse the building to stronger excitation demands. For that it was decided not to reduce the strength of the materials, knowing that the final response data would not be correct to safety assessment project, even if the values are more accurate. Actually, the code does not inform the designer about how the analysis should be performed, so the use of full knowledge level may not be wrong, since the results may be more similar to the real response. The tensile strength, f_{ct}, is 1.9 MPa and the strain at peak stress, ε_c, is 0.002 m/m (values varies between 0.002 and 0.0022 m/m). Two slightly different concrete materials were defined for all sections regarding the cover and confined concrete. In fact, this does not take any major effect on the results because, from the calculations, using Mander [Mander *et al.* 1988] recommendations and the available drawings of the amount of stirrups and its properties, the result for confinement factor was 1.005. This value could be greater but since there is no information on how the hoops were performed, it should take some care not to lead to inaccurate results, therefore it is evident that

concrete has a less ductile behaviour. It is used a concrete cover of 30 mm.

The steel main properties are specific weight of 77 kN/m^3, yield strength, f_{sym}, of 235 MPa, elastic modulus, E_{sm}, of 200 GPa and strain hardening parameter, μ , of 0.005 (values usually varies between 0.005 and 0.015) which is the most conservative. The rest of defined parameters are the recommended ones, namely the transition curve of initial shape, R_0, which is defined with 20. The used fracture/buckling strain, ε_{ult}, was 0.2, a conservative value for this kind of steel A235NL, hot rolled, which was fabricated without much strength capacity but was very ductile. Traction tests show an average extension of 24%. The yield strength which was used is the characteristic value, so, it could be increased to at least 300 MPa, and buckling strain to 24%, but due to uncertainties regarding the slippage, and because the steel has less impact on the global response compared to the concrete, it was decided to integrate more conservative values.

4.3 Definition of Loads and Masses

To integrate the loads on the model, it is needed to account with all permanent loads, as weight from frame elements (beams and columns which are directly calculated by the program), slabs, exterior and interior walls, stairs, and non permanent loads, which are defined ahead.

According to Eurocode 8 (EC8) [CEN 2003], the load combination which should be used for an earthquake occurrence is

$$\sum G_{\text{k},j} \text{ “+” } \sum \psi_{\text{E},i}.Q_{\text{k},i} \tag{4.1}$$

where the coefficient for variable action “E, i” is calculated as $\psi_{\text{E},i} = \varphi.\psi_{2,i}$, of Eurocode 0 [CEN 2001]. For buildings from categories specified on the EC0, the values of the coefficient φ are 1.0 for roof, 0.8 for storeys with correlated occupancies and 0.5 for independently occupied storeys. For $\psi_{2,i}$, the code predicts different values depending on the categories in which the buildings are integrated. Both buildings are integrated on category A, described on Eurocode 1 as, *i.e.* “use for domestic and residential activities”.

From technical tables, project information and previous studies [Freitas 2008], the used loads for both buildings are defined according to table 4.1, for permanent loads, and table 4.2, for variable loads, and calculated according to combination referred as equation 4.1.

Table 4.1: Permanent loads.

Weight [kN/m^2]	Costa Cabral	Parnaso
Waffle Slab	3.35	3.18
Thick Slab	2.85	2.88
Other elements	1.20	1.20
Finishings	0.60	0.60
Interior Walls	-	1.00

After the definition of loads for all the specific and individual areas in kN/m^3 should be converted to masses. In order to perform the analysis of modal vibrations and shapes, the used formulation needs to use the weights in masses, in order to be in line with some

Table 4.2: Tabled overloads and reduction factors.

Location	Q [kN/m^2]	ψ_2 (EC0)
Habitation	2.0	0.2
Balcony	2.0	0.2
Roof	0.3	0.0

dynamic definitions. The mode is characterized as the shape that a structure, without damping, would naturally undergo without a change of deflections after an excitation. The change of deflections can change according to the number of degree of freedoms. Therefore, it is described its free vibration equation,

$$u(t) = q_n(t)\phi_n \,, \tag{4.2}$$

where $q_n(t)$ is the variation of displacements along the time in each degree of freedom and ϕ_n the deflected shape. The vibration can be integrated on the equation of motion which gives

$$\left[-w_n^2 m\phi_n + k\phi_n\right] q_n(t) = 0 \,, \tag{4.3}$$

where ϕ_n and w_n are unknown. Equation 4.3, where $q_n(t)$ is different than zero, can be solved through the determinant definition, where the n roots of the solution are the natural frequencies of vibration [Chopra 2006], as

$$\det\left[k - w_n^2 m\right] = 0 \,. \tag{4.4}$$

This serves as a practical guide of the need to correctly define the loads on the structure. Having said it, the masses are assigned as distributed along the beams chosen according the specified on the drawings of slabs reinforcement way to perform, in terms of directions. For unidirectional slabs, the loads are divided 50% for each side. For bidirectional slabs, the loads are divided with a concept of area of action/influence, changing it according to the columns place/typology. If beams have continuity or not changes creates different angles which affects the amount of area which should unload on the beams. This exercise needs to be done because the program do not allow to associate a mass on the slabs, since these elements are defined differently, without possibility of define an area load/mass. One possibility, would be the definition of lumped masses on the centre of mass of the slabs, but since this is intended to achieve the most accurate results possible, the masses are introduced individually.

4.4 Definition of the Elements

The section dimensions are defined as accurate as possible by the extraction of information from the technical drawings and the descriptive documentations. In terms of cross-section dimensions there are just a few doubts, but the reinforcement is not so clear in all cases and storeys. The definition of reinforcement was accounted as being the same in all the length of the elements, using the amount of steel bars near the joints, from the last section of the element until where it is considered to form the spread of

the plastic hinges. Thus, the elements were defined in a way which has more strength to negative moments. The only difference is for beams where columns are directly supporting on them, creating high positive moments. In these cases, two different sections are defined with different amounts of steel for indirect supports and continuous frame (column-column).

The various frame elements are defined as force-based element with concentrated inelasticity on the fixed end lengths (plastic-hinge), divided in an average of 200 fibres each.

The plastic hinges were defined with a general/average value for each cross-section and/or amount of steel, to avoid too much time consumption, both in computing and in assigning stages. The used simplification consists in calculating an average of all the section strong-axis separated by columns and beams. Dividing the result by 2, it is possible to estimate the length which separates the face of the perpendicular element (section) from the geometrical node (centre of the joint). With this value, it is summed the 0.25 of the transverse height in each element to which plastic length is being calculated. That estimation comes from conclusions taken from reference [Varum 2003]. It was used a proposed formulation by Paulay and Priestley, for typical beam and column proportions and smooth bars, where the effective plastic hinge length can be estimated as approximately 25% of the height on beams and 25% of the height of the strong-axis on columns, counting from the face of the adjacent element. Getting l_p, plastic-hinge length, it was necessary to divide it by the actual element length in order to introduce it on the program as the required percentage of plastic length on the element, l_p/L.

An exhaustive list of the cross-sections for both buildings is not present on the dissertation. This information can be found in [Freitas 2008, Milheiro 2008]. Replacing it, it is given next an overall view of the dimensions. For the Costa Cabral building, the columns are rectangular, varying dimensions from 0.2/0.3 m and 0.4/0.5/0.8 m, and beams varying dimensions from 0.15/0.25/0.35 m and 0.4/0.7/1.1 m, on both axes. For the Parnaso building, the columns are squared, varying dimensions of about 0.2/0.3/0.4 m, and rectangular beams varying dimensions from 0.25/0.35 m and 0.4/0.8 m, on both axes.

4.5 Definition of Other Elements

4.5.1 Concrete Wall

The Parnaso building, on the exterior block for stairs, has a concrete wall on the far end. This stiff element, far from the centre mass of the building, is very important to model because it is expectable to take an important influence on global torsion effects. To model the wall, and because no information is given about it, it was considered as being 20 cm thick and 2.5 meters wide along the building height, with constructive reinforce steel bars. To model it on the program it was necessary to create beams for each floor, linking the structural beams which came from the block laterally, with extremely high bending stiffness and no mass. Then the wall section was attached to these stiff beams on their centre, as it is a long column on each floor, restricted on the ground. All material proprieties are the same as the rest of the frame but the element type was chosen to be calculated as force-based formulation with distributed inelastic along the elements, instead of concentrating on the fixed-end lengths.

4.5.2 Infill Panels

SeismoStruct has an implementation of a model developed by Crisafulli [Crisafulli 1997] which is a four node panel infilled in framed structures, describing its non-linear response. The model considers six strut members using hysteresis rules. Two diagonal and parallel struts in each direction, which carry the axial loads on the panel, and another pair to describe shear from the top and bottom of the panel, which are activated in each direction, depending on the activation due to axial compressive loads while the panel is deformed. The internal and dummy points to which the struts are linked, are the delimitation of the concrete frame and the actual contact of the infill panel when is deformed (*vd.* Figs. 4.2 and 4.3).

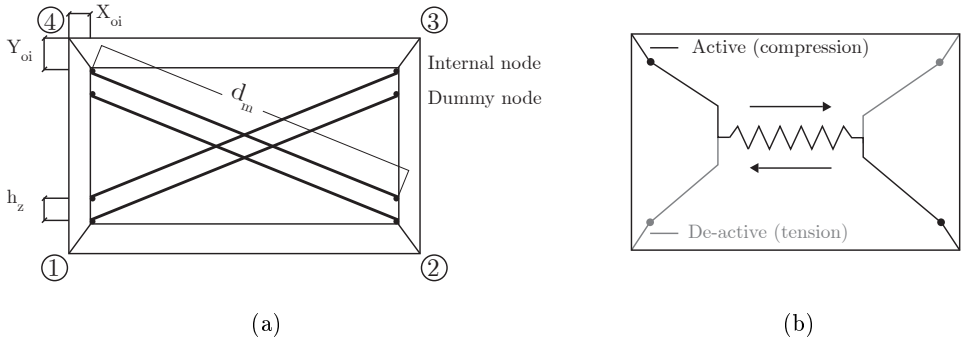

Figure 4.2: Crisafulli model for (a) compression/tension struts and (b) shear struts (adapted from [SeismoSoft 2012]).

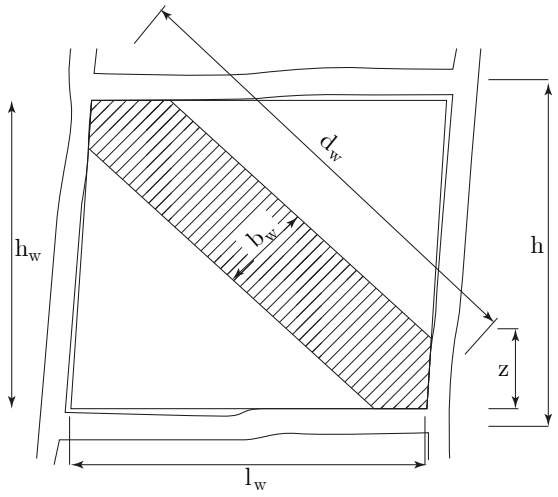

Figure 4.3: Infill panel parameters (adapted from [Smyrou 2006]).

The definition of properties on the current modelling was performed using Smyrou's infill panel implementation/procedure [Smyrou 2006] for the framework of the ICONS

research programme [Carvalho *et al.* 1999]. It is assumed that the used infills are representative of the ones also applied on the construction in Portugal. No tests have been done on the two buildings, so it is considered that the both have the same characteristics and that are similar to the next referred results.

The compressive strength values used for some masonry specimens are available in [Varum 2003], with 1.1 MPa of average compressive strength in the direction perpendicular to the bed joints (f_{n}).

The compressive strength of the struts, $f_{\mathrm{m}\theta}$, was calculated with a equation [Crisafulli 1997]

$$f_{\mathrm{n}} = f_{\mathrm{l}} \sin^2 \theta \,. \tag{4.5}$$

f_{l} is the principal stress and θ is the angle formed by the two corners of the infilled frames.

As expectable, during the process of calibration of the model, it was verified that the model was too stiff for what it should be. The strength calculated did not take into account the openings (windows and doors) of the panels of the buildings. To get a better calibration, some tests on both models were done and introduced with same exact modifications on both models. Therefore, the results of $f_{\mathrm{m}\theta}$ were post-processed reducing the capacity of the panels with openings in 50% the first results, which induced a good calibration. For panels without openings, no modification of the results of equation 4.5 were done. In the Parnaso building, the infills of the plane next to the stairs block, with no openings, had the strength increased in 50% because the drawings show a different kind of line (expected a different material) on that façade.

From these values, the elastic modulus was calculated multiplying $f_{\mathrm{m}\theta}$ by 1000, as proposed by Paulay [Paulay and Priestley 1992] and others.

The value for tensile strength was also consulted in [Varum 2003] from which work an average strength of 575 kPa was achieved. The introduced value was 500 kPa for all panels on both models.

The next referred values were also adopted by [Smyrou 2006]. Shear bond strength with 300 kPa, a coefficient of friction of 0.7, a maximum shear stress of 1 MPa, strain at max stress (ε_{m}) of 0.0012, and ultimate strain (ε_{u}) of 0.024.

It was also needed to calculate the horizontal and vertical offsets $x_{\mathrm{o}i}$ and $y_{\mathrm{o}i}$, which correspond to half width of the strong axis on columns and half depth on beams, respectively. To overcome the complexity of the geometries, on both models, averages of these values were calculated to avoid description of too many slightly different panel proprieties. The procedure was done just for the cross sections (depth of beams or width of columns), as the length for the elements was the real value. The offsets are calculated as $y_{\mathrm{o}i} = 0.5 h_{\mathrm{beam}}/h_{\mathrm{column}}$.

The contact length is calculated with equation

$$z = \frac{\pi}{2\lambda} \,, \tag{4.6}$$

where

$$\lambda = \sqrt[4]{\frac{E_{\mathrm{m}} t_{\mathrm{w}} \sin(2\theta)}{4 E_{\mathrm{c}} I_{\mathrm{c}} h_{\mathrm{w}}}} \,, \tag{4.7}$$

as proposed by Stafford Smith. [Stafford-Smith 1966] On these equations, t_w is the thickness of the panels, considered as equal to 0.15 m, according to the architecture definitions, and h_w the height of the wall. The vertical separation between struts fluctuates in the interval $1/3z \leq h_z \leq 1/2z$. The considered lengths to define the struts were chosen to be close to the inferior limit $(1/3z)$ for short-bay and to the superior limit $(1/2z)$ for long-bay panel, introduced as percentages in comparison to the height of the panel.

The area of the strut, is calculated with $A_m = b_w t_w$, where $b_w = d_w/3$, according the formulation of Holmes [Holmes 1961].

The assigned weight is close to zero, as the loads are already considering the walls.

A collection of other parameters were selected through some recommendations available on [Smyrou 2006]. These empirical parameters were already introduced by default SeismoStruct, so no modification was done at this level.

It is recommended to consult the documents [Smyrou 2006] and [Crisafulli 1997] for further informations.

The location of the infills can be found on the appendix section B.1.

4.6 Moment/Force Releases

The stairs were not modelled on both structures. The stairs case on both buildings are made as being just "resting" instead of attached, causing no increase of stiffness on the building. Thus, no extra elements were modelled and the respective zone was considered as being a hole with the correspondent permanent loads, supporting on the beams where they are resting.

In the Costa Cabral building no releases on frames were done. Some releases are referred on the middle of the building but it is related with the expansion joints of the slab and not with the actual framed system.

In Parnaso, according to the available drawings, some moment and axial load releases were included on modelling for some beams of the exterior stairs block and on the façade of the same block.

4.7 Damping

As highly responsible for dissipating energy of an earthquake, damping is an important issue on dynamic analysis. Global damping parameters were not defined in the model properties, letting the actual proprieties of materials do it without artificially imposing it. The fibre model formulations implemented on the program can already take into account the hysteretic damping. The program is capable of considering a "small quantity of non-hysteretic type of damping that is also mobilised during dynamic response of structures, through phenomena such friction between structural and non-structural members, friction in opened concrete cracks, energy radiation through foundation, *etc.*, that might not have been modelled in the analysis" [SeismoSoft 2012]. To model it, the program gives a possibility to define Rayleigh damping. Among the scientific community, no full agreement on how to define it has been achieved, therefore, was chosen not to define a Rayleigh damping and just use the calculated on the dissipation on frames defined by the material models.

4.8 Soil-Structure Interaction

All the columns were considered to be perfectly restrained on the ground level. No elastic properties are defined for the way the ground acceleration impact, as the an integration of some kind of strings.

Because a partial portion of the two main longitudinal façades of the Costa Cabral building are underground, some modelling on this matter were made. Taking it into account, the influence of the soil was defined through perfect restricted nodes, at 2 meters of height, linked to the correspondent columns as elastic elements. These element links are modelled as springs, with a behaviour with elastic stiffness towards the perpendicular direction of the soil, defined with a 20 MPa value, using soil data from Oporto city documented in [Martins *et al.* 2003], and with no resistance on all the other directions. So, a limited resistance on deformations against the soil, and free movement on the moving out deformations of the columns.

4.9 Short-Beams

The short beams are a problem on the building Parnaso which could not be solved, after many attempts and strategies. On the first floor, the columns from the upper floors are unloading on small continuing beams of 0.5 meters. This modelling, even for static analysis was showing some numerical errors, therefore, the found solution was to remove those 0.5 of beams, having in mind that it could bring some inaccuracy computing the structure response.

To perform later modelling with the program, one strategy which still could not solve numerical instability, was to combine a displacement-based formulation for those short beams, instead of forces-based. The formulation does not allow the definition of plastic hinge lengths but should help on this kind of convergence difficulties.

4.10 Constraints

The slabs were modelled as rigid diaphragm constraints, restricting degrees of freedom on the horizontal plane, linking the nodes from each floor, unifying its behaviour. The chosen type makes all the nodes on the same constriction get the same relative position on the defined plane, with its individual rotation and displacements but on the same plane. A chosen master node needs to be defined on this formulation and is this case was the near centre mass one of the diaphragm.

In a case of a very fragmented number of beams forming the structure, it is advised to have care while choosing the nodes which integrates the constraint diaphragms. Since elements subjected to flexure develop axial deformation, the constraint of all the nodes can lead to an artificial stiffening because it can prevent this natural deformation. On the specific case of this work, because the spans are naturally long, almost all the nodes were constrained.

4.11 Natural Frequencies

To get an accurate behaviour of the model, it is important to understand how to consider the natural frequency of the building to calibrate it. These experimental frequencies are necessary to get the best post-results possible. With them, it is possible to have a notion if there is not a big error on the modelling, reducing the discrepancy between the virtual and real structure. On this dissertation, the used results are extracted from the existing experimental work available in Milheiro Master's dissertation [Milheiro 2008], and showed on the next subsections.

The resorted program ARTeMIS® uses information of geometry, Degrees of Freedom (DoF) and measurements in a way to read the results from the accelerometers in order to calculate the natural frequencies from the provided information. It was used the Enhanced Frequency Domain Decomposition (EFDD) method which estimates damping ratio and natural frequency from calculation of the resonance peaks of the modes, based on some criteria that transforms the auto-spectral density of a Single-DoF to a time domain. [ARTeMIS 2008] The program is able to give the mode shapes of the structure, but they are not assumed.

The discussion and analysis of the results are made on the specific chapter 7.1.

4.11.1 Costa Cabral

Nine longitudinal and transversal measurements were performed, distributed in all the stories and repeated on third and fifth one. The dispositions of the accelerometers were applied according to the recommendations to achieve good results for vibration modes and experimental frequencies.

The mode shapes provided by the program show a reduction of drift on the first storey and a big one on the last, for both first and second modes of vibration. Results are shown on the appendix figure B.4 and table 4.3.

4.11.2 Parnaso

On this building, nine longitudinal and transversal measurements were applied, distributed in all the stories and repeated on the technical and penultimate ones.

The shape of the first mode (transversal direction) shows a small drift on the last storey and a big drift on the previous one. Regarding the second mode, the results show a normal shape of similar drift in height with some reduction on the last and first floors. Results are shown on the appendix figure B.5 and table 4.3.

Table 4.3: Experimental frequencies.

Mode	Parnaso		C. Cabral	
1	2.178	Hz	2.914	Hz
2	2.343	Hz	3.863	Hz
3	2.999	Hz	4.365	Hz
4	4.000	Hz	6.000	Hz
5	4.469	Hz		
6	6.002	Hz		

4.12 Final Comments on Modelling

All the process of modelling should be monitored with visits to the real building, with a previous careful study of all the available drawings and descriptive memories. Tests on the structure, as the extraction of samples, to confirm the information on descriptions is very important. With the definition of the proprieties and how well the building is known, some coefficient factors for security level should be applied, according to the description on the codes. The modelling should not end with the definition of all the elements and materials, to perform a good modelling, the calibration process should be also taken with care and attention.

Experimental work to know natural frequencies should increase the accuracy of the modelling. This definition is of the most importance because it can affect decisively on how the earthquake affect the structure and how it responds. Since is decision of the engineer to consider infills or not on the assessment, it is more complete considering that all the built concrete structures have indeed these elements which changes the stiffness of the structure, at least while these elements do not achieve the rupture. Because is not possible to extract the infills for the experimental work, and then rejoin them, this experimental work is only useful if the infills are considered on the analysis. The iterative process which follows to calibrate the experimental and numerical frequencies serves to track possible spurious proprieties of infills, which can have completely different proprieties from one country, city, or factory to another.

If the considered modelling is just of concrete framed skeleton, it is impossible to calibrate. It can be useful to use some empirical simplified equations to see if the frequencies are not too different. Of course, such simple approaches do not take into account dimensions of the building and proprieties of materials, therefore are just illustrative.

The final maximum times for convergences, after an iterative process are summarised on the table 4.4. The convergence on Costa Cabral without infills was impossible, to medium earthquakes, due to some deficiencies explained on sections ahead.

The final aspect of the modelled structures are available on the appendix section B.3.

Table 4.4: Convergence times of the analysis on modelling.

		INFILL		NO INFILL	
Return Period	Dir.	Parnaso	C. Cabral	Parnaso	C. Cabral
73 yrs	x	15.00 sec	15.00 sec	15.00 sec	15.00 sec
	y	15.00 sec	15.00 sec	15.00 sec	15.00 sec
170 yrs	x	15.00 sec	15.00 sec	15.00 sec	15.00 sec
	y	15.00 sec	15.00 sec	15.00 sec	15.00 sec
475 yrs	x	15.00 sec	15.00 sec	15.00 sec	8.22 sec
	y	15.00 sec	15.00 sec	15.00 sec	8.20 sec
975 yrs	x	15.00 sec	14.78 sec	15.00 sec	7.88 sec
	y	15.00 sec	12.78 sec	15.00 sec	- sec
2000 yrs	x	15.00 sec	14.99 sec	15.00 sec	- sec
	y	15.00 sec	6.14 sec	15.00 sec	- sec
5000 yrs	x	7.50 sec	5.86 sec	9.42 sec	- sec
	y	3.97 sec	2.80 sec	8.42 sec	- sec

Chapter 5

Earthquake Loading

5.1 Accelerograms

Artificial accelerograms implemented on the modelling were created for a medium/high risk for Europe used on ICONS programme. Even if these are not the exact expectable accelerations for buildings located in Oporto, academically it is more relevant to see the behaviour of a typical building which can be found averagely on Europe. In Portugal, one of the most concern areas is located in Lisbon where a lot of assessments have to be performed for the expected future, and actually these accelerograms are suitable due the proximity of maximum accelerations. The implemented accelerograms have a return period of 73, 170, 475 (demonstrated in figure 5.1), 975, 2000 and 5000 years. These

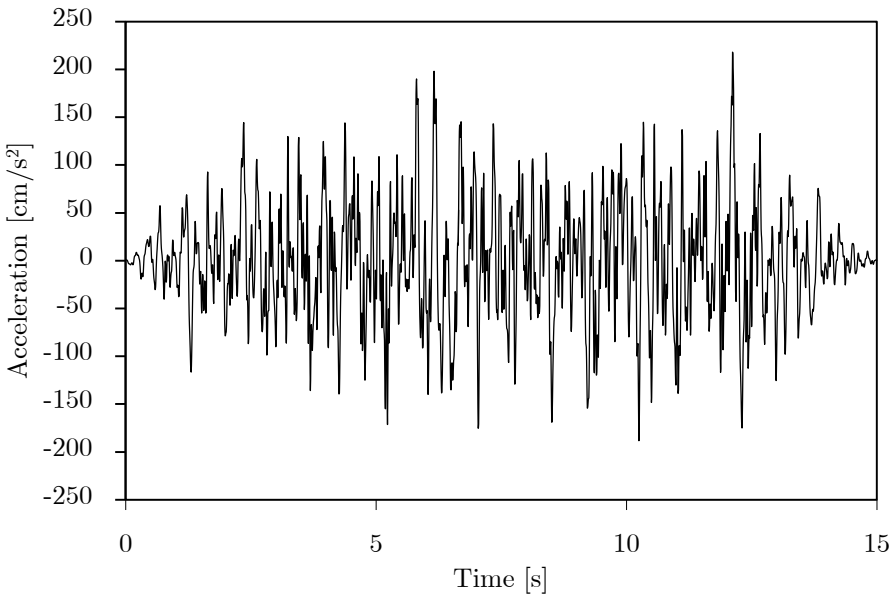

Figure 5.1: Accelerogram of the earthquake with a return period of 475 years.

data are the sets introduced on the program to perform the calculations, each in both directions on ground plane, corresponding to transversal and longitudinal directions of the buildings. The table 5.1 shows the peak ground motion of the used return periods.

Table 5.1: Peak accelerations of all the implemented earthquakes.

Return Period [years]	Peak Acceleration [m/s^2]	Peak Acceleration [g]
73	0.89	0.091
170	1.40	0.143
475	2.18	0.222
975	2.88	0.294
2000	3.73	0.380
5000	5.04	0.513

To better understand the earthquake, some calculations have been performed. The data were handled with simple classical mechanic definitions for velocity, $v_i = \sum[v_{i-1} + 0.5(a_i + a_{i-1})\Delta t]$, and for displacement, $u_i = \sum[u_{i-1} + 0.5(v_i + v_{i-1})\Delta t + 0.25(a_i + a_{i-1})\Delta t^2]$, where constants v_0 and u_0 for time equal to zero are naturally null. Figures 5.2 and 5.3 are showing the final plots, of velocity and displacement for the earthquake.

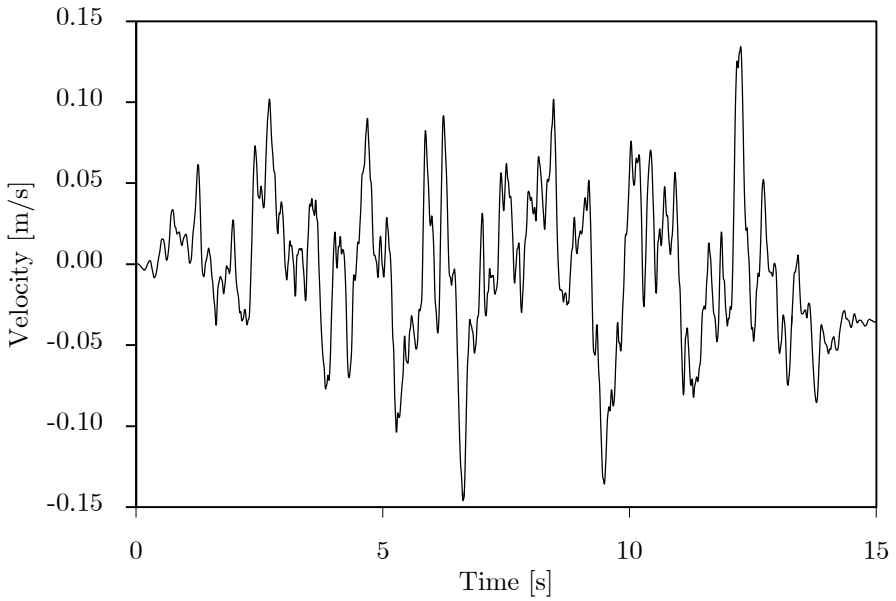

Figure 5.2: Velocity of the earthquake with a return period of 475 years.

5.2 Response Spectra

From the accelerograms is important to know, for example, the peak ground motion, but other informations, even more important needs to be worked, to compute velocities and displacements which depends on the variation and intensity of the accelerations, or their range according to the natural frequencies of the buildings. The first point was already shown, the second is dependent on the elaboration of the response spectra which is obtained from the peak historic response, changing the natural period on the equation

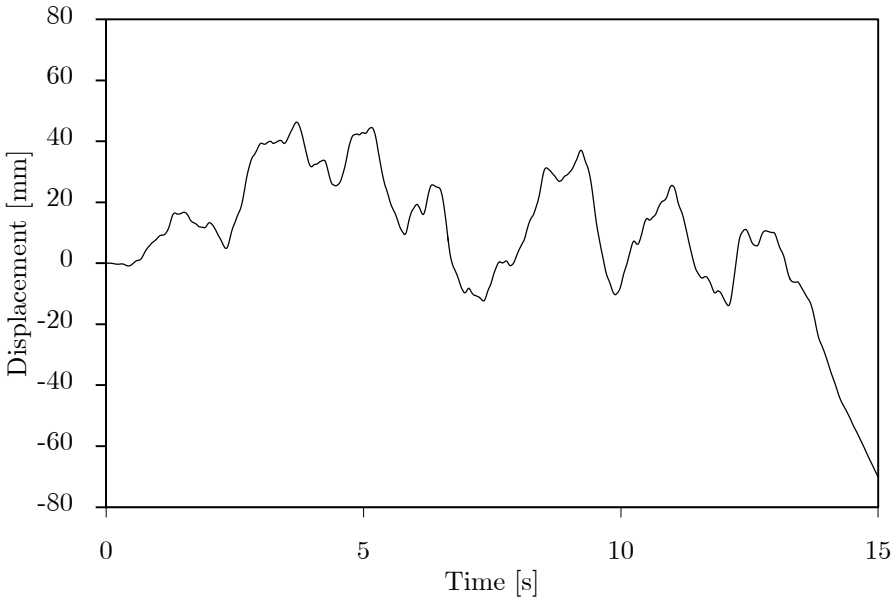

Figure 5.3: Displacement of the earthquake with a return period of 475 years.

of motion. A natural period equal to zero is obtained by the peak ground motion (PGA) on the actual accelerogram and the rest calculated through the formulation ahead.

The equation of motion for multiple degrees of freedom (MDoF) is defined as

$$[M]\ddot{\vec{u}}(t) + [C]\dot{\vec{u}}(t) + [K]\vec{u}(t) = [M]\vec{\jmath}\ddot{u}_{\mathrm{g}}(t) \; . \tag{5.1}$$

The response can be obtained by the development of the equation of motion both for the complex MDoF or SDoF through [Chopra 2006]

$$m\ddot{u}(t) + c\dot{u}(t) + ku(t) = -m\ddot{u}_{\mathrm{g}}(t) \;\Rightarrow\; \ddot{u}(t) + 2\zeta w_{\mathrm{n}}\dot{u}(t) + w_{\mathrm{n}}^2 u(t) = -\ddot{u}_{\mathrm{g}}(t) \; . \tag{5.2}$$

To convert the accelerogram, analysing its excitation on a response spectra, an easier formulation should be used, calculated for a single degree of freedom system (SDoF), as a cantilever with a unit mass on top and variable stiffness to plot different frequencies for the response. It is performed solving Duhamel's integral (*vd.* Eqn. 5.3),

$$u(t) = -\frac{1}{w_{\mathrm{D}}} \int_0^t \ddot{u}_{\mathrm{g}}(\tau) e^{-\zeta w_{\mathrm{n}}(t-\tau)} \sin\left[w_{\mathrm{D}}(t-\tau)\right] d\tau \; , \tag{5.3}$$

valid for a SDoF. The results are dependent on the damping ratio (ζ), usually considered as 5% for R.C. buildings and on the selected ground motion. For each chosen period, that changes the natural period of vibration (w_{D}), a plot of the response for all the different values is done. From those plots, only the peak values are selected to plot the response spectra of (maximum) accelerations for the chosen natural period range. Despite not being the exact information needed to analyse the structure, due to simplifications, this formulation is presented to be easier to read and analyse the results, knowing better the possible effects on the structure [Chopra 2006].

The figures 5.4 to 5.6 show the results of maximum displacements (by solved equation 5.3) for different structure period, pseudo-velocity (equal to $v = w_{\mathrm{n}}.u$) and pseudo-acceleration (equal to $v = w_{\mathrm{n}}^2.u$).

In order to compare the different accelerograms (medium/high risk for Europe) with the demand provided by the Eurocode 8, two spectrums for Lisbon were computed and then plotted together (*vd.* figure 5.4 and 5.6). According to the EC8, the two different

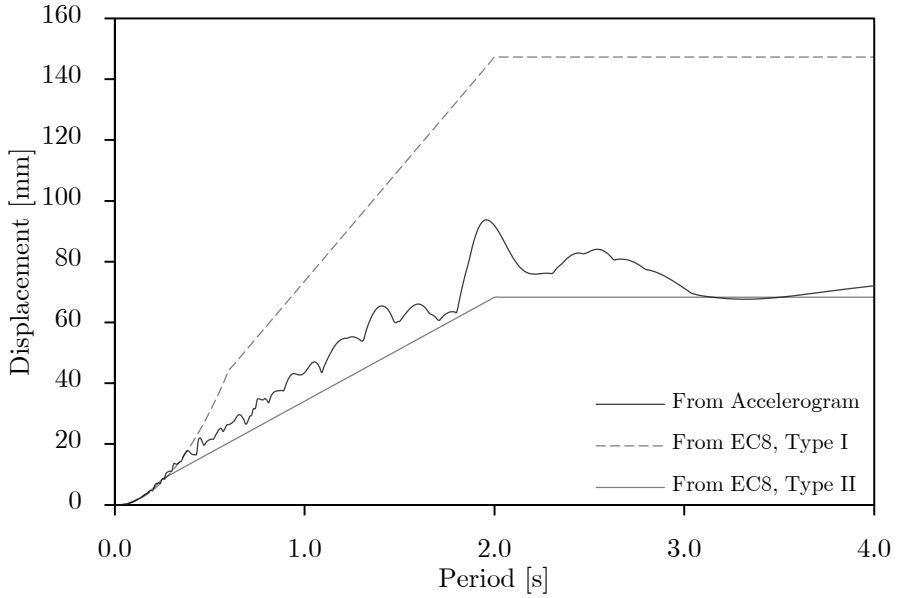

Figure 5.4: Displacement of SDoF response spectra.

types of spectrums have their distinction on the localization of the epicentre, for type I, a far earthquake taking place on the Atlantic Region, and another, type II, a close earthquake, happening in the continental territory. A close earthquake has a much more higher vertical demand than one with epicentre far away, and higher horizontal accelerations from higher frequencies which can inflict higher level of forces due to the matching with stiffer structures. The type I earthquakes can excite lower stiff modes of vibration with higher accelerations, which can increase the displacement demand of the building.

Respecting the procedure of the EC8-1, the two design spectrums were calculated for Lisbon, assuming a soil of type B to the adoption of some parameters, directly from the national annex of Portugal, for a return period of 475 years and viscous damping of 5%.

The overlaid graphs (figures 5.4 and 5.6) show the accordance between the accelerogram of ICONS and the type II spectrum for Lisbon. Observing them, it is possible to conclude that the spectrum is almost like a inferior envelope of the pseudo-accelerogram. The accelerograms can be used as a good match for the assessment of the buildings, and from the previous conclusions it is expectable a "less displacements" and "higher acceleration" type of demand on the structures.

The accelerations of the earthquake (with return period of 475 years) shows a range between up to 2 m/s^2 for accelerations, 0.15 m/s for velocities and up to 60 mm on displacements. Regarding these values, as already referred, just a few information is

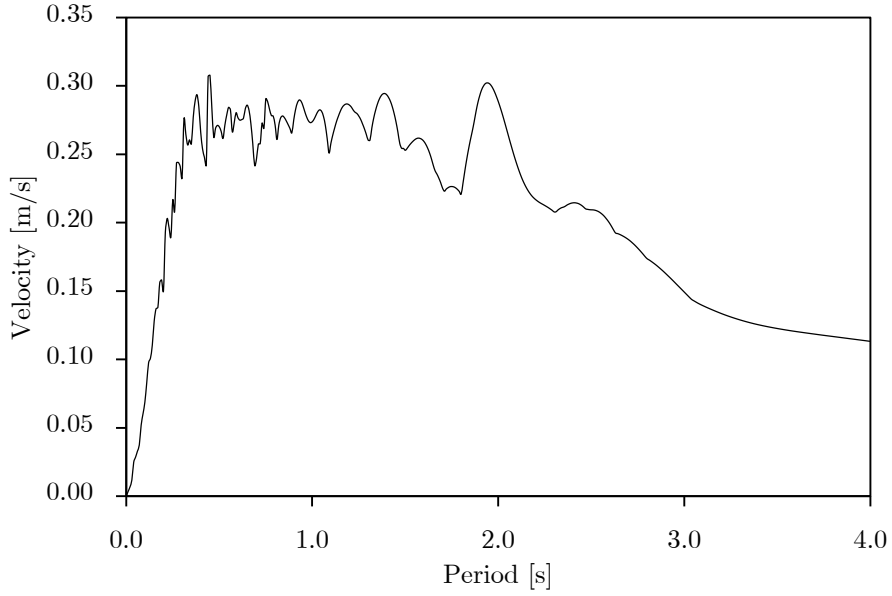

Figure 5.5: Pseudo-velocity of SDoF response spectra.

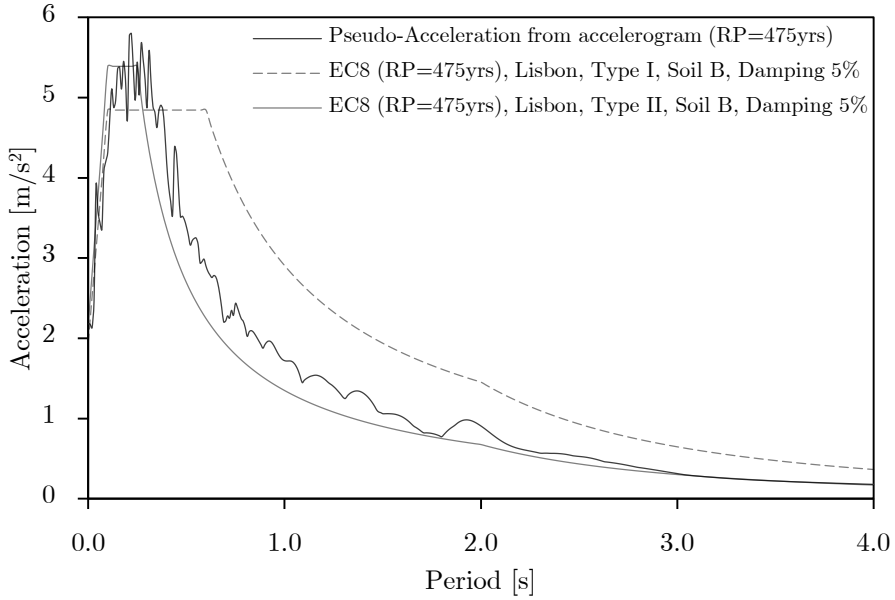

Figure 5.6: Pseudo-acceleration of SDoF response spectra.

given in terms of response of structures. Looking to the response spectra, and assuming that a normal concrete structure would not have a period higher than 1 second, then the real maximum accelerations which are expected on the structure are between 2 and 6 m/s^2. Thus, the accelerations can be intensified 300% on the top of the building. Accelerations can go up to 0.30 m/s, twice as much, and displacements up to 30/40 mm. These values serves only as a reference because the analysed results are very simplified compared to the real modelling, so they serve as a big picture of what is expectable.

Part III

Discussion

Chapter 6

Seismic Assessment

6.1 Safety Guides

The assessment of buildings for the seismic behaviour finds vast lines of orientation from which is possible to be guided. An important matter is to know how to separate and understand the differences between the uncertainties of construction and design in different countries, which has direct implications on the respective guides. To filtrate some line guides it is necessary to know accurately for which kind of structure are referred to new or old, with smooth or deformed bars, the type and strength of the expectable ground excitation, or even the techniques of construction on the specific country from where the guides are created. One important issue related to these topic is the economical impracticability (or maybe the impossibility) of making the assessment to respond to an earthquake with the same level of safety as a new building. The subjectivity of the level of safety to which the assessment is performed turns into a complicated exercise to the designer, owner of the building or even the safety authorities. All recent technical seismic regulations/guides, such as ATC-40, Vision-2000, FEMA-356, Italian Code or Eurocode 8 are pointing different levels of safety level regarding the expectable occurrence of an earthquake. The four different levels of damage limitation which regulates the first step for the assessment has no specific discussing on the quantitative limitations itself, but to associate a performance to an expected damage. This group can be referred as:

- Operational performance - no structural or non-structural damage is experienced;
- Immediate occupancy performance - non-structural elements problems and light structural damages;
- Life-Safety performance - guarantee of life-safety with high damage, which may lead to not economic reparability;
- Near-collapse performance - structure stable with capacity of carrying the remaining vertical loads but structurally unsafe, obligating its posterior demolition.

Vision-2000 committee present an interesting matrix of performance objectives (see figure 6.1), guiding to an adjustable level of intervention needed, in order to achieve the needs according to the typology of the building for which the assessment is made. Permanent structures, like residential buildings as the ones assessed on this dissertation, usually have a basic objective level, which should be attained, at least for new structures.

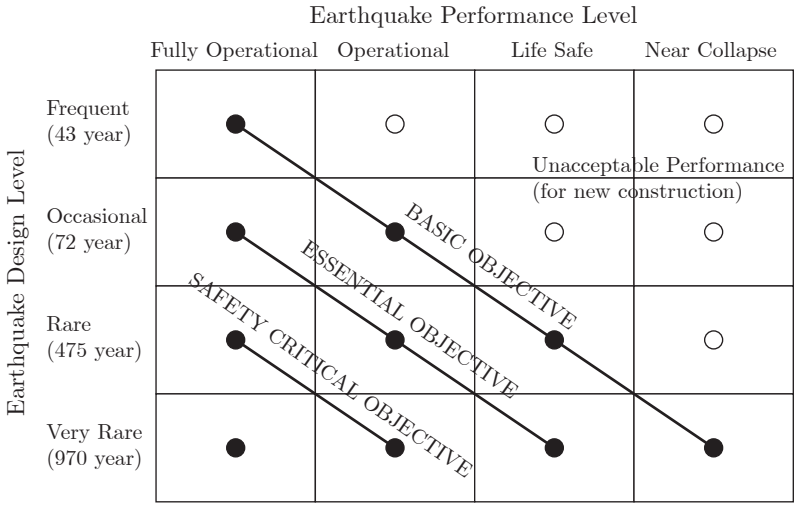

Figure 6.1: Seismic performance/design objective matrix (adapted from [SEAOC 2005]).

The committee points to the verification of the latter groups referred to specific return periods of the earthquakes. The basic level is pointed as fully operational for a return period of 43 years, operational for 72 years, life-safety for 475 years and near-collapse for 970/2000 years. An important structure, like a nuclear plant, because its failure is very dangerous to human safety, must have a higher level, to the point of performing fully-operational even for a very rare earthquake with a return period of 970, 2000 years or more.

Regarding the existing buildings the design level can be different, and they are not rigorously specified. The committee points that it is unacceptable not to design a new structure for at least a near-collapse performance for an earthquake with a return period of 475 years, so it is acceptable a different level for an existing building to which the rehabilitation is performed. As economy has a key role on the assessment, the Italian Code will adopt an important measure by reducing the nominal life period for existing structures, which reduces the return period of the earthquake for the design procedure. The direct impact on this reduction for existing structures, the performance level gets to 60% compared to a new one. (Exampling differently, for a new habitation building, the structure is design for at least 50 years, and a retrofitted can be designed for at least 30 years, which reduces the near-collapse level from 975 to 682 years of return period.) The Eurocode 8 points some informative levels in terms of return period, which are not regulative, but informative to locate basic performance and adjustable economical levels for the assessment of new buildings but is still lacking on informing a more adjustable limits for existing/old ones.

In this work, and because the intensity level of earthquakes for Portugal is not highly demanding, a return period of 975 years for design level for a ultimate state of near-collapse performance level is performed and reviewed on the next sections.

6.2 Main Deficiencies

To understand the kind of challenges that can be found in the analysis results, in Varum's PhD Thesis is presented an extremely insightful description of which are the main deficiencies of non-ductile R.C. Buildings [Varum 2003].

- Stirrups/hoops, confinement and ductility;
- Bond, anchorage, lap-splices and bond splitting;
- Inadequate shear capacity and failure;
- Inadequate flexural capacity and failure;
- Inadequate shear strength of the joints;
- Influence of the infill masonry on the seismic behaviour of frames;
- Vertical and horizontal irregularities;
- Higher modes effect;
- Strong-beam weak-column mechanism;
- Structural deficiencies due to architectural requirements.

This is a recommendable reference for further readings and better understanding of the topics, when performing seismic assessments. In a general way, the study encounters all these items, in different rates of intensity.

6.3 Assessment and Interventions

The assessment of existing structures should be performed to evaluate if the structure still has capacity to sustain the demands, the seismic excitation or the static loads because of an accident, change of typology or degradation of material, without strengthening interventions improving the capacity or changing the use of the building. The seismic interventions can be performed to respond to the safety levels on the codes, provided by a full rehabilitation; or to introduce improvements of the safety level, to provide better response, even if it does not achieve the regulative levels, increasing the global capacity by solving some deficiencies; or finally, to repair or strengthen some local members which solves just a few and immediate issues.

The possible interventions can introduce global or local improvements, like:

- Repairing damaged elements, strengthening weak structural or non-structural elements or even the completely change of some elements as a last resort
- Addition of other elements, like bracings, infill walls, concrete walls.
- Modification of the structure, erasing or limiting irregularities, vulnerable elements or introducing joints on some elements, like the system of stairs.
- Addiction of new structural systems to deal with higher amount of seismic actions or modification of non-structural system to structural to improve seismic response.

- Introduction of passive devices, like base isolation or other dissipative mechanisms.
- If possible, mass reduction or demolition can also be a good resort to improve the structures.

The seismic design philosophy of the new codes is based on a hierarchy principle in which the existing structures should also follow, if possible, while the intervention is prepared and thought. The strength hierarchy is based on that the ductile mechanisms should always be in advance regarding the fragile mechanisms. This is applicable in terms of various levels. One is the material hierarchy like reinforced concrete elements, where the steel is much more ductile than the concrete. The sections and reinforcement, for new elements, should be designed with low longitudinal reinforcement ratio so the failure occurs as a result of the crushing of the concrete but with steel using its non-linear capacity. The failures in terms of stresses should be designed to the point where the brittle failures, like shear, is obtained after the ductile ones, like flexure, with a factor which majors the difference between the two strengths. A good ductile behaviour of a structure, before it collapses, should also form plastic hinges on all the beams before the forming a global mechanism collapse instead of a local mechanism like a soft-storey.

Chapter 7

Response and Safety Assessment at the Global Level

The global analysis of a building serves the purpose of understanding how the structure behaves. Knowing more generalized information about it, it is possible to expose some deficiencies of the building, like tendency for the formation of soft-storey, torsion effects, evaluation of weaknesses by floor or by direction, distribution of loads and deformations, and as the ultimate verification, the formation of mechanisms. The mechanism can be obtained, for example, by the formation of plastic hinges in all of the columns of a specific floor or, the collapse of columns which brings high amount of stress to the near elements, creating a domino effect.

7.1 Modes of Vibration

The analysis of modal results is an important step to understand the global behaviour of the building, to check if it has a harmful tendency for developing unwanted patterns, like torsion. From that analysis is possible to understand the global stiffness of the building and to predict what may be the response to the earthquakes.

As explained on the sections 4.5.2 and 4.11, both structures were calibrated with their natural frequencies, according to the experimental work. The experimental work has been taken on its natural state of the buildings, in other words, with its infill walls. Therefore, the calibration had to achieve those values considering the growth of stiffness provided by the integration of walls on the frames.

The calibration had taken as an assumption the reduction of stiffness on some panels, from the reduction of material and non-homogeneous behaviour. The main façades of both buildings are designed with openings for windows and balcony doors, which naturally reduces the stiffness of the panels. For the respective panels, a reduction of 50% on the compressive strength is adopted as a simplified ratio. Actually, this same adopted ratio has shown to be accurate on the calibration for both buildings. As pointed before, the reduction of the compressive strength has effects on the elastic modulus and on the vertical separation between struts (which as a beneficial effect of increasing the percentage separation of struts, distributing more the amount of unloading on the columns). On the rest of the infills, as for the panels without openings on the transversal or longitudinal façades and on the interior walls, the proprieties obtained from the results of the

empirical proposed formulas were maintained.

7.1.1 Calibration of the Infill Panels

The tables 7.1 and 7.2 are describing the results of the modelling for the building Costa Cabral and Parnaso, respectively. According to the previous assumptions, the percentage of stiffness reduction was defined to approximate the calibration, mainly concerning the first two natural modes of vibration. With the same assumptions, both results showed a discrepancy of less than 4.5% in average, which was considered to be acceptable for the possibility of error from the experimental results and difficulties in perfectly model the buildings. Since usually, these are the important frequencies for the type of excitation demand and its response, is expected to get accurate results from the program.

Table 7.1: Costa Cabral numerical & experimental difference.

	Experimental		Error
Mode 1	2.178	Hz	-3.0%
Mode 2	2.343	Hz	3.3%
Mode 3	2.999	Hz	1.0%
Mode 4	4.000	Hz	31.1%
Mode 5	4.469	Hz	28.5%
Mode 6	6.002	Hz	14.3%

Table 7.2: Parnaso numerical & experimental difference.

	Experimental		Error
Mode 1	2.914	Hz	1.5%
Mode 2	3.863	Hz	-4.4%
Mode 3	4.365	Hz	8.2%
Mode 4	6.000	Hz	4.5%

The calibration is possible to be performed with the accounting of the infill panels. For the framed structure, there are some empirical formulas to get a general idea of the expected period of the buildings. A very simple one (proposed by Aničić) is the division of the number of storeys per ten ($T = nr.storey/10$). The number of storeys is 9 for Costa Cabral and 6 for Parnaso, which tells that the period may be near 0.90 and 0.60 seconds respectively. It means a difference of 50% and 5% compared to the first and second modes of Costa Cabral and 25% compared to the first mode of Parnaso. From the Eurocode 8, $0.075H^{3/4}$, Costa Cabral has a difference of 130% and 6% when compared to the first and second periods, and 22% for the first mode of Parnaso. This shows that no accordance to the predictions has been achieved. One substantial dependent which affects the natural frequencies is the mass of the building. It is on the slabs where a big amount of the permanent weight is accumulated in. On this matter, the dimensions of the building have a direct influence because the mass is increasing linearly with the loads. From other side, as the mass increases, so the number of structural elements, which can balance the determination of the stiffness to compute the natural frequency. One possible

big discrepancy can be found on the slender columns due to the non-provision designs to sustain lateral loads. Therefore, it may be recommendable to consider an increase of flexibility of the structure when compared to old existing structures of concrete.

Some simplified, and potential useful formulations are the two pointed before and also 0.05 N from Navarro or 0.105 N from Kobayashi. The formulations have different range of 0.1 to 0.5 seconds of period, concluding that are gaps on the accordance between the different calibrations. [Draganić *et al.* 2010]

As a summarize, is recommendable to look at the figure 7.1 to have an idea of the progression and differences of the various exposed models.

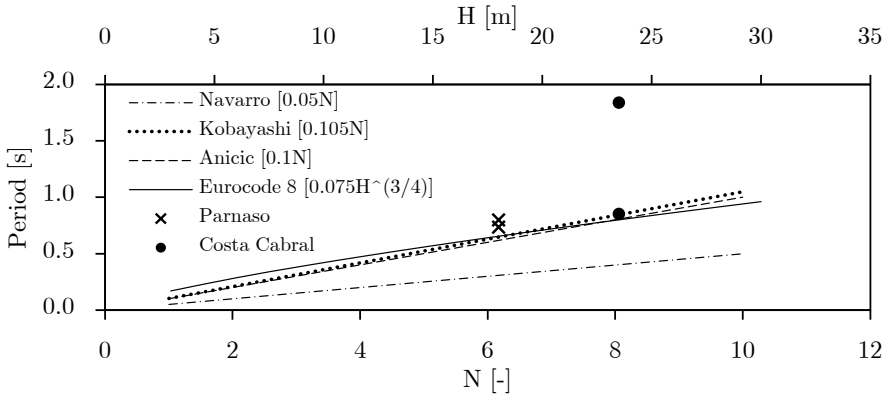

Figure 7.1: Different calibrations for concrete framed structures with the first two modes of both analysed buildings.

7.1.2 Natural Frequencies and Modal Shapes

The buildings have an expected behaviour of the two first modal shape of vibration (vd. figure 7.2). By just an exception for the Parnaso building, which has a concrete wall on the exterior stairs box, generally the buildings have an uniform architecture with equally distributed assigned loads. On some floors, because of the greater amount of beams and higher dimensions, thickness of the slab and height of the columns, the building is influenced by small variations of the modal shapes. The shapes of the two first modes have a similar deformation progression along the different storeys, in both directions, with predominance of translations instead of rotations. Costa Cabral building, on the transversal direction (U_y) has a stiffer behaviour than the longitudinal, provided by the orientation of some of its columns, which have the higher width in that direction. At a first sight could be predictable to believe that the building would have its first mode with translational for transverse deformations, due to a less frame span and quantity of columns on its opposite direction. The inertia of the columns is powered to three, therefore, the average double dimension of the sections on the transverse direction is enough to compensate the dimension span. Without infills, the mass participation percentages varies between 60% and 80%, for U_x and U_y, and 10% to 15% of rotational participation of R_y and R_x, respectively. The third mode has a concerned behaviour that develops a torsion mode shape which is very near to the second mode, 0.01 Hz of difference which can lead to response deficits. With the incorporation of the infills on the

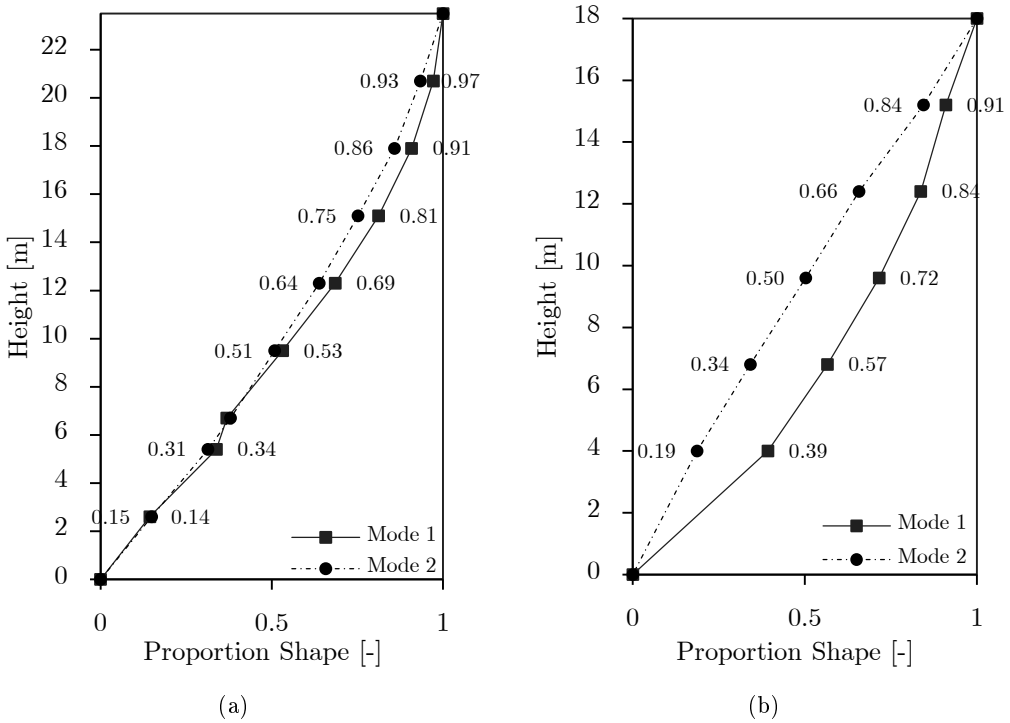

Figure 7.2: Modal shapes of (a) Costa Cabral and (b) Parnaso.

building, it is verified a change of more than twice of the frequencies for the first mode. The biggest increase is verified on the longitudinal directions due to a bigger amount of infills, increasing the effective participation from 60% to 80%. The second and third modes, with the participations of infills, are separated by 0.61 Hz. These greater natural frequencies, relating them to the results of a single degree of freedom response spectra, on figure 5.6, are located on the peak acceleration, which can lead to a tougher demand on the structure. The results are summarized on the table 7.3.

The natural frequencies of Parnaso considering the framed structure shows some interesting behaviour due to the concrete wall. The columns cross-sections have a generalized square shape, so it is not expected a bigger stiffness on some of the directions, as it happens with Costa Cabral. What prevails on the translational shapes are the actual locations of the columns which is much stronger for the longitudinal direction. Therefore, even with the increase of stiffness of the wall on the transversal direction, the structure finds the first mode on that direction with effective participation of 76%. Along with this participation, the first mode, as it translates on U_y sees the participation of the wall, a stiff element further from the centre of mass of the building, creates torsion effects, with participation of 7%. The slender architecture of the building on the transversal direction, where just two frame sets are contributing for the rotation capacity so, is verified 13% of rotational mass participation (R_x). The second mode has mainly a translation participation of 90% on the longitudinal direction and the third, torsion shape, with 70% of mass participation of the rotation on vertical axis. With the incorporation of the infills on the model, the model has as increase of 2.5 times of the frequencies, increasing them to va-

Table 7.3: Costa Cabral frequencies comparison, with and without infills.

	Frequency [Hz]		Change		Participation				
	Infills	No Inf.	Hz	%	Infills		No Inf.		
Mode 1	2.11	0.54	1.57	389%	82.79%	[Ux]	61.18%	[Ux]	21.61%
Mode 2	2.42	1.17	1.25	207%	82.93%	[Uy]	77.19%	[Uy]	5.74%
Mode 3	3.03	1.18	1.85	256%	85.77%	[Rz]	74.62%	[Rz]	11.15%
Mode 4	5.81	1.60	4.21	364%	20.47%	[Ry]	14.95%	[Ux]	Switch
Mode 5	6.25	2.48	3.77	252%	52.82%	[Rx]	12.91%	[Ux]	Switch
Mode 6	7.00	2.75	4.25	255%	1.15%	[Ry]	27.41%	[Rx]	Switch
Mode 7	7.01	2.78	4.23	252%	4.43%	[Uz]	14.46%	[Rz]	Switch
Mode 8	7.09	3.30	3.79	215%	1.51%	[Uz]	5.64%	[Ux]	Switch
Mode 9	7.48	4.39	3.10	171%	1.83%	[Uz]	1.28%	[Ux]	Switch
Mode 10	7.75	4.55	3.19	170%	4.63%	[Ry]	2.66%	[Rz]	Switch

lues between 3 and 3.7 Hz for the first two modes. Once again, these changes, according to the figure 5.6, can mean a transition of these modes to higher levels of acceleration demands. It is interesting to verify that the integration of infills, creates a flip on the modes: the first with infills has a mass participation of 91% of longitudinal translations and the second mode has 70% of translation on the transversal direction. Due to the architecture, the translations on this direction takes a key roll, so it continues to be verified a torsion effect due to the wall, mass participation of 11% of rotational on vertical axis, and 17% of rotation on the longitudinal axis. The third mode has its correspondent frequency increased, due to the global increase of stiffness but no big change of rotation mass participation is verified. Despite this, the translation on transverse has a bigger participation, increased from 4% to 12%. The flip on the mode shapes shows one of the great importance in taking into account the integration of the infills on the modelling of structures. Because the structure has more amount of walls infilled on frames on the transverse direction, together with the wall, is sufficient to change the expected way that the building responds to an seismic excitation, and which direction may appear more deformations or stresses. The results are summarized on the table 7.4.

Table 7.4: Parnaso frequencies comparison, with and without infills.

	Frequency [Hz]		Change		Participation				
	Infills	No Inf.	Hz	%	Infills		No Inf.		
Mode 1	2.96	1.25	1.71	236%	91.88%	[Ux]	76.52%	[Uy]	Switch
Mode 2	3.70	1.36	2.34	272%	68.31%	[Uy]	88.40%	[Ux]	Switch
Mode 3	4.76	1.73	3.03	275%	70.59%	[Rz]	70.26%	[Rz]	0.34%
Mode 4	6.28	3.50	2.78	180%	0.11%	[Uz]	36.98%	[Rx]	Switch
Mode 5	7.14	3.98	3.16	179%	0.01%	[Ry]	20.44%	[Ry]	-20.43%
Mode 6	7.33	5.96	1.36	123%	0.04%	[Uz]	4.38%	[Rx]	Switch
Mode 7	7.80	6.21	1.58	125%	0.03%	[Ry]	0.09%	[Uz]	Switch
Mode 8	8.32	6.53	1.79	127%	30.19%	[Ry]	0.04%	[Uz]	Switch
Mode 9	8.66	6.60	2.06	131%	0.21%	[Ry]	1.67%	[Ux]	Switch
Mode 10	9.01	7.06	1.95	128%	0.15%	[Ry]	11.30%	[Rz]	Switch

7.2 Acceleration of the Structure

The natural periods of Parnaso for the first two modes 0.34/0.27 and 0.80/0.74 seconds, for infilled and framed structure, compared to the response spectra on the figue 5.6, the expected accelerations are in a range of 4.6–5.5 and 2.0–2.5 m/s^2, respectively for infilled and framed structure. The figure 7.3 is showing the variations of accelerations by floor for an earthquake with a return period of 475 years. Comparing it to the response spectra, made for a SDoF, is concluded that a good match is achieved. Thus, a proximate value of acceleration for the real MDoF structure can be expeditiously calculated for simplified assessments. Of course, if the building is behaving with a lot of torsion effects, or have big differences of stiffness along the height, the accelerations can be strongly modified, not accounted on this simplification. The figure shows it in a small way, regarding global rotation, where for the transversal direction the difference is slightly bigger.

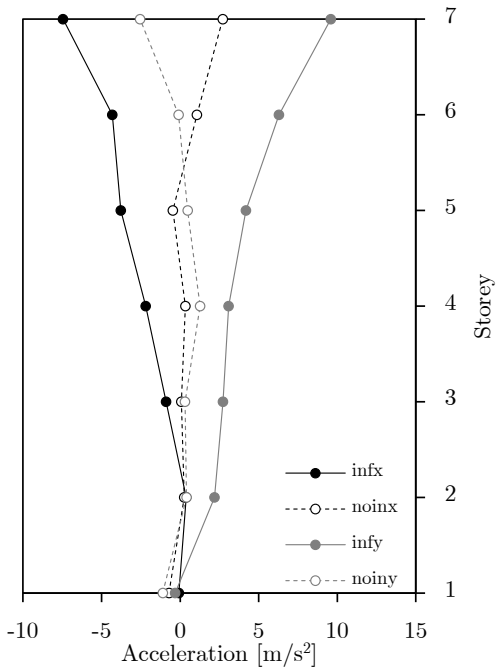

Figure 7.3: Accelerations of Parnaso on a central column.

7.3 Displacement Profiles and Drifts

7.3.1 Costa Cabral

From the modal analysis, the building presents an expected and linear behaviour which is confirmed through the first earthquake, where the building behaves almost perfectly linear. It shows a reduction of displacement along its height. On the first three storeys the displacement progression changes. On the second storey, without partial soil support that exists on the first floor and with a higher height of the columns, is verified more intense drifts right from the weakest excitations. The higher drifts appear mostly on these bottom

storeys for all earthquakes. For excitations on the transversal direction deformations are more intense on the second storey, clearly evident for intense earthquakes up to 975 years of return period, and for longitudinal excitations the drifts are almost equally intense on the first two storeys, visualized on figures 7.4.

These displacements show the importance in assuming the effects of the soil on the structure. The infills have a protective effect in terms of displacements until the cracking starts to happen. On the longitudinal direction, the crush of the infill panels starts to be evident for a 2000 year earthquake, and is continually providing support on the transversal direction even for a strong earthquake. Because the soft-storey is only happening for a high return period, it is possible to conclude that the panels may have a good contribution by giving confinement to the frames.

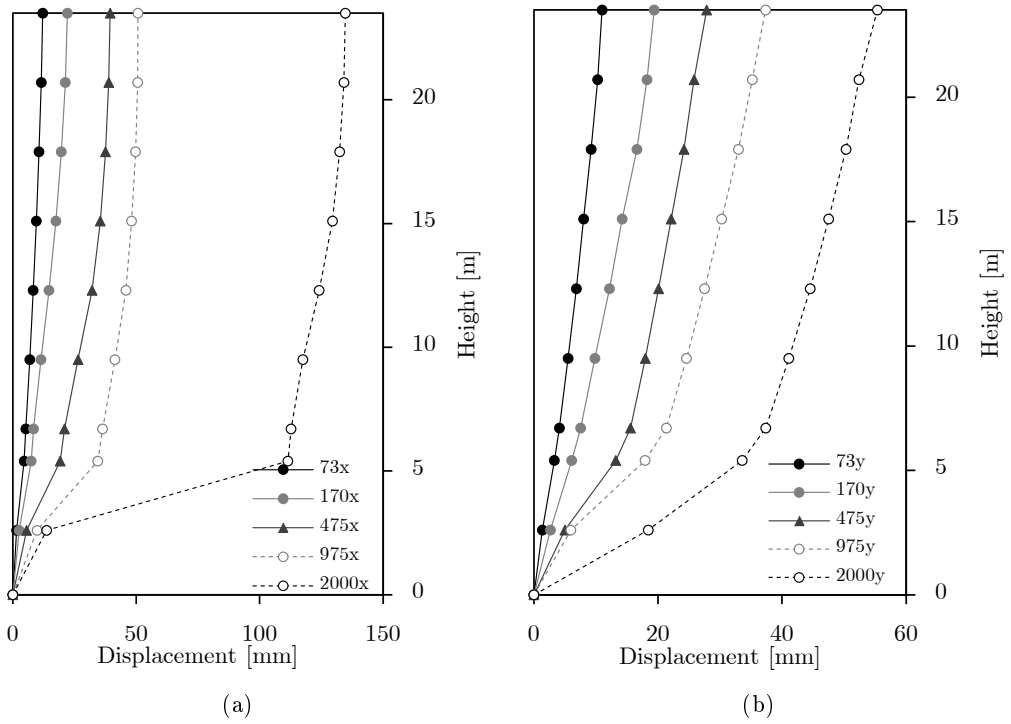

Figure 7.4: Lateral displacement profile for maximum top displacement of Costa Cabral with infill panels for (a) longitudinal earthquake and (b) transversal earthquake.

In the case of analysing the structure without its panels (figures 7.5), the shape of the deformation is completely different. Starting with the excitation of 73 years, the top displacements do not change much but the shape of it does. This shows that just by looking to the top displacements can be misleading. Right from the elastic behaviour, where the building with infills had showed an evenly deformation, which means a distributed contribution of the structural elements, this shows a very flexible/weak set of columns on the last storeys. Intensifying the demand, the structure continues to confirm the tendency, where the top displacements, which are accumulated on the last storeys, have already similar values for a 170 years demand without infills compared to the distributed deformation on the earthquake 975 years with infills. For the earthquake

with RP of 475 years, in both directions, the thin columns, which are designed to sustain vertical loads, do not have capacity to sustain higher accelerations. The formation of plastic hinges on the columns, if they are distributed on all the storey means a formation mechanism, where floor is "swallowed" by the upper ones. This, actually, is expectable to happen from the analysis on both directions, meaning that the structure does not perform at the wanted level.

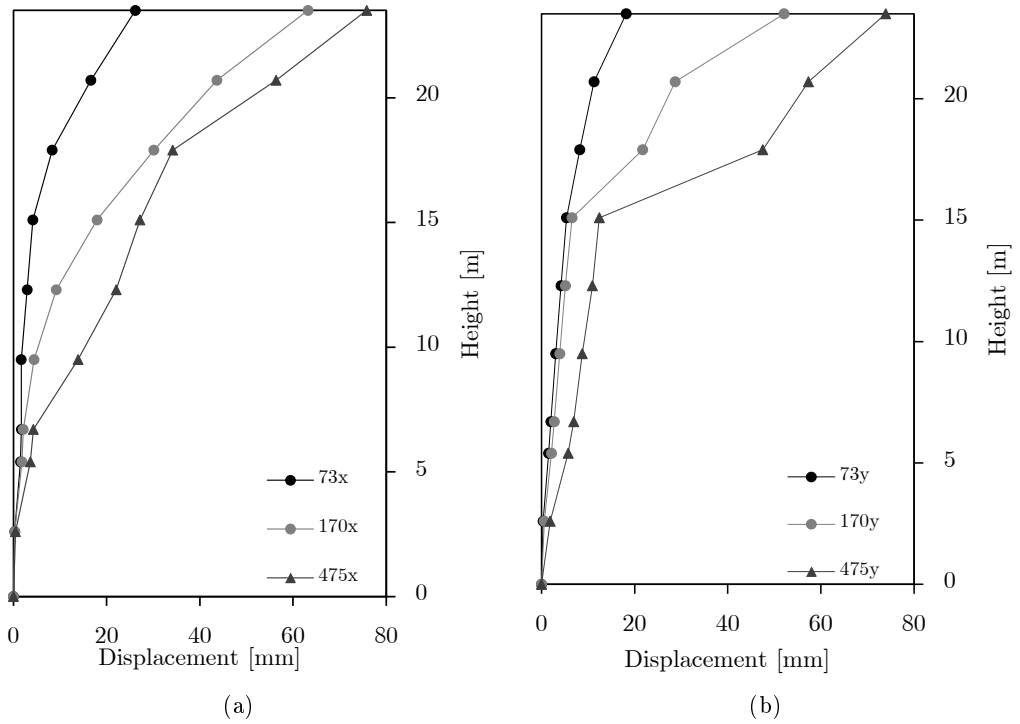

Figure 7.5: Lateral displacement profile for maximum top displacement of Costa Cabral without infill panels for (a) longitudinal earthquake and (b) transversal earthquake.

Figures C.1 to C.8 presents the deformations and drift progressions for the building with and without infill panels, for an earthquake with a return period of 475 years. The legends are referring to the columns used to plot the graphs. The point "13" and "94*" are the two central columns on the two shorter façades which limits the length (perpendicular to longitudinal direction), "53" and "65" are the two central columns on the two long façades which limits the width (perpendicular to transversal direction), and finally "53" is a central column on the interior of the building. (The numbers were given by the references on the modelling.) The plots are made for the instant in which the maximum top displacement deformation is attained.

The graphs, once again, show the tendency of forming the soft-storeys on the first and second storeys for the structure without infills and a slightly rotation effect by the transverse excitation (confirmed ahead on the figure 7.7). On the perpendicular directions, regarding the excitation, a negligible rotation is seen, with drifts of a range of 0.01%, and top (perpendicular) displacement of 2 mm. For the framed structure, no rotation is happening on the principal direction where the higher drifts are concentrated

on the upper levels, the reverse seen before. The drifts reach 1%, which may not seem much if the actual capacity of the columns is ignored. In other words, drifts up to 1.5% or 2% can be reasonable, but the columns must have the ductility to support it in safety. On the perpendicular directions, the torsion effects takes place for the step were the structure is already unstable. The only purpose of figure C.8 is to show the instability of the numerical convergence at some step, because no valuable information is given by that shape. The figure C.8 is showing the instant where the mechanism of collapses is starting, where the upper floors starts to rotate, anticipating their total collapse.

This result shows the importance on these global analyses meaning that, before going to local verification, is important to know how it responds globally. A good and complete global assessment can be very useful on helping and limiting the deepening which anticipates a local analysis, since is possible to limit the demands right from its origin.

The drifts (see figure 7.6) are less than the recommended ones on FEMA-356 [FEMA356 2000] and VISION2000 [SEAOC 2005], where it does not overtake 1% for the near-collapse performance level, in any of the floors. It is important to mention that for the structure without infills, the 475 return period earthquake result, which is represented on the peak ground acceleration of 0.22 g, would be much higher if the analysis would not encounter convergence difficulties. No more results are presented because the other earthquakes encounters the same deficiency, so no further information is given by showing plots.

One concern with this building, due to the proximate mode shapes, second and third, for the framed structure without infills, would be a formation of torsion effects. It is not confirmed on the rotation envelope results on figure 7.6, where the maximum rotation does not overtake the 0.003°, which is virtually nothing. The 475 year earthquake seems have a higher, but still small, influence on the rotation effects, but may be linked to some numerical "noise" during the iterative process of convergence. The inter-storey rotations between storeys are very small but the slight higher ones are located on the second (higher height), fifth and sixth storeys. The smaller rotations are located on the third storey, where the columns are much shorter compared to the other floors.

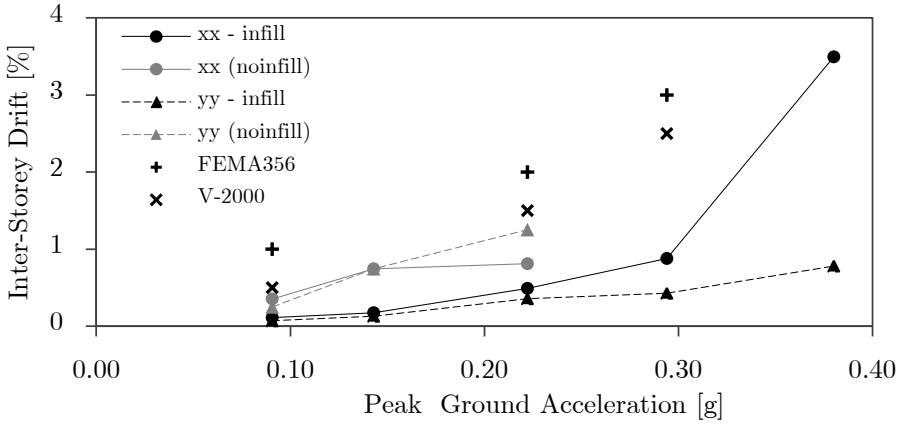

Figure 7.6: Higher drifts for central columns and different intensities of earthquake for Costa Cabral.

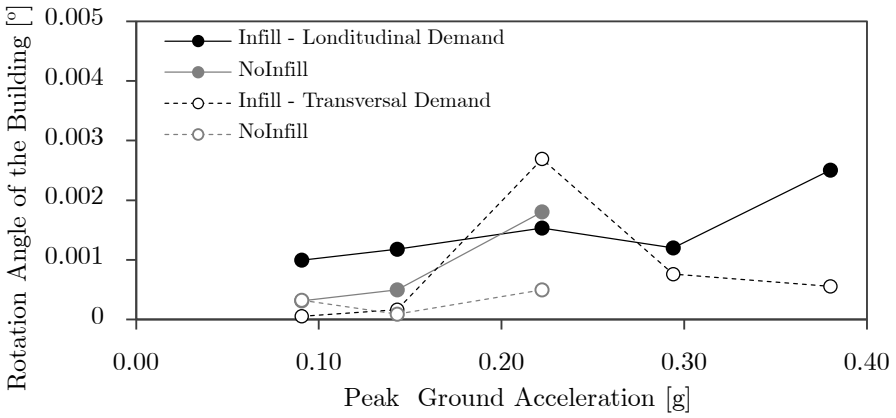

Figure 7.7: Maximum inter-storey rotation with and without infill panels for each earthquakes for Costa Cabral.

7.3.2 Parnaso

Some of the deformations and drift progressions for the building, with and without infill panels, can be checked on the figures C.12 to C.19, for an earthquake with a return period of 475 years. The legends are referring to the columns used to plot the graphs. The point "12" and "92" are the two central columns on the two shorter façades which limits the length (perpendicular to longitudinal direction), "51" and "53" are the two central columns on the two long façades which limits the width (perpendicular to transversal direction), "52" is a central column on the interior of the building, and "wall" is the concrete wall element of the stairs block. The plots are also made for the instant with higher top displacement.

The displacement profiles shows that the building, with the infill panels integrated, presents regular translations in its height for both demand directions, until an earthquake with a return period of 475 years, showing that the building has a similar stiffness on all storeys, or, in other words, until degradation of the infills, the building is highly controlled by them. (See figures C.12 to C.15 and 7.8, for a visual understanding of the topics.)

As expected from the separation of the centre of inertia and centre of mass on the transversal direction, rotational effects are evident for a transverse earthquake. This is true and is confirmed further ahead on the analysis of framed structure. The key point is on the slender shape of the building and its infill panels. As was already said before, the panels on the transverse façades are more stiff than the other panels, and are fully filling the frames of the façade which is far from the wall, and not fully present on the other façade because of the stairs block. Actually, those are the most stiff elements of the structure on the transversal direction, therefore, as a consequence, the deformations are controlled by that system, showing the great influence of the infills, which increases even more stiffness of the structure than the wall linked through beams. The figure C.14 is showing this conclusion. For the higher top displacement, the shape shows a rotation because the lines are not over-lined (do not have the same deformation), and the column "12" is actually static, confirming the high stiffness of those infills, and that the defor-

mations are dominated by the rotations. This may lead to an expectable higher demand on the columns near the wall until the limit of resistance of the infill walls.

On the perpendicular directions relatively to the earthquakes, the transversal deformation on a longitudinal earthquake is negligible, with a top displacement of 1 mm in 18 meters, but 5 times higher on the response dominated by the infills, where the differential between the far transversal top points gets to 10 mm, even though with small drifts.

Overlaying the displacements for each level of excitations, it is possible to compare the evolution and a formation of soft-storey on the ground storey for a longitudinal earthquake, described on figure 7.8. It begins to show the tendency on the earthquake with a return period of 475 years. It has a clear formation of a mechanism for return period of 5000 years, and for that reason, is not presented on this work. The soft-storey for 2000 years, is still stable, at least in a global aspect. The tendency on the first storey is due to a higher height, which has a direct impact on the lateral resistance, and also because has less infills on the longitudinal direction compared to the rest of the storeys. Thus, a soft-storey is progressively formed, leading to a possible mechanism. The drift on the first storey increases from 0.4% to 2% from 475 years to 2000 years of RP. With

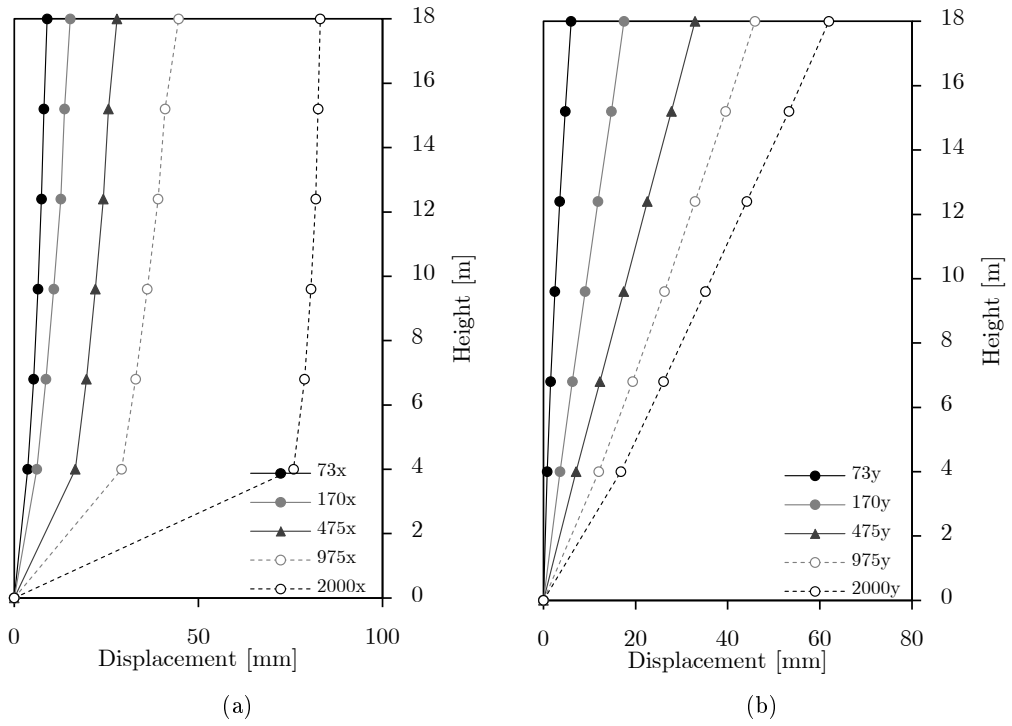

Figure 7.8: Lateral displacement profile for maximum top displacement of Parnaso with infill panels for (a) longitudinal earthquake and (b) transversal earthquake.

exception to this storey the usual drifts are 0.1%, corresponding roughly to 3 millimetres for 2.8 meters of column height, assumed to be a safe limit. Now, on the transversal direction, it shows a linearly increase of deformations without any softening in any of the storeys. The drift is slightly greater on the first storey, a little more than 0.4%, and for

a RP of 2000 years. In this direction, the amount of infills is similar along the parallel frames, and has also on the first storey, informing a similar stiffness and behaviour in all storeys.

The issue with the torsion effects, from a global and assess point of view, may be solved by calibrating the stiffness of the wall and those frames. It could be done reducing the stiffness with a integration of calibrated bracing struts, to a point where the rotational behaviour of the building is reduced and performance increased.

Regarding the behaviour of the building without infill panels (see figures C.16 to C.19 and 7.9), the difference of the deformation shapes and magnitudes of displacements are evident. Due to a less stiff structure, provided just by the concrete frames, the drifts are less constant in its height for a transverse earthquake, where it presents rotations on the plane (Rz). For a 975 years of return period, the structure seems to be forming a soft-storey on the third floor, confirming the drift tendency until then. But, continuing to higher accelerations, the influence of the height on the first storey takes its importance where the higher axial load together with the top-displacement induces higher moments, leading to more bending, then formation of a soft-storey in the first one. The analysis on the other direction shows once more the presence of torsion on the building. Without infills, the top displacement is now less variable near the wall, meaning a whip on the opposite side of the building, in other words, the stiffness on this direction is this way controlled by the concrete wall and the columns which supports the interior stairs.

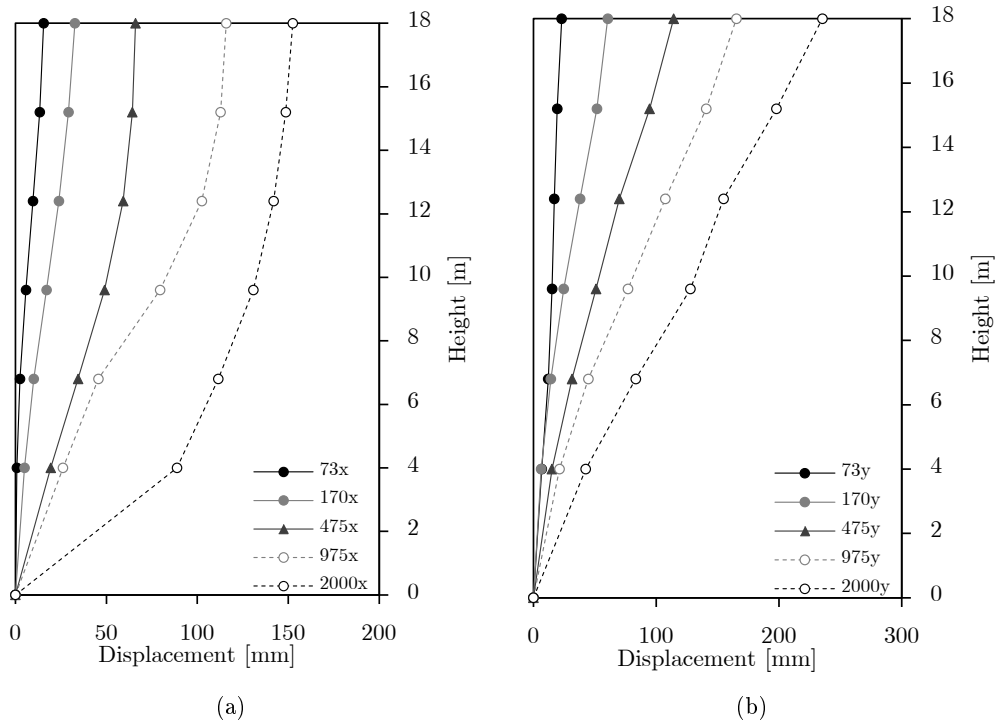

Figure 7.9: Lateral displacement profile for maximum top displacement of Parnaso without infill panels for (a) longitudinal earthquake and (b) transversal earthquake.

The displacements without infills are about three times higher, as showed on the

figure 7.10, the drifts do not have such difference. (The graphs were plotted for the middle structural column.) As previously mentioned, the building with infills, for higher accelerations, has a tendency to lose stiffness on the first floor for the longitudinal direction, which happens more distributed if the infills are considered. This is important because those results are only comparing higher drift on the building, which is occurring for both on the same storey. For the transversal direction, the building has a more uniform response with and without infills, but without is much more flexible, showed by the displacements. The response without the infill panels has a higher amount of energy being canalised and dissipated by the concrete wall which is protecting the extension of higher deformations.

Comparing the drifts with the limits recommended by FEMA-356 or VISION2000 (vd. figure 7.10) it is concluded that the values are bellow the limitations. These limits were defined having in mind different types of construction techniques and different levels of possible demand. As the earthquakes are more intense in the U.S., for instance, inferior drift limitations would create an impracticability on the assessment of concrete buildings. Therefore, the limitations serves as informative of good practise.

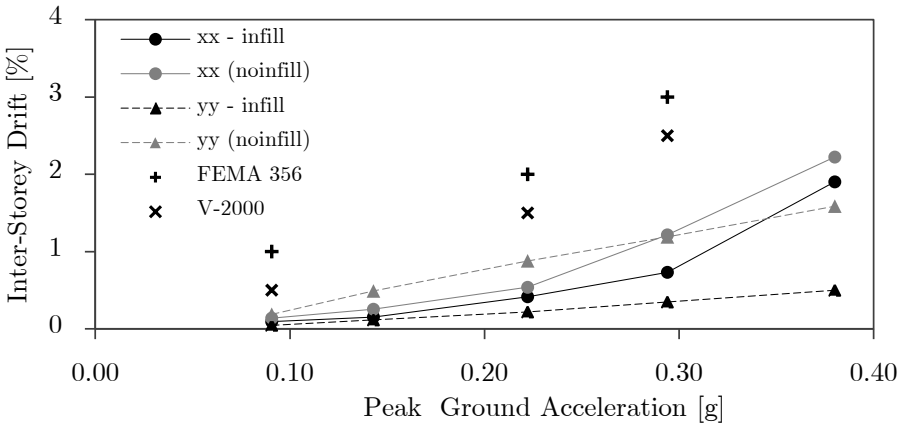

Figure 7.10: Higher drifts for central columns and different intensities of earthquakes for Parnaso.

The building has a rotation on the top of the building of 0.16 and 0.31 degrees (see figure 7.11), respectively with and without infills for a return period of 2000 years, which increases almost linearly for excitations on the transverse direction. The top rotation on the other direction is just roughly 0.01 degrees, not a noteworthy value.

The inter-storey rotations, which better represents the torsion demand, are generally 50% more intense on the first storey compared to the other storeys with infills and are similar in height for the bare structure. The transverse earthquake has an impact of 0.045 and 0.07, respectively with and without infills for a return period of 2000 years.

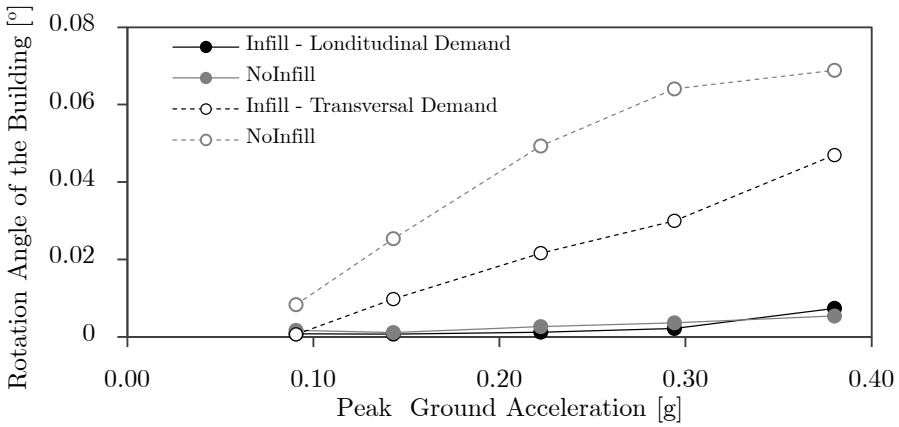

Figure 7.11: Maximum inter-storey rotation with and without infill panels for each earthquake for Parnaso.

7.4 Global Force Demands

7.4.1 Foundations

This section is dedicated to the analysis of the demand on the base of the building for an earthquake of 475 return period.

Costa Cabral

The total load on the foundations for the static combination of Costa Cabral building has a total of 36500 kN. For the longitudinal direction, the global variation of axial load is more intense, with stresses growing 1600 kN and, for the transverse direction, the growth is 1100 kN where the actual individual variation on each column member is more intense due to the smaller length of the moment equilibrium on that shorter span direction, showing a higher demand on the stress moments. The axial variations on the elements have its higher variations located at the expected far extremities of the direction of the earthquake, until a limit up to even more than 1000 kN in one or more individual elements. Those levels are extremely high, not much in compression, because the combination of loads does not increase so much as for ultimate design combinations, but variations which decreases the axial stress can lead to tractions. In terms of shear and moment variations are occurring more on the columns which limits the infills. The base shear is between 7000 and 9000 kN on the directions of the earthquake, and the total base shear on the perpendicular direction varies from 200 to 300 kN. The moments on the foundations for a transversal earthquake can the achieved up to 300 and 400 kNm, for columns close to infill panels. On the longitudinal excitation, the moments are less intense, with maximum moments on the range of 150 and 200 kNm. The total axial variations are similar with or without infills, but in terms of total shear is verified a high drop of the stresses, as is shown on figure 7.12. The perpendicular shear due to rotational effects, has a drop from near 250 kN to 80 kN in average with and without infills, respectively.

Summarising, the infilled building has a maximum base shear capacity of 10000 kN,

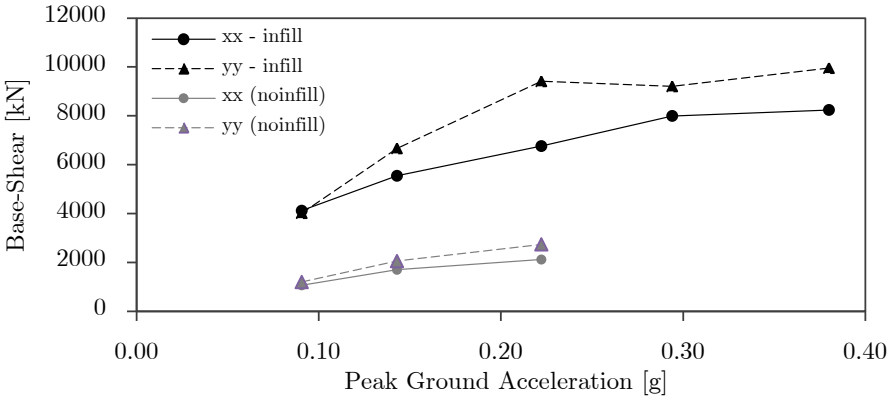

Figure 7.12: Base-shear variations with and without infill panels for each earthquake for Costa Cabral.

achieved for 0.22 g and 8000 kN achieved for 0.29 g, for longitudinal and transversal directions, respectively. The bare structure has a base shear capacity of 2000 kN for both directions, so is verified the increase of the capacity due to the existence of infills.

Parnaso

The Parnaso building, has a total vertical load on foundations of 11200 kN, three times less than the Costa Cabral, therefore, with less nominal shear and axial variation demands. The total axial variations on the foundations are similar for both directions but different for infilled and framed structure rounded to 1000 and 3500 kN, respectively. The figure 7.13 summarizes the base-shear levels, where the transversal direction has a constant growth of shear stress, due to the strong infills, which continues to hold and unload stress to the foundations. For the perpendicular shear stresses according to the excitation direction, the stresses are two times higher for earthquakes for the transversal direction, where is happening the torsion effects, in a range of 350 and 150 kN with and without infills, respectively.

Summarising, the infilled building has a maximum base shear capacity of 3500 kN, achieved for 0.22 g for the longitudinal direction. On the transversal direction, the building has a continuously growth of base shear stresses, which shows that, even for earthquakes with a PGA higher than 0.38 g, the infills still have capacity left, higher than 6500 kN. The bare structure has a base shear capacity of 1000 kN for both directions, achieved 0.29 g. The infill panels are increasing the global capacity of the building.

7.4.2 Columns Axial Force Variation

The variations of axial loads are analysed only for the Parnaso building, comparing earthquakes with a return period of 73 and 975 years. The plotted results are presented on the appendix, by the six different schemes, on the figures C.20 to C.25, for different localizations and different earthquake directions.

Beginning with figures C.20 and C.21, with infill panels, and the figures C.26 and C.27, for framed structure, are compared columns located in the interior, corners and

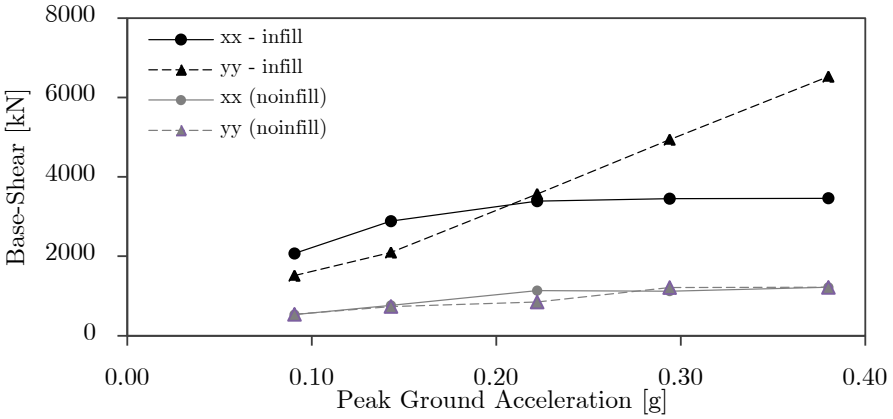

Figure 7.13: Base-shear variations with and without infill panels for each earthquake for Parnaso.

façades (longitudinal and transversal). The variation on the solicitation is higher for the corner columns than for other locations. The columns located on the interior of the building have a lot less variations, even if the translations are almost the same as the others, as the stiffness is almost the same on both directions, the global "neutral" axis of the building (making the parallel with concrete sections) is near to the centre. The variations usually do not exceed 20% and increase similarly until the top height. As the eccentricity increases, so the variations. The façade columns have from 50% to 100% less variations than corner ones.

The torsion effects on the transverse earthquake have an evident increase on the variations, where the same columns can go up to the twice verified variations.

The figures C.22, C.23 and C.28, C.29, summarizes differences between different corner columns for the building with and without infills. The graphs confirm a higher increase on the variations for columns confined within infill walls. The corner columns on the infilled structure have its variations between 100%, and on the framed structure proximately on the 50% variation. One exception is the columns 1 (far from the stairs block) on the main façade which presents strong variations on transverse direction. With infills, the variation goes up to 200% due to the explained reason, and for the framed structure, the same column goes up to 70%/80% due to the torsional effects verified on that column. The columns close to the stairs block have an increase of stiffness dominated by the wall and columns supporting interior stairs, deformation is higher on the opposite far column, named as column 1.

The figures C.24, C.25 and C.30, C.31, summarizes differences between different façade columns. The variations by height are not so linear comparing the transversal direction of the earthquakes with the longitudinal ones. The rotation component of the vertical plane is higher on the slender direction of the building which explains the less linear variation by height.

As a summarize, the corner columns have the biggest variations in an average range of 100%, followed by the façade columns with 50% and interior with less than 20% for a strong earthquake with a return period of 975 years. For an earthquake with a return period of 73 years, the variations are more concentrated do not overcome 20% for both

framed and infilled structure. For columns which are limiting the infills, the variations can be doubled.

7.5 Shear Profile on R.C. Structure

The shear progression for the structures with infill panels is not presented because of the way results given by the SeismoStruct. The shear and moments are plotted on the plastic hinge and the (un)loading of the infills is made near the frame joints. The actual variation would be a very concentrated shear demand near the joints which is reduced until the end of the contact of the infill with the column. Because the stresses are plotted on a middle section of the plastic hinges, is not possible to capture the real shear demand. To plot the correct shear values would be necessary to correctly connect the infills with the correspondent columns, project the correct component of the struts for the six struts that the model defines for the panels. The profit of the conclusions towards the time consumption for the automation of the task has not been attempted, whereby, only the shear profile envelope for the buildings without infills is shown. For the same reason, the later local analysis can only be performed for the building without the infill panels.

The shear by floor is calculated by summing all the stresses on the same floor.

7.5.1 Costa Cabral

The shear progression is plotted for the first three intensities of earthquakes, with the third incomplete until the collapse. The figure 7.14 is showing the envelope progression of shear stresses by the floor. In the appendix, is shown the shear progression on the moment of maximum base-shear, on the figure C.9. The envelope shows a proximate constant shear diminution along the height. The variation of shear for different stronger earthquakes is much higher on the bottom levels.

It would be interesting to compare the shear progression with and without the infill panels. As the global stiffness increases and deformation decreases, the restriction of movement is made by an increase of forces. The expectable global stresses with the infills depend on the characteristics of the panels. A reasonable increase could be two times higher. If the infills have a capacity of 70% of the shear strength, it would mean that the columns could be supporting less shear than the demand without infills. It is not possible to check in this current dissertation.

The increase of shear from one floor to an upper one indicates the occurrence of higher modes of vibration. It is only visualised as a small variation in some middle storeys, for earthquakes with a low intensity.

7.5.2 Parnaso

The results, with the same assumptions as the ones for Costa Cabral are presented on the figure 7.15 (and also C.32).

The shear demand on this building is inferior compared with the shear of Costa Cabral. As is known, the base-shear is dependent on the ground acceleration and on the weight of the building. It shows also a very constant reduction of shear demand along the storeys, which can be expected for framed concrete structures.

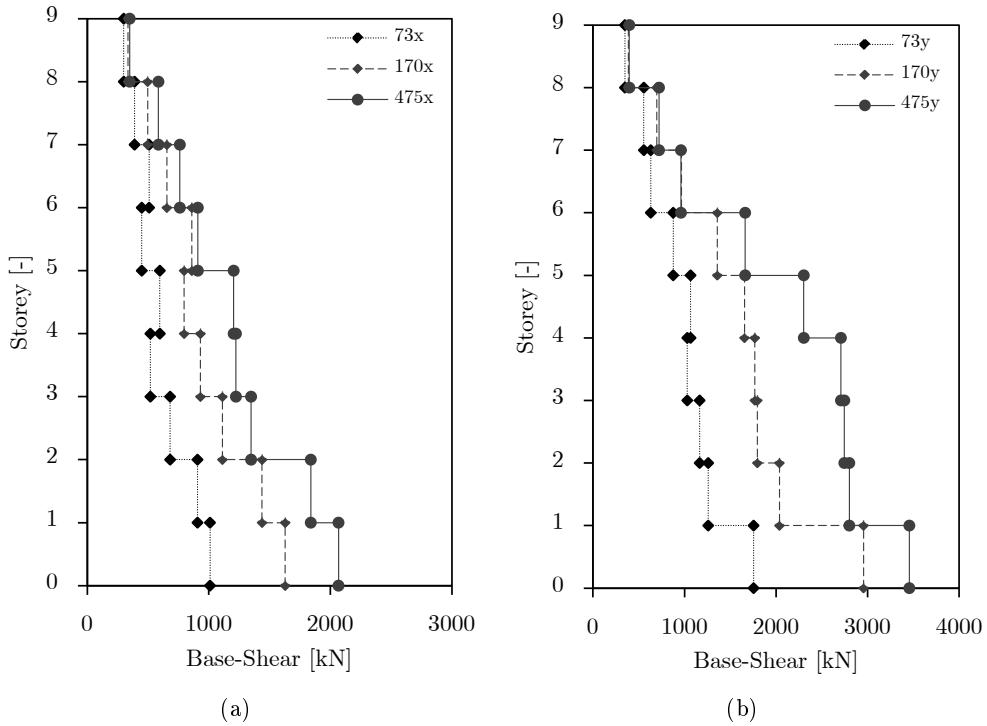

Figure 7.14: Envelope of total shear by storey of Costa Cabral for (a) longitudinal earthquake and demand and (b) transversal earthquake and demand.

Checking more structures, would also be interesting to study an expectable reduction of shear until the top storey. To compute the base-shear demand without complex modelling, is possible with empirical formulations which computes it with the acceleration and weight. If a reasonable reduction is 50% of base-shear until the top (which seems to be adaptable for both studied buildings), is possible to have an idea of the total shear in a specific floor, which can be divided by the number of columns to check the average strength. A quick assessment can be handy, on some urgent situations or for the need of cataloguing general characteristics of a big amount of building to make a decision of post-rehabilitation by level of need.

As happens on Costa Cabral, the increase of shear stress on the second and third storeys indicates the influence of higher modes of vibration. The shear rise is small and is only verified for low intense earthquakes.

7.6 Shear-Drift

In this section, the base-shear is plotted along with the drifts helping to understand the progression of the forces towards deformations, and also the ductility moved by the structure on the two directions.

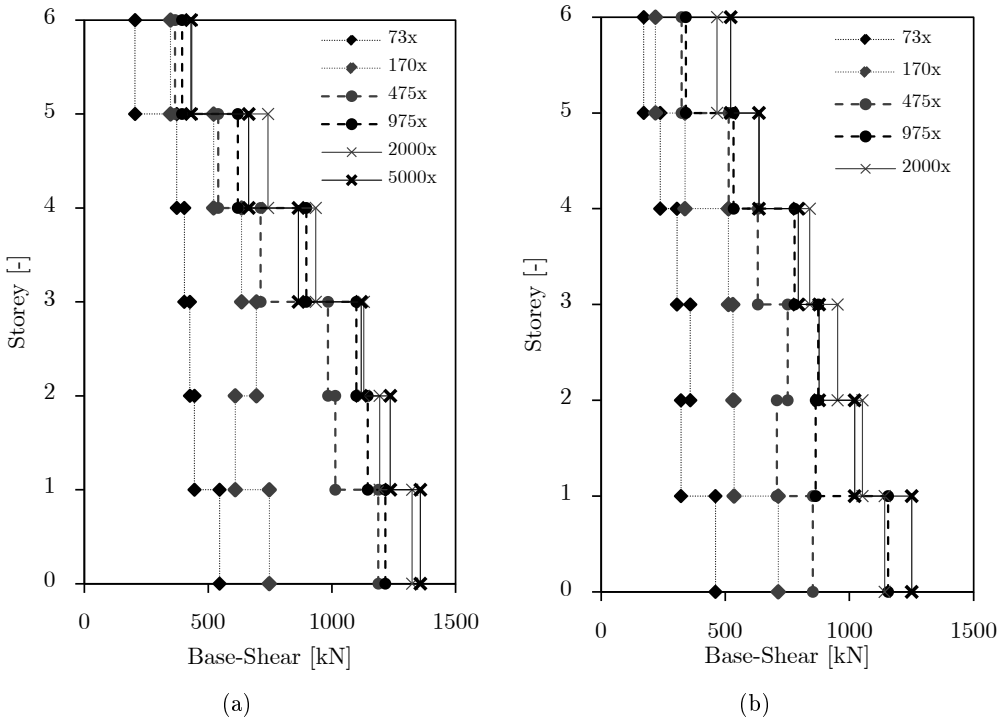

Figure 7.15: Envelope of total shear by storey of Parnaso for (a) longitudinal earthquake and demand and (b) transversal earthquake and demand.

7.6.1 Costa Cabral

Both directions are showing a similar stiffness at the ground level, with deformations and shear capacity growing along with the excitations. The earthquake with a return period of 475 years starts to show a more evident non-linear behaviour, but only for earthquakes with a return period of 975 and 2000 years which have higher deformations starts to take place at the bottom level, by figures C.10.

From the type of curves on the figures C.11, drift-shear by floor, for an earthquake with a return period of 475 years, the bottom floors present some hardening on the columns in a small level. As already verified by the deformation graphs, is proved that higher issues are present on the upper floors. In general, the figures are showing an increased loss of stiffness on the height of the building, where the bottom columns support higher amount of shear stresses and less drifts.

On the last three floors, the figures are showing interesting information from the collapse point of view. As expected, the shear canalised to the upper floors is less than the amount on the bottom, but, is evident a big drop of shear on the last three floors due to the reduction of cross-section dimensions. While the other floors are having a slight linear reductions, on these three levels have an uncontrolled progression of deformation, indicating a formed mechanism. Looking carefully to the figures is possible to conclude that after a 0.50% drifts, the floors starts to behave unstably.

7.6.2 Parnaso

The figures C.33 and C.34 are related to the floor shear-drift for structure with infill panels and figures C.35 and C.36 are related to the structure without infills, for both directions. As is expected by the deformation results, both highest stresses and deformations are located at the bottom floor. Starting from the infilled structure, once again the stiffness of the structure is proved to be higher on the transverse direction where the slope of the building is higher. As showed by the displacements, the soft-storey is happening on the longitudinal direction where is possible to see a much more evident non-linear progression on the curves. This starts to appear for a RP of 975 years and the ductility of the materials starts to yield where the maximum base-shear capacity is achieved near the 4000kN, but more energy is constantly being dissipated through the ductile capacity of the materials. The longitudinal direction, less stiff by the infills, presents more ductility compared to the transverse direction. The transverse direction, due to high stiff elements as those infill walls on the extremities and the concrete wall, the structure deals with more forces and a smaller amount of deformations. Discarding the influence of the concrete wall in terms of torsion effects, this resistant element is actually protecting the structure, absorbing great amount of forces which is not going to affect the other elements. For a return period of 2000 years, a decrease of stiffness for the transverse direction, and reduction of stresses is visible at the base level, due to what may be the fracture of the infills and transference of energy to the wall. On the appendix is shown the plots of the moment-rotation of the concrete wall, with infills, for the two directions of earthquake on figures C.42 and C.43, showing the big differences between both directions. The earthquake on the transverse direction has more than three times higher moments and 50 to 200% less chord rotations when compared to the longitudinal direction, which shows the influence of the wall regarding the absorption and limitation of deformations on the direction in which the earthquake of acting.

Discarding the infill panels, the stiffness of both directions and global behaviour at the base level is very similar between them, for deformations and base-shear capacity. The structure starts to yield for an earthquake of 475 years of RP. For an earthquake of 2000 years, the level of viewable deformation starts to increase exponentially which leads to conclude that the global capacity is yet to be achieved but not far from an unsafe perspective. The amount of shear stress at the foundations, for the transverse direction is 5 times less for the structure without infills, a great difference.

The figures C.37 to C.40 are comparing together the two structure modelling, with and without infills. The main conclusion is that for the longitudinal direction, there are similar drifts but higher stresses with infills, and on the transversal direction, higher stresses but more than two times less drifts. The stiff panels together with the concrete wall provide strong elements which restricts the deformations.

The figures C.41, for a 975 years of return period, without infill panels, are showing two big differences between this building and Costa Cabral. The Costa Cabral building has an evident scale of differences along the floor and drifts increasing with the height, in Parnaso, all the storeys have a similar shear-drift relationship slope and with higher demands at the bottom floors. On the transversal direction top floors shows a slight decrease on the stress levels and increase of drifts, showing a reduction on stiffness, due to the lack of influence of the concrete wall along the height.

Chapter 8

Safety Assessment at the Local Level

Only the building Parnaso is assessed locally. As pointed before, the building Costa Cabral develops a mechanism on the last floors, due to the slender columns which does not hold capacity to avoid formation of soft-storey. Hereby, Costa Cabral is not globally stable for the return period of 975 years for which brittle mechanisms should be assessed, and also for the ultimate assessments performed for ductile mechanisms.

The verifications are just performed for the bare framed structure (without infill panels) because the program gives the stresses on end of the elements, and model of the infills unloads the stresses of the panels on specific length near the nodes. Therefore, a complex routine would be needed to link the six struts of the infill model to the exterior frame, projecting the components, for a large amount of elements, and for 1500 steps of the 15 seconds of the earthquake.

8.1 Ductile Mechanism

To each second of an earthquake, the conditions are changing and the strength of the elements evolves with it. Axial, shear and moment stresses, deformations and degradation changes during the earthquake causing direct impact on the material proprieties and on its final resistance. Therefore, to compute the moment and chord-rotation capacity and to plot it, is needed to make a decision on what are the expectable envelope limits. On a first approach, it was used the static axial loads from the gravitational seismic combination together with a shear span considered to be equal to half the length of each element. Another used approach was extracted from the analysis, using the maximum and minimum axial load, corresponding respectively to the high and less stress on the elements, and its correspondent moment and shear to calculate the shear span.

It is also compared the empirical approach of the EC8 and the theoretical one, with the same assumptions. The theoretical is used for comparison since it is not recommended for non-seismic designed structures. The empirical formula was calibrated taking into account the cyclic degradations on the elements, and has reduction factors to decrease verification limits for structures with seismic deficiencies. The limits and formulation were slightly changed on the last update of the code.

To compute the chord-rotation with the theoretical approach and the plastic chord-

rotation is necessary to calculate the neutral depth of the elements for both yield and ultimate states. A general formulation, from the strength of materials is formulated through the equation 8.1,

$$y = \frac{N_{\mathrm{E}} + A_{\mathrm{s}} f_{\mathrm{s}} - A'_{\mathrm{s}} f'_{\mathrm{s}}}{b\sigma_{\mathrm{c}}} \ , \tag{8.1}$$

where f_{s} and f'_{s} are the tensile and compressive stress on reinforcement bars, respectively, N_{E} the axial force (positive for compression, and y neutral depth converted from the parabolic curve of the concrete formulation (vd. equation 8.2) to an equivalent rectangular for the total strength. The concrete proprieties and strength are calculated through the formulation on EC2,

$$\sigma_{\mathrm{c}} = f_{\mathrm{c}} \left[1 - \left(1 - \frac{\varepsilon_{\mathrm{c}}}{\varepsilon_{\mathrm{c2}}} \right)^2 \right] \quad \text{for } \varepsilon_{\mathrm{c}} \leq \varepsilon_{\mathrm{c2}} \ . \tag{8.2}$$

The neutral depth x, for the ultimate is usually considered to be 0.8 (simplification of 0.809). Since the value for yielding is not achieved through the resistance of the concrete, the area should be calculated with a different estimation. The calculation was performed on a spreadsheet, so, the integration of the formulas has no direct implementation. To control the neutral depth, a linear and polynomial regression was done from the numerical variation of this factor. It was chosen the linear envelope regression, with more percentage of error, $y = 0.1x + .45$, but more useful for eventual hand calculations. It gives a conservative values for the neutral depth with just a maximum difference of 6%. (see figure 8.1)

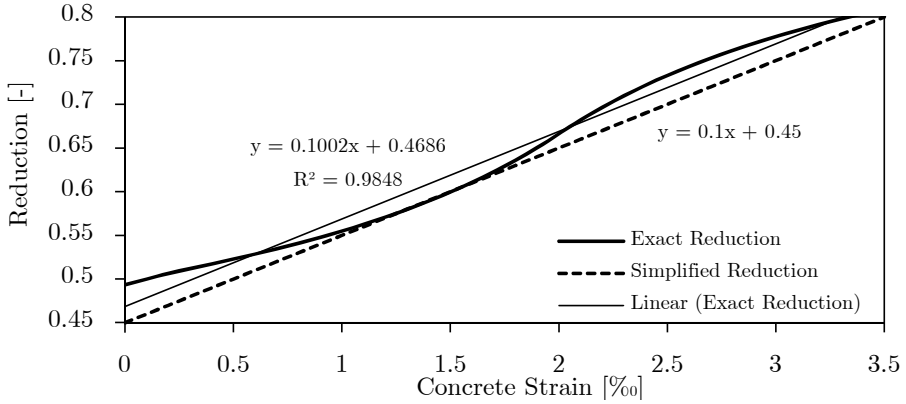

Figure 8.1: Variation of the conversion factor for the neutral depth.

The moment capacity, on yielding or ultimate, can be computed by

$$M_{\mathrm{R}} = yb\sigma_{\mathrm{c}} \left(\frac{h-y}{2} \right) + \left(A_{\mathrm{s}} f_{\mathrm{s}} + A'_{\mathrm{s}} f'_{\mathrm{s}} \right) \left(\frac{h}{2} - c \right) \ , \tag{8.3}$$

also formulated by the strength of materials but it is not used because the program itself, solves this kind of verifications, triggering the formations of the plastic hinge, for yielding case.

As already stated, to compute the chord rotation is necessary to get the respective neutral axis depth (x) for the yielding limit and for the ultimate limit, therefore, the formula is written to calculate the neutral axis of yielding to the limit where the first compressive or tensile reinforcement bars achieve the yielding point. Knowing that the compressive axial load deepens the neutral axis, for small to medium of axial load range, the yielding is limited by the tensile reinforcement, and for high axial loads, the yielding is limited by the compressive reinforcement of the section. Considering that the elastic modulus is, for this work, $E_{\mathrm{s}} = 200$ GPa, and the $f_{\mathrm{sy}} = 235$ MPa, the yielding strain is $\varepsilon_{\mathrm{sy}}{=}f_{\mathrm{sy}}/E_{\mathrm{s}}{=}1.175‰$.

The chord rotation is the angle formed by the element, from the fixed-end section and the zero moment section. So, the rotation can be simply explained as $\theta = \Delta/L_{\mathrm{v}}$, where Δ is the deflection of the element. Since the deflection compared with the length is much higher, the angle calculated with the tangent or with that way, has a negligible error associated. It is important to refer some differences on the calculation of the length of the zero moment, known as shear span, which can be calculated as $L_{\mathrm{v}} = M/V$ (or $L_{\mathrm{v}} = L/2$). If we are dealing with a shear wall (cantilever) or if the two fixed-ends have moments on the same direction, the shear span is equal to the length of the element because there is no deflection, if the case of opposite moments on both fixed-ends, for beams and columns, the shear span can be calculated by the definition. The simplified $L/2$ can be defined because of the way, for example, a column deforms laterally. With both ends fixed, one on a constrain slab and the other on a restrain support on also on a slab, the rotations/deformation on both ends are similar, so just the translational component of the element, it is actually controlling the deflection/chord rotation.

Having the equations prepared, and the theory in mind, some assumptions needs to be integrated on the calculations to compute the theoretical formulation proposed by the EC8-3 (Corrigenda) [CEN 2009], the chord-rotation for the damage limit state,

$$\theta_{\mathrm{y}} = \phi_{\mathrm{y}}\frac{L_{\mathrm{v}} + \alpha_{\mathrm{v}}(d - d')}{3} + 0.0014\left(1 + 1.5\frac{h}{L_{\mathrm{v}}}\right) + \phi_{\mathrm{y}}\frac{d_{\mathrm{bl}}f_{\mathrm{ylm}}/\mathrm{CF}}{8\sqrt{f_{\mathrm{c}}/\mathrm{CF}}}\ , \tag{8.4}$$

already with the other points of the EC8 implemented. ("CF" is the coefficient factor, considered to be equal to 1.2, the higher value allowed by the code for non-linear analysis.) This formulation is divided on three summed members, flexure, shear and fixed-end rotation (slippage) contribution. Some assumptions to calculate the rotation limits are recommended by Fardis [Fardis 2009] to assume a minimum value for the steel yielding curvature,

$$\phi_{\mathrm{y,tens}} = \frac{f_{\mathrm{ylm}}/\mathrm{CF}}{E_{\mathrm{s}}(d - x_{\mathrm{y}})}\ , \tag{8.5}$$

and for the compressive concrete "apparent yielding" curvature,

$$\phi_{\mathrm{y,comp}} = \frac{1.8f_{\mathrm{cm}}/\mathrm{CF}}{E_{\mathrm{c}}x_{\mathrm{y}}}\ . \tag{8.6}$$

Fardis also suggests a limitation for the concrete strain for yielding verifications on cyclic excitations by the equation

$$\varepsilon_{\mathrm{c,max}} = \frac{1.8f_{\mathrm{cm}}/\mathrm{CF}}{E_{\mathrm{c}}}\ , \tag{8.7}$$

The theoretical limit for the ultimate chord-rotation capacity is calculated through,

$$\theta_{\mathrm{u}} = \frac{1}{\gamma_{\mathrm{el}}}\left[\theta_{\mathrm{y}} + (\phi_{\mathrm{u}} - \phi_{\mathrm{y}})L_{\mathrm{pl}}\left(1 - \frac{L_{\mathrm{pl}}}{2L_{\mathrm{v}}}\right)\right] \tag{8.8}$$

where safety factor γ_{el} takes the value of 2, for present the assumed conditions, and L_{pl} are the plastic hinge length considered to be equal to the ones implemented on the modelling.

The code also presents an empirical formulation which should be used to compute the chord-rotation for this kind of structure without seismic provisions by

$$\theta_{\mathrm{um}} = \frac{1}{\gamma_{\mathrm{el}}}0.016(0.3^{v})\left[\frac{\max(0.01; w')}{\max(0.01; w)}f_{\mathrm{cm}}\right]^{0.225}\left(\frac{L_{\mathrm{v}}}{h}\right)^{0.35}25^{\alpha\rho_{\mathrm{sx}}\frac{f_{\mathrm{yw}}}{f_{\mathrm{cm}}}}\ , \tag{8.9}$$

where w are mechanical reinforcement ratio for tension and compression, α the confinement effectiveness, ρ_{sx} the ratio of transverse steel, and the safety factor γ_{el} equal to 1.5 for primary seismic elements. This empirical approach has some reductions factors, among them division by 1.2 for structures with no seismic provisions, multiplied by 0.8 if the structure has smooth bars and a also multiplication accounting the lapped bars by $0.019[10 + \min(40; l_0/d_{\mathrm{bL}})]$. The lapped length, l_0, is considered to be 40cm, and d_{bL} is the longitudinal diameter bar.

The reason to use and compare both empirical and theoretical limitations of the code, it is the way the analyses have been performed. As was referred, the program does not calculate the effect of the slippage of steel, and to overcome this limitation the introduced plastic-hinges were taken as half the expected for structures with deformed bars, different from the length that the code describes for that specific verification. This was the best known way to introduce the effect of smooth bars. Therefore, the modelling those not match perfectly with any of the verification approaches. The code gives no information about the way to calculate the demand chord-rotations, just applies the limitations. This creates the indefinition of not knowing exactly what to compare to what, so verifications are performed for both equations and with different parameters.

The verifications can be performed for a near collapse limit (ultimate capacity), significant damage (3/4 of the ultimate capacity) and for damage limitation (yield capacity). Even if the code tells the designer to all these limits, on the present work, just the near collapse is verified, for two main reasons: to use the non-linear capacities of the modelling comparing it to the code formulations, and to verify if the buildings still holds some capacity left to sustain the earthquake until the end. The used earthquake to perform it is the 975 years of return period, meaning the ultimate capacity.

8.1.1 Parnaso

The caption on figure 8.2 are referring to the longitudinal earthquakes (xx) demanding rotations on the same direction, with the same happening on the perpendicular transversal direction (yy). The beams, on both directions, are calculated for the rotation on the strong axis (vertical axis), the most demanding which naturally affects different beams according to the direction of the analysed earthquake.

The results from the analysis shown on the figure 8.2 are divided by groups with the envelope combination of all the elements which did not pass on of the present verifications, for empirical, for theoretical and for merged verifications. The first individual group is

for axial loads of the seismic combination, and shear span equal to half of the length of the element. The next two groups are referring to maximum and minimum axial loads for individual different elements taken from the analysis, again, considering the shear span equal to "L/2". On the last two groups, the difference regarding the latter is on the shear span which were done according to the formulation "M/V". The moment and shear loads which were used are the exact ones acting on the element on the actual maximum and minimum axial loads. This is actually, one of the difficulties which was referred on

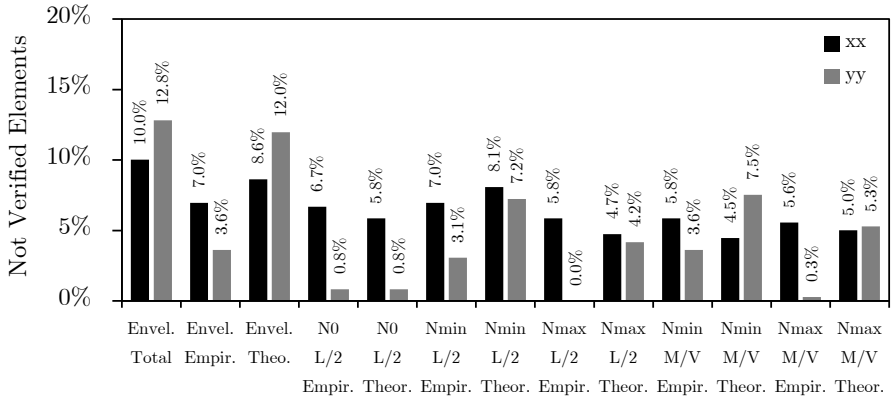

Figure 8.2: Elements failing in chord-rotation limitation.

the beginning of this section, the indefinition of what should be considered and how. The axial load on the elements, mainly on columns, takes an important part, since the amount of axial load can affect the behaviour of the element on rotation capacity, as is easily seen by the first equation of this chapter, equation 8.1.

The first group is formulated with the loads from seismic combinations and shear span equal to "L/2". This approach is important because is one of the most simplified verifications, and compared to the others, the fastest one. The drawback is the lower conservative results.

Then, comparing the two more complex equations, assuming maximum and minimum stresses, the not verified elements are similar in percentage. The tendency is to get higher percentage for higher compressive loads, but on the transversal direction some verifications got more percentage of not verified elements. On an earthquake acting on the transversal direction, the range of axial load is bigger and, on some elements, it is verified tractions which affects greatly the neutral axis, reducing the verification of chord-rotation. Comparing M/V approach to the L/2, it is found a slightly higher amount of not verified elements for L/2. This shows that the most conservative limit is expected on the theoretical approach with higher tensile forces and shear span equal to L/2. The conclusion is also valid on the empirical formulation.

The different considerations of length of plastic hinge, shear span length, consideration of maximum strain of concrete, the lap-splice, induces big differences on the model, when referred to these kind of concerns, assessing a structure which, for one side is very complex to perform the modelling, and on the other side, it is difficult to guarantee which is the best approach for each case.

Looking to the last member of the theoretical ultimate chord-rotation formula, $(1 -$

$.5L_{pl}/L_v$), it is evident the importance of both lengths of shear span and plastic hinges. As an example, for low moments, the shear span can get to the point were the quotient is higher than 1, the actual ultimate chord-rotation is smaller than the yielding one. The ultimate strain for computing the ultimate curvature has also a big impact on the last results. On the empirical verifications, the lapped length of bars can also have a big influence, with a direct reduction of the limit on a range of 50% to 95%.

For the empirical verifications, two other parameters were analysed but are not presented. The proposed a correction to the reduction in case of lapped bars by Ricci [Ricci 2010], $0.02\min(50; l_0/d_{bL})$, has a slight influence with less conservative results. It was also compared lapped bars of 40 cm and 80 cm, were almost all elements become limited by l_0/d_{bL}, affecting by a lot less conservative results.

The results are not matching perfectly, therefore the assessment may be performed from the combination of the various approaches. If such analyses are not possible to be performed, the results should be taken from the combination of both earthquakes, using the theoretical approach, with maximum compressive stress and shear span equal to half length of the element.

From the longitudinal earthquake, the few beams which did not pass are located on the opposite extremity side of concrete wall (evidently with the same direction) and the columns are distributed along the buildings. The problems mainly appear up to the third level, but are more evident on the second and third storeys. From the transversal earthquake, the main deficiencies are located on the same places, but more concentrated on the opposite side of the concrete wall, confirming what was already predictable from the global analysis, due to the rotational characteristics of this response.

Annexed is described the progression of the non-verified elements, separated by figures D.1, D.2, D.3 and D.4. It shows a much higher demand on columns than beams, for both earthquakes, and that the building still hold a lot of capacity to sustain deformations, with 50% of capacity left for more than 90% of the columns. The high demand is concentrated on specific zones of the building. The progression on columns confirms that the distribution of capacity left is higher on the bottom storeys than the top storeys.

The figures D.5 and D.6 are summarizing the verification of the rotations for different return periods of earthquake, for its respective limits, yielding for 170 years, 3/4 of ultimate for 475 years and ultimate chord-rotation for the 975 years. The graphs inform that the building retains chord-capacity for all levels. Even for the yield level is shown a big amount of chord-rotation capacity left. Without infills the structure has more elements which holds less rotation capacity.

The chord-rotation response of the building is better with infills, as the building becomes stiffer, the deformations are less, increasing the safety level of the building to just a very few columns which does not verify the limit imposed on the code.

The ductility of the elements, regarding the chord-rotation deformations is schematically presented on the figure 8.3. The assumed limit for this evaluation was the theoretical formulation of the EC8 to compute the yielded chord-rotation, referring to the parameters of seismic combination with shear span equal to half the length of the element. In this case, the ultimate chord-rotation is not used because the elements which did not pass on the verification are not considered. It is separated by groups of beams and columns, and by storey, for the two demand directions. The average lines are for the average ductility of safe elements, and the max is referred to the still safe element with more ductility. In average, only the columns on the storeys three and four are performing in its plastic

behaviour. Of course, this does not contradicts the conclusions of the global analysis showing the big influence that the variation of axial load can take on the response of elements. The other groups, in average, do not perform on ductile response, but it is shown that columns are showing higher plastic response.

Regarding the maximum ductility, on the first three storeys, all have at least beams and columns which did perform in plastic performance and still maintaining the safety limits.

In general is possible to check that for both beams and columns, the plastic demand on rotations is stricter on the three first storeys.

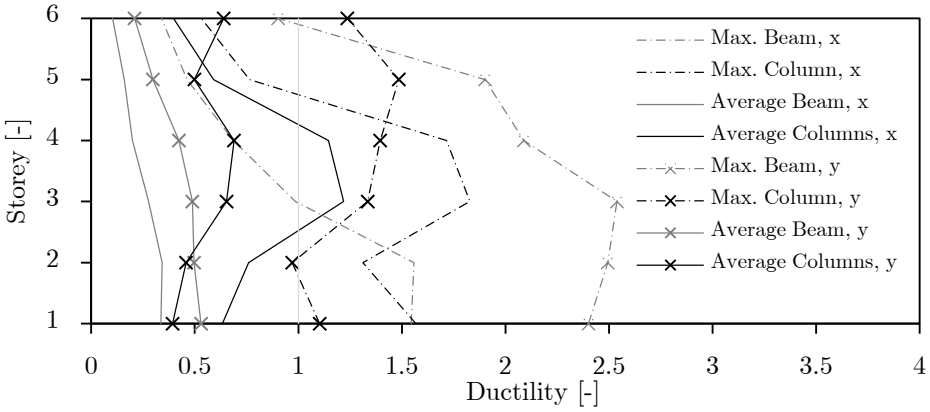

Figure 8.3: Ductility of beams and columns, regarding the chord-rotation, for the Parnaso building. Average and maximum ductility by floors.

8.1.2 Costa Cabral

No results are shown because the earthquake did not fully run. Even though, the results until then were studied and some main deficiencies were found. Of course, the failing chord-rotations are localized on the last three storeys, where the collapse has occur. Excluding those floors, an amount of 10% of more than 1500 elements, do not verify the safety level and are spread on the second and third floors.

8.2 Brittle Mechanism

The failure obtained by a shear mechanism is brittle because no plastic deformation, or residual capacity to dissipate energy is expected to happen on the R.C. materials. This type of failure is dangerous for the structures, since it can bring the total collapse of the structure without a warning. This kind of mechanism does not allow the redistribution of stresses for the equilibrium.

Eurocode 8 suggests the verification of the shear strength by the influence of axial

load, concrete and transverse steel strength, with

$$V_{\mathrm{R}} = \frac{1}{\gamma_{\mathrm{el}}} \left\{ V_{\mathrm{N}} + \left[1 - 0.05 \min\left(5; \mu_{\Delta}^{\mathrm{pl}}\right) \right] .(V_{\mathrm{C}} + V_{\mathrm{W}}) \right\} \ , \quad \text{where} \tag{8.10a}$$

$$V_{\mathrm{N}} = \frac{h - x_{\mathrm{dem}}}{2L_{\mathrm{v}}} \min\left(N; 0.55 A_{\mathrm{c}} \frac{f_{\mathrm{cm}}}{\gamma_{\mathrm{c}} \mathrm{CF}} \right) \ , \tag{8.10b}$$

$$V_{\mathrm{C}} = 0.16 \max(0.5; 100\rho_{\mathrm{tot}}) \left[1 - 0.16 min\left(5; \frac{L_{\mathrm{v}}}{h}\right) \right] \sqrt{\frac{f_{\mathrm{cm}}}{\gamma_{\mathrm{c}} \mathrm{CF}}} A_{\mathrm{c}} \quad \text{and} \tag{8.10c}$$

$$V_{\mathrm{W}} = \frac{A_{\mathrm{sw}}}{s} b_{\mathrm{w}} (d - d') \frac{f_{\mathrm{ywm}}}{\gamma_{\mathrm{s}} \mathrm{CF}} \ , \tag{8.10d}$$

where almost all the components are already known by latter formulas but, $\mu_{\Delta}^{\mathrm{pl}}$, which is the ratio of the plastic of the chord rotation normalized to the chord rotation at yielding, that can be extracted from the previous verifications, and $\rho_{tot} = A_{sl}/bd$ the total longitudinal ratio. The axial load component should be considered as positive for compression and null for tension. Analysing the formula, it is possible to understand three main influences on the shear strength. One is the amount of axial load, beneficial until a certain point, the cross-section characteristics and concrete proprieties, and the transversal amount of reinforcement, this last with a major impact.

The shear capacity is limited to

$$V_{\mathrm{R,max}} = \frac{1}{\gamma_{\mathrm{el}}} 4/7 \left[1 - 0.02 \min\left(5; \mu_{\Delta}^{\mathrm{pl}}\right) \right] \left(1 + 1.35 \frac{N}{A_{\mathrm{c}} f_{\mathrm{c}}} \right) \left[1 + 0.45 \left(100 \rho_{\mathrm{tot}} \right) \right] \times \sqrt{\min(40; f_{\mathrm{c}})} b_{\mathrm{w}} z \sin[2 \arctan(h/2L_{\mathrm{v}})] \tag{8.11a}$$

for columns characterized by $L_{\mathrm{s}}/h < 2$.

The formulations are based on empirical calibration for new constructions, therefore, for assessment purposes, the results may not represent exactly what the limit should be for an existing old building. Nothing can be done to guarantee the accuracy of the results for this structure without seismic provisions. Just to introduce the best possible way all the information about transversal and longitudinal reinforcement, cross-section dimensions, and the get the loads from a good modelling.

8.2.1 Parnaso

The drawings are not very elucidative about the amount of transversal reinforcement. From some of them, is possible to check that some elements have stirrups of 8 mm spaced by 15, 20 and 25 cm. Because that information is not available, an average of $8\phi//.20$ is considered on the verifications.

The verifications were performed with the values from the analysis, for the envelope shear stresses. The moment stresses on the same specific instant were computed the shear span length which was acting for that shear demand. The results are described on the table 8.1.

The results show that the structure is vulnerable to shear stress, both on columns and beams.

The beams have shear problems on its strong axis on the transversal earthquakes, more than for longitudinal. The not verified beams are spread along the floors. It is

Table 8.1: nsafe elements in shear demand for Parnaso without infill panels (with stirrups of $8\phi//.20$).

Earthquake	Longitudinal		Transversal	
Direction	22	33	22	33
Total	0.0%	16.1%	4.8%	15.9%
Beams	0.0%	14.5%	0.0%	24.2%
Columns	0.0%	19.0%	13.5%	0.8%

not verified a concentration on a specific zone by floor, but prevails on the first three floors. In terms of vertical elements, for a longitudinal earthquake, the central columns on the two exterior transversal façades have a big shear demand in its height until the fifth floor, which makes those elements unsafe. On the transversal earthquake, the not verified columns are more concentrated near, and in, the opposite façade to the concrete wall.

In general, the elements have a lack of less than 15% of shear capacity for longitudinal earthquakes. For transversal ones, the percentage is higher. Some elements have 50% lack of capacity. Without the safety factors, using the average proprieties of the materials, the percentage of not verified elements drops to 2% and 10% for longitudinal and transversal earthquakes.

On a assessment project, the lack of knowledge should be surpassed with some verification with equipment which allows a better tracking and definition of the reinforcement on the elements. If the considered transverse reinforcement is $10\phi//.20$ or $8\phi//.15$, the percentage of not verified would decrease a lot. As an example, the difference of considering transverse reinforcement equal to $6\phi//.20$, almost doubles the percentage of unsafe elements on the structure. Therefore, it is very important to be very accurate while establishing these values.

8.2.2 Costa Cabral

Until the mechanism is formed, it is possible to check that the building has a better behaviour for longitudinal demand where an average of 2% of elements presents some shear failures. For transversal excitation, both columns and beams performs worst, achieving 5% and 30% of failures on shear verifications. This show that the columns are under designed for the shear stress than beams, which have larger cross-sections to deal with the level of stresses. Corresponding to each type, the non verified elements are not exclusive on the higher floors, the verified deficiencies are concentrated on the second, third, seventh and eighth floors, spread on the storeys.

8.3 Joint Shear Strength

The shear on joints is another very important matter on the assessment of structures. The lack of capacity in one joint can put two columns and 4 beams in danger of affecting its dependants. Therefore, this may be one of the most important issues on seismic demand. Together with the ineffectiveness of the joint projected by the old codes, where

the longitudinal reinforcement is not properly tied, lack of reinforcement and the slippage of the smooth bars, can be potentially harmful.

To verify the shear capacity on joints, the EC8-1 [CEN 2003] suggests to use the next formulation,

$$V_{\text{jhd}} \leq \eta f_{\text{cd}} \sqrt{1 - \frac{\nu_{\text{d}}}{\eta}} b_{\text{j}} h_{\text{jc}} \quad \text{where} \tag{8.12a}$$

$$\eta = 0.6(1 - f_{\text{ck}}/250)\ ,\ f_{\text{ck}} \text{ in MPa}, \tag{8.12b}$$

$$h_{\text{jc}} = b - 2c \quad \text{or} \quad h_{\text{jc}} = h - 2c\ , \tag{8.12c}$$

$$b_{\text{j}} \Rightarrow b_{\text{c}} > b_{\text{w}}\ :\ b_{\text{j}} = \min[b_{\text{c}}; (b_{\text{w}} + 0.5h_{\text{c}})]\ , \tag{8.12d}$$

$$b_{\text{j}} \Rightarrow b_{\text{c}} < b_{\text{w}}\ :\ b_{\text{j}} = \min[b_{\text{w}}; (b_{\text{c}} + 0.5h_{\text{c}})] \quad \text{and} \tag{8.12e}$$

$$\upsilon_{\text{d}} = \frac{N}{f_{\text{cm}} b_{\text{j}} h_{\text{jc}}}\ , \tag{8.12f}$$

where h_{jc} is the distance between the reinforcement layers on columns, b_{j} is the effective width of the joint, υ_{d} the normalized axial load for the axial load on the above column. The equation is valid for interior joints, but should be considered as, at least, 80% when is applied for exterior joints. V_{jhd} should be compared to the next simplified equations,

$$V_{\text{jhd}} = \gamma_{\text{Rd}}(A_{\text{sl}} + A_{\text{s2}}) f_{\text{yd}} - V_{\text{c}} \quad \text{(for interior joints) and} \tag{8.13a}$$

$$V_{\text{jhd}} = \gamma_{\text{Rd}} A_{\text{sl}} f_{\text{yd}} - V_{\text{c}} \quad \text{(for exterior joints).} \tag{8.13b}$$

γ_{Rd} is equal to 1.2, A_{sl} and A_{s2} are the beam top and bottom reinforcement, and V_{c} is the shear force in the columns above the joint, taken from the analysis.

To have a comparison on these important local assessments, the formulation of the Italian Code [DM 2008] is used. The major difference between both approaches is that this code is specifically prepared to verify this failure on existing buildings, structures without seismic provisions. It separates the maximum diagonal compression and tensile stress in the joint core which needs to be compared with the concrete strength, respectively suggested through the equations,

$$\sigma_{\text{nt}} = \left| \frac{N}{2A_{\text{g}}} - \sqrt{\left(\frac{N}{2A_{\text{g}}}\right)^2 + \left(\frac{V_{\text{n}}}{A_{\text{g}}}\right)^2} \right| \quad \leqslant 0.3\sqrt{f_{\text{c}}} \quad \text{and} \tag{8.14a}$$

$$\sigma_{\text{nc}} = \frac{N}{2A_{\text{g}}} + \sqrt{\left(\frac{N}{2A_{\text{g}}}\right)^2 + \left(\frac{V_{\text{n}}}{A_{\text{g}}}\right)^2} \quad \leqslant 0.5 f_{\text{c}}\ . \tag{8.14b}$$

The concrete strength, f_{c}, should be used in MPa, A_{g} is the horizontal section area of the joint core, N is the axial force on the upper column and V_{n} is the shear on the upper column plus the shear transmitted by the reinforcement bars of the beams, calculated by,

$$V_{\text{n}} = \gamma_{\text{Rd}} A_{\text{sl}} f_{\text{yd}} (1 - 0.8\upsilon_{\text{d}}) \quad \text{(for interior joints) and} \tag{8.15a}$$

$$V_{\text{n}} = \gamma_{\text{Rd}} (A_{\text{sl,inf}} + A_{\text{sl,sup}}) (1 - 0.8\upsilon_{\text{d}}) \quad \text{(for exterior joints),} \tag{8.15b}$$

where υ_d is the normalized axial load on the joint.

8.3.1 Parnaso

The final results for all the verifications are summarized on the table 8.2. The analyses were made considering two different envelopes, one with the higher compressive load, and its respective shear, and also the reverse. The formulation by the Italian Code, for the compressive strength of the diagonal strut is slightly more conservative, and is higher using the maximum shear stress as parameter. The safety verifications from both codes are not very different on these results, by the ratio of strength and capacity. The higher conservative character is adequate to the verifications on joints and type of structure because of the reason pointed before.

Table 8.2: Joints failing in shear demand according to EC8 and NTC8 for diagonal compressive and tensile(*) strength for Parnaso.

Earthquake	Longitudinal			Transversal		
	Compressive		Tensile	Compressive		Tensile
Code	EC8	NTC8	NTC8*	EC8	NTC8	NTC8*
N_{max}	2.7%	3.6%	66.4%	2.7%	2.7%	70.0%
V_{max}	2.7%	6.4%	62.7%	2.7%	6.4%	61.8%

Regarding the joint failure on the tensile diagonal strut the results show a very conservative verification. According to Paulay [Paulay and Priestley 1992], even with the joint cracked, the joint panel and reinforcement can continue to transfer shear forces, therefore the joint failure should be only considered by the compressed strut crush. It is also referred that for high axial loads, the compressed crushing should be verified before the tensile cracking.

The joints which are failing on compressive crush are the located on the first and second storey, the three interior columns of the building, and on the three columns of the longitudinal façade which has no indirect columns. This is valid for both earthquakes. The percentage is referring to 110 nodes, so no more than 10 joints are failing. Without the use of the safety factor, the achieved verification would be 100%.

Even if the building still holds capacity left without, the importance of joints is high, so the correction should be performed without restrictions.

8.3.2 Costa Cabral

The compressive failures on this building, until the convergence problems, are verified on about 10% of 400 joints and mainly on the interior joints of the second floor.

8.4 Local Interventions

Among some solutions for local retrofitting, are the bracing, the concrete (or steel) jacketing and introduction of Fibre-Reinforced Plastic (FRP) on elements. Bracing would not be a good intervention on this structure because it does not need to be increased in terms of stiffness, with a consequence of increasing also the stresses on the rest of the elements. Jacketing would be a good intervention since it would correct some design issues of strong beam-weak column, with masses, stresses and ductility increased. This would

be particularly recommendable for the thin columns on Costa Cabral building. FRP is a solution which does not increase directly the strength of the elements, does not increase the masses of the building but takes a key role on increase of ductility and confinement of concrete elements. This is very applicable on structures which have deficiencies on the construction techniques like hoops on stirrups made by 90 degrees, where some lapped bars needs to be confined and where the slippage of bars has a big influence on global response.

The option consists on using the characteristics of composite materials formed by polymer matrix, which is reinforced with fibres. The union has high strength towards tensile stresses, and can be applied on the elements like a jacket, by strips or even continuously by sheets. For seismic reinforcement, is required to apply the material fully wrapped in the case of columns and at least U-wrapped on beam elements, and the fibres should be parallel with the parallel with the development of the elements. Summarizing, the benefits of this material are the increasing of the shear capacity of columns and walls (introduced by the capacity of the aligned fibres with the transverse demand), increasing of the flexural strength on beams and columns (by the fibres which are along the member) and increasing of ductility (by the wrapped cross-sections, which increase the confinement and length of the plastic-hinges).

Some calculations, according to the EC8-3 were made to check the influence of the FRP on the Parnaso building. Using a FRP commercial product, based on carbon fibre, SikaWrap Hex-230C, with a thickness of 0.12 mm, all the shear failures in all the members are corrected with just one layer. Fully wrapped on the columns and U-wrapped on the beams were applied with results shown on the table 8.3.

Table 8.3: Verification of shear with FRP.

Shear Elements		Assessment		FRP	
	Direction	22	33	22	33
a	max	0%	10.6%	0%	0%
	min	0%	7.2%	0%	0%
b	max	0%	9.7%	0%	0%
	min	0%	5.8%	0%	0%

In terms of rotations no verifications have been performed but, from the confinement of the sheets, which increase the ultimate deformation of the concrete has a direct impact on the increase of the ultimate rotations capacity. Some experimental work shows that its application can decrease the plastic hinge length, therefore no further conclusions should be taken on this topic before the available final results.

A superficial verification in terms of jacketing was performed to check what was lacking on the columns of the Costa Cabral building. The conclusion is that, just by increasing the cross-section of the very thin columns on the last three floors by 5 cm (from 20x20 cm to 25x25 cm), the collapse on those last floors are not achieved for even for an earthquake with a return period of 975 years, therefore, the global capacity on the building can be achieved by some small but important interventions.

8.5 Fixed-End Rotation

The slippage is a very complex topic and there is no easy way to implement it on the analysis. The actual integration with the length of the plastic hinges has been one prompt way to include it on the analysis. The most accurate possible analysis would be the consideration of the tensions between the steel and the concrete, along all the length in all the elements. These type of analysis should be extremely time consumer, and maybe with convergence difficulties due to the increase of complexity. Although the SeismoStruct has no current integration of the steel slippage, other programs like OpenSees it can be modelled for some simple examples.

One simulation to check the possibility of having another simplified integration was through a decrease of the young modulus of the steel. From experimental works comparing the moment-curvature of elements with deformed bars and smooth bars is possible to calibrate the elastic modulus of steel of the steel bars to achieve the same levels of deformations. In a paper yet to be published, by the researcher José Melo, is proposed a correction of relationship of stress-strain to compute a closer behaviour of moment-curvature when in presence of slippage. The proposed model upgrades the well-known bi-linear relationship to a tri-linear relationship which increases the extensions for similar stresses. The corrected relationship is presented on the figure 8.4. Through this approach

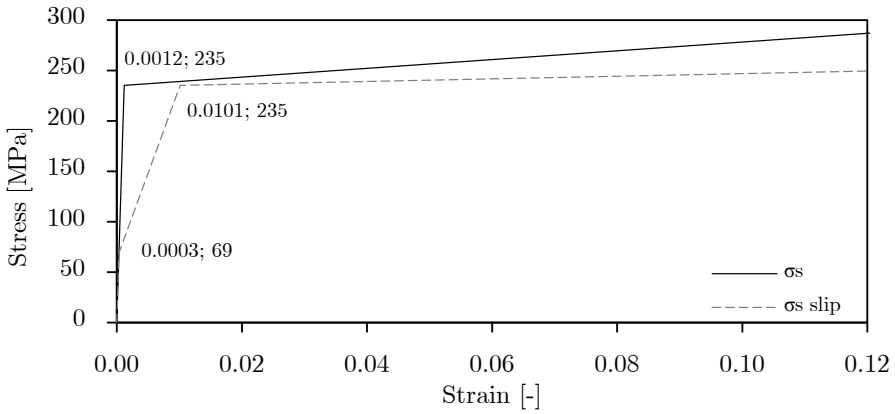

Figure 8.4: Stress-strain relationship with and without the consideration of slippage.

is possible to simulate higher strains (deformations) for a similar level of stress.

To integrate it on the analysis, the steel proprieties were corrected with this reduction of elastic modulus and, it was used a half height of the centre column on the first storey of the Parnaso building, as a cantilever, assuming that the shear span of the element is L/2. The top of the column was loaded with the static axial load from the seismic combinations and with a variable lateral load also on top, analysed for both direction separately.

The results are summarized in the figures D.7 to D.10 on the appendix. It was plotted the hysteretic curves of base-shear with top displacement, and moment-rotation for both directions of the cross-section. It is shown that, using the reduction of the young modulus on steel to track slippage, the results tends to present higher deformations and less capacities of shear and moments, compared with the "half plastic-hinge length" of

the initial modelling. For the direction of the reinforcement, it shows a progression of deformation 100% for the "slip" model.

To check both modellings may be necessary to perform a comparison with experimental results, to guarantee if the deformations are still lacking in terms of accuracy. Even if the present results are not completely conclusive, they prove the importance in considering the steel slippage and, alerts for the possibility that the performed modelling in the dissertation may still lack on the deformation accuracy of existing old buildings.

Chapter 9

Final Remarks

This chapter intends to provide an overview of the main conclusions of this dissertation and the prospects of future works which can be continued and completed ahead.

9.1 Main Conclusions

The main objectives for the dissertation were the modelling and calibration of existing concrete buildings followed by dynamic characterizations and assessments according to informative and regulative formulations. To perform the work were used two existing buildings of reinforced concrete, built without seismic provisions which were lacking on the first concrete codes.

The modelling of existing structures lack formulations to compute the influence of slippage, so as a consequence, there is no accurate way to compute real rotations of the fixed-ends. Thus, the global assessment should be performed through some assumptions, such as the reduction of the plastic hinge (concentrating the curvature progression in a smaller length) and the introduction of spring elements on nodes (linking the various elements through some strength/deformation limits in accordance with experimental work), this latter more laborious. Analysing in an element level, the contribution of the slippage on the fixed-end rotation may have an impact up to 90% on the total deformation of the element, according to [Verderame *et al.* 2008a, Verderame *et al.* 2008b].

The modelling surpassed various challenges of research and iterative correction until having the final numerical structures, with and without the infill panels. Some important conclusions on this theme are summarized. A good way to proceed on modelling is to use force-based formulation with concentrated inelasticity in the fixed-ends of the elements. The force-based analyses are faster, stable, and allow the definition of plastic hinges to indirectly integrate the influence of the smooth bars. For short elements may be useful to use a displacement-based formulation to avoid convergence deficiencies. To avoid spurious results, the constraints of floors to simulate the stiffness provided by the slabs should be carefully defined, avoiding excessive flexibility of the beams, or introduction of an unreal stiffness if the slabs are expected to have high flexibility, by carefully choosing the parameters and nodes to constraint. The calibration of Crisafuli for the infill panels may be accurately adaptable to most cases, with a reduction of 50% or none, respectively for panels with and without openings, relating to the exposed procedure. Therefore, if there is no possibility to perform experimental work to know the natural frequencies, a

reasonable application with this procedure may be applied with a small reduction factor to increase the safety accordance.

Various formulations to expeditiously compute the natural frequency have a good match. Hereupon, the simpler formulation of Aničić may be used as a fast/direct to have a general idea of the natural frequencies for concrete buildings in Portugal, for regular architecture. This may not be considered an accurate value in directions with very slender elements, to which has the possibility of a higher period due the higher flexibility. The infills increase the frequencies from 2 up to 2.5 times the frequencies without infill panels. Combining the formulation Aničić and then adding up these factors, a good agreement of range to the natural frequencies may be achieved.

The infills have a big impact. If somewhat they are not equally distributed on the building, or if the building is slender, it can not only affect the modal shape, but more importantly, switch the directions of the natural mode shapes, and so, introducing different participation on different directions.

If the infills are distributed on all height of the building, there is a tendency to have higher drift demands on the bottom floors due to the collapse of infills on these storeys. If some floor, on the ground level or another, is striped from infills, there is a tendency to occur soft-storey mechanisms to which should be addressed retrofitting techniques. As the higher shear stresses are located on the base levels, so the relative deformation demand is higher on those levels. Usually, the first or second floors have a higher height, compared to the rest of the building, so the soft-storey mechanism may happen on that higher and consequently more flexible floor. If on the top levels, the columns are very thin, mechanisms may occur from there. The infilled structures tends to form soft-storey for strong earthquakes on the base level. The infills have a key role on protecting the deformations of the building until the cracking. Once it is achieved on the ground level, which has higher demand, then the other floors are continuously protected, creating a stiff body supported by these "new" unprotected columns, happening for strong earthquakes with a return period of 2000 years. The R.C. bare frame has a tendency to develop soft-storey mechanisms for much lower earthquakes at the ground level but, if upper floors have very thin columns, the strong-beam weak-columns mechanism happens, provoking the collapse.

The presence of stiff elements, as concrete walls, or a set of secondary elements, as for supporting the stairs, have a big impact on the global response due to rotation effects, a consequence of the modification of uncentred stiffness and mass.

The axial stress on columns can achieve high levels of variation. In a summarized conclusion, for high earthquake, in average it can happen in a range up to 100% for corner columns, 50% for façade columns and less than 20% for interior columns. For columns limiting the infill panels, these limits can be increased somewhere up to 2 times higher variations.

In terms of local verifications, there are a lot of different ways to compute the limits and there is no individual one which can be considered as the most conservative. The results tend to be more conservative for the theoretical approach than the empirical one. To calculate these checks, it may be safer to use the most conservative approaches regarding the uncertainties to respect the assumptions made for the R.C. building with smooth bars. If there is no possibility to compute the envelope of all combinations expected to be more demanding, the most conservative is a less axial load (reduction of compressive axial load) with shear span equal to half the length of the element. The

theoretical approach is more complex to be applied but guarantees, at least, slightly more conservative results which seem to be adjustable. Around 15% of the elements, located mostly on the first floors, do not check the imposed limits. The buildings show some deficiencies too in shear strength for both beams and columns, and also on joints. The verification of safety on just a small amount of joints is not attained, but is a very dangerous failure which should be avoided at any cost.

The verifications, at local level, have been performed with the safety factors which decreases the limits, increasing the safety margin. Without the coefficients, just a small amount of failures would be verified. From the numerical results, which are a limited portion of just two study cases, the results led to believe that, if an earthquake with similar intensity occurs in Portugal, the collapse should not occur. In Portugal, a lot of buildings tend to be built in band, so deformations are limited and lateral global strength tend to increase. In other way, the pitching effect of structures may crack some structural elements, but further investigation in these matter may be developed in future work. To avoid the formation of mechanisms due to slender columns, primary columns, the results show that these identified elements need to be strengthened through jacketing (steel or concrete) or some calibrated bracing. Reinforcing this idea, the buildings do not check the safety levels for the ultimate limit states, thus existing buildings do need retrofit, but without a predictable global collapse/failure.

The main deficiencies on existing buildings without seismic provisions, described in Varum's work [Varum 2003] are confirmed. The stirrups should be more abundant to both increase the confinement of the concrete and the ductility. Another possible harmful deficiency is on the 90 degree hoops which are easily opened due to concrete spalling. The bond and existence of lap-splice decrease the capacity, showed on the chord-rotation verifications, also contributing for the lack of flexure capacity and shear strength for both elements and joints. The influence of the infills was shown as beneficial for the building until some point, when the failure of the panels is attained, it creates an opposite effect due to increase of flexibility to where it occurs and consequently, the soft-storey mechanism. The strong-beam weak-column mechanism is evident right from the structural drawings and confirmed in terms of demands, where the columns tends to fail previously to the beams.

The steel slippage is a very complex mechanism which should be accounted to achieve accurate results for the structure response. Considering a perfect bond between the steel and the concrete, in presence of smooth bars, means an overestimation of stiffness of the structures and overestimation of energy dissipation capacity on the critical regions (beam-column), leading to an underestimation of deformations. The reduction of the plastic hinge length assumption, with empirical values, is not enough to surpass the numerical limitations. It should be combined with other approaches to approximate it to the real behaviour of these type of structures.

9.2 Future Developments

Further developments on the modelling with dynamic non-linear analysis may be taken to extent the comparison of the results. Some ways to improve it are summarised:

- The work on this dissertation is lacking on influence of direct stresses on the elements of the R.C. structure when the infill panels are integrated. To do it, is

missing the elaboration of a procedure which projects all the components of the struts by time, and combining it with the same nodes and elements.

- More and different buildings, with different dimensions, shapes, material proprieties and/or higher irregularities would increase the confidence or show some discrepancy of some of the taken conclusions.
- To compare the modelling of a building designed to sustain seismic excitation with a designed one, to check if tendencies of old existing buildings are also verified on the new ones.
- The different used earthquakes are the same one scaled to different peak ground accelerations, representing different return periods. Even if this artificial earthquake has been created to have vast and adjustable type of excitation, the analysis are only agreeable for this earthquake. If the different accelerograms with similar peak ground acceleration are used, some other deficiencies may be tracked and is a good way to understand how different and real earthquakes affects differently a structure.
- The inclusion of link elements on the elements to simulate the fixed-end rotation, and also, in a expedite way, would be useful to try to check the influence of different plastic-hinge lengths and its influence on the deformations.
- Perform further calibrations on the stress-strain curves for the Menegotto-Pinto steel model to approximate the numerical response of various elements to the existing or new empirical tests.

Appendix A

Study Case Description Support

A.1 Building Costa Cabral

A.1.1 Architecture

(a) (b) (c)

Figure A.1: Architecture of Costa Cabral. (a) Front façade. (b) Back façade. (c) Lateral section of the building.

A.1.2 Engineering

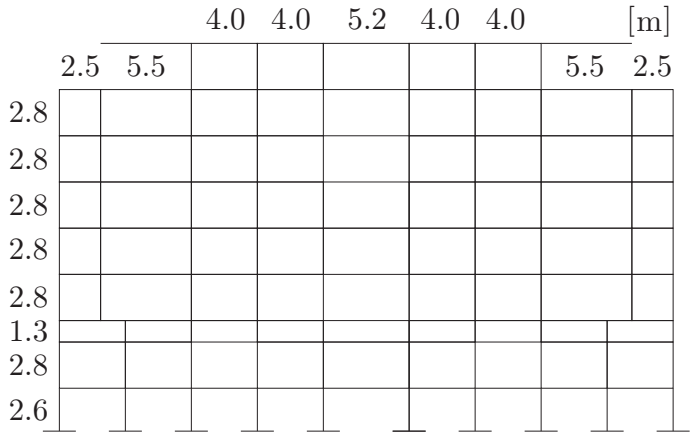

(a)

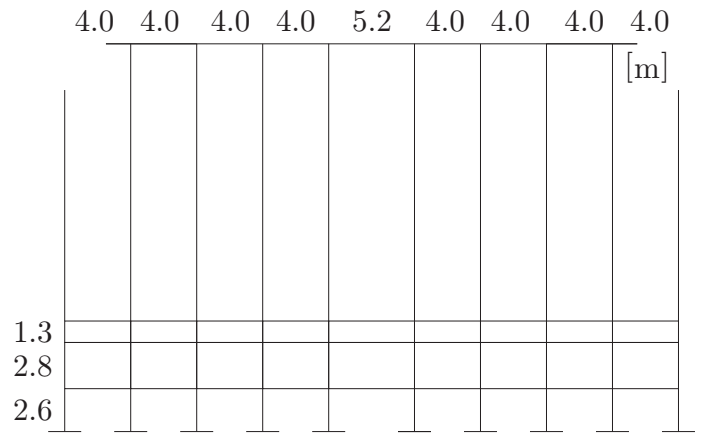

(b)

Figure A.2: Longitudinal extremity frame of (a) main façade and (b) back façade, with measurements.

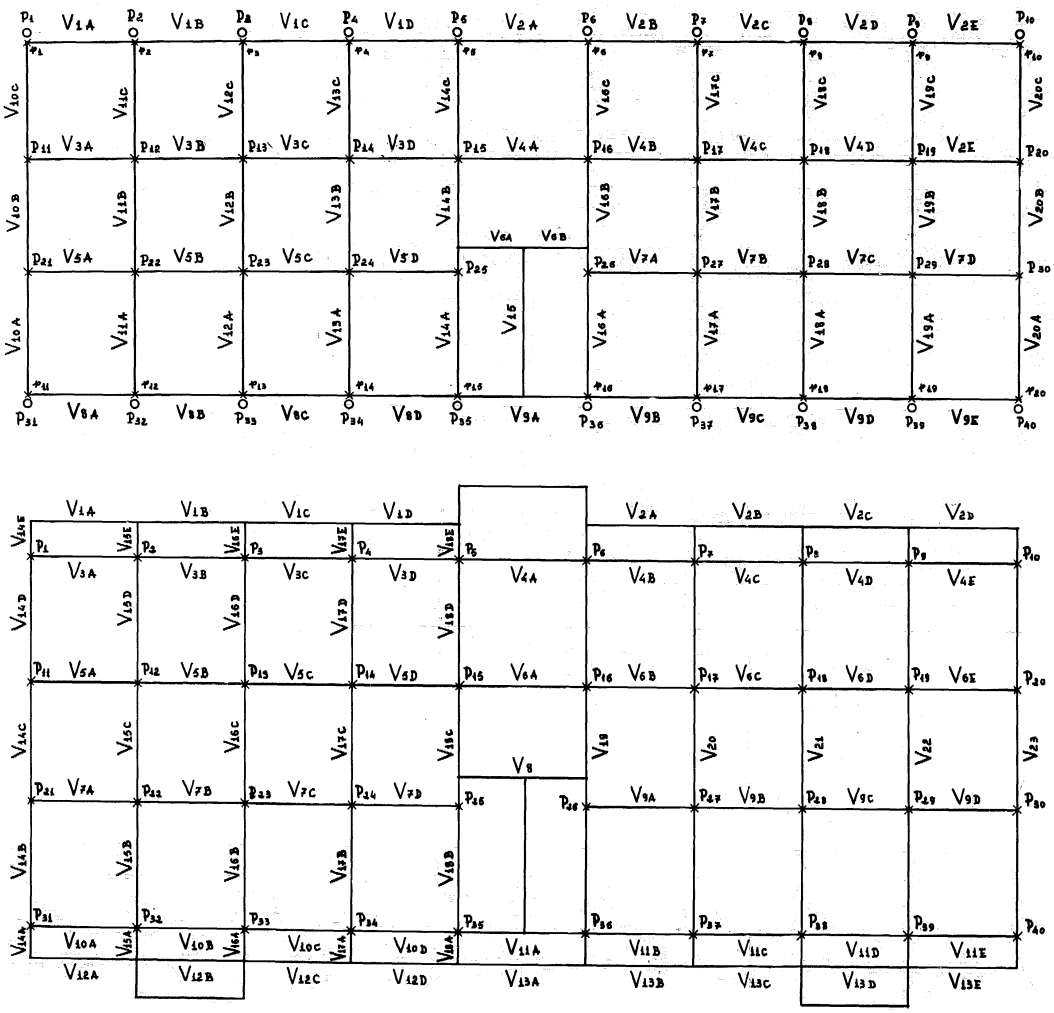

Figure A.3: Structural design for cellar and ground floor.

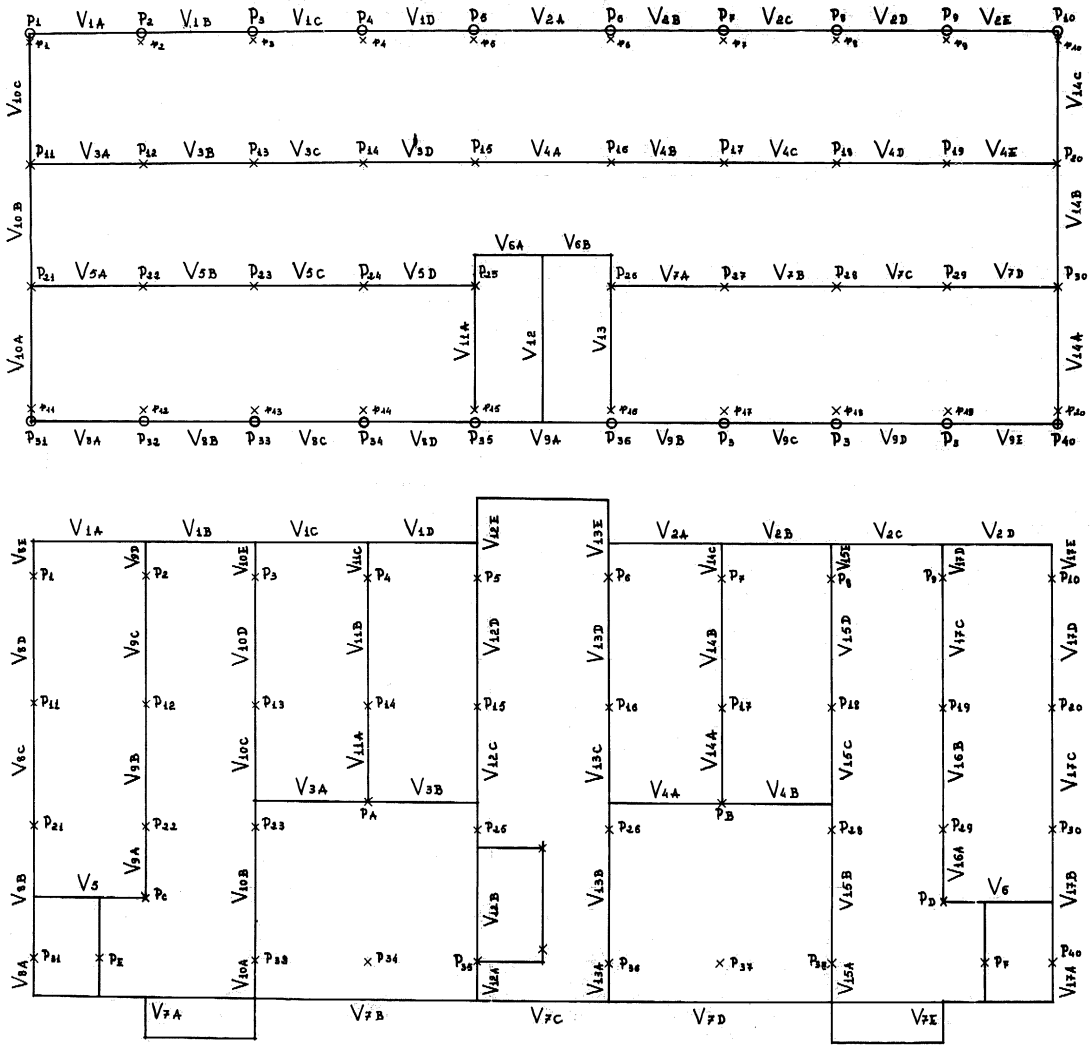

Figure A.4: Structural design for service floor and "type" floor.

A.2 Building Parnaso

A.2.1 Architecture

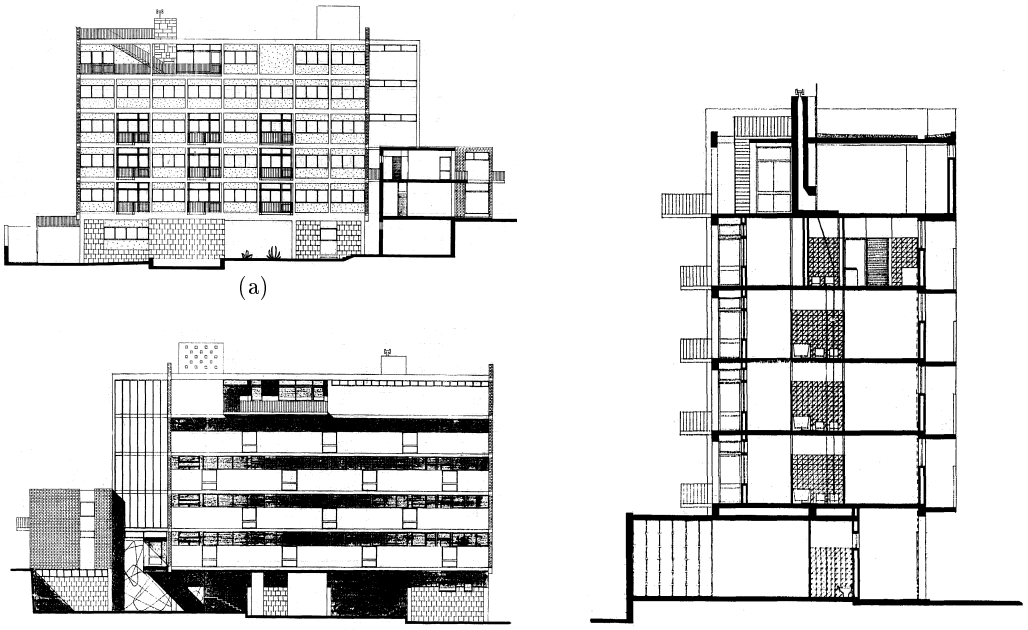

(a) (b) (c)

Figure A.5: Architecture of Parnaso. (a) Front façade. (b) Back façade. (c) Lateral section of the building.

A.2.2 Engineering

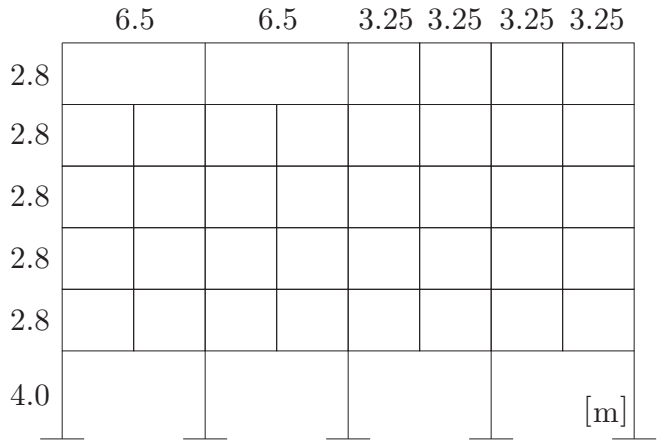

(a)

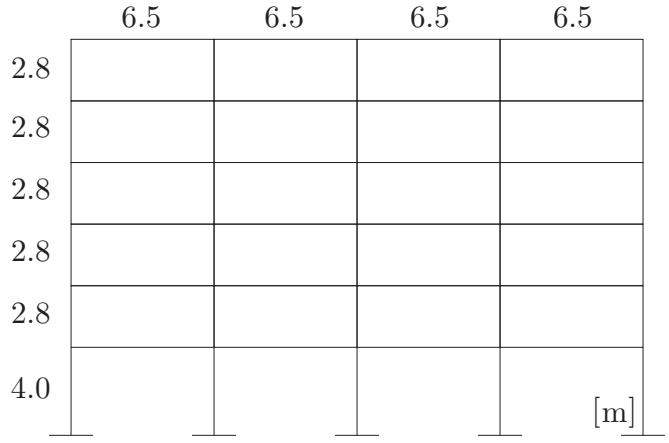

(b)

Figure A.6: Longitudinal extremity frame of (a) main façade and (b) back façade, with measurements.

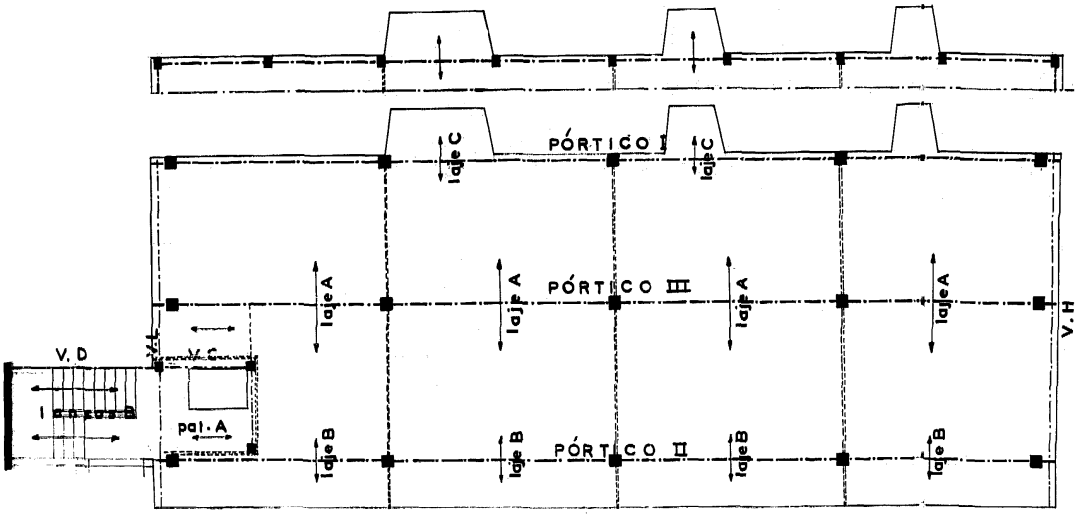

(a)

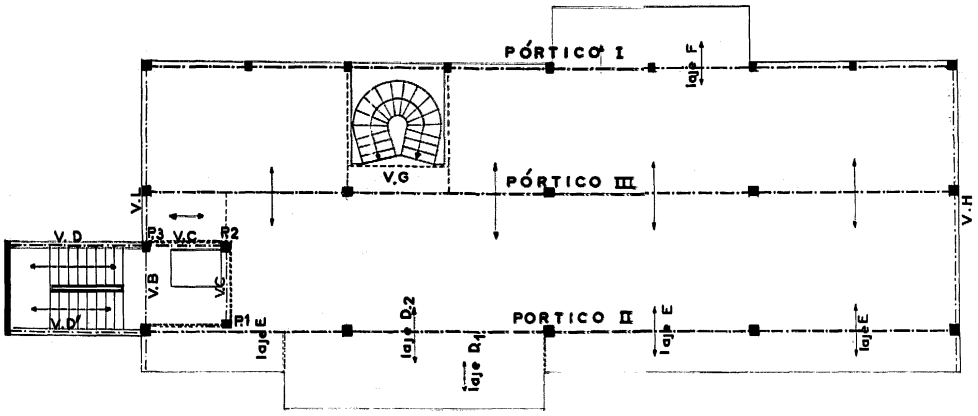

(b)

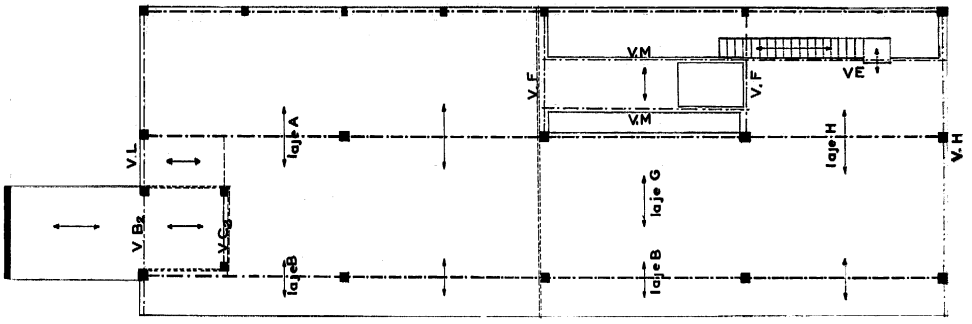

(c)

Figure A.7: Structural design. (a) First to fourth floor. (b) Fifth floor. (c) Sixth Floor.

Intentionally blank page.

Appendix B

Modelling and Assumptions Support

B.1 Location of the Infill Panels

B.1.1 Costa Cabral Building

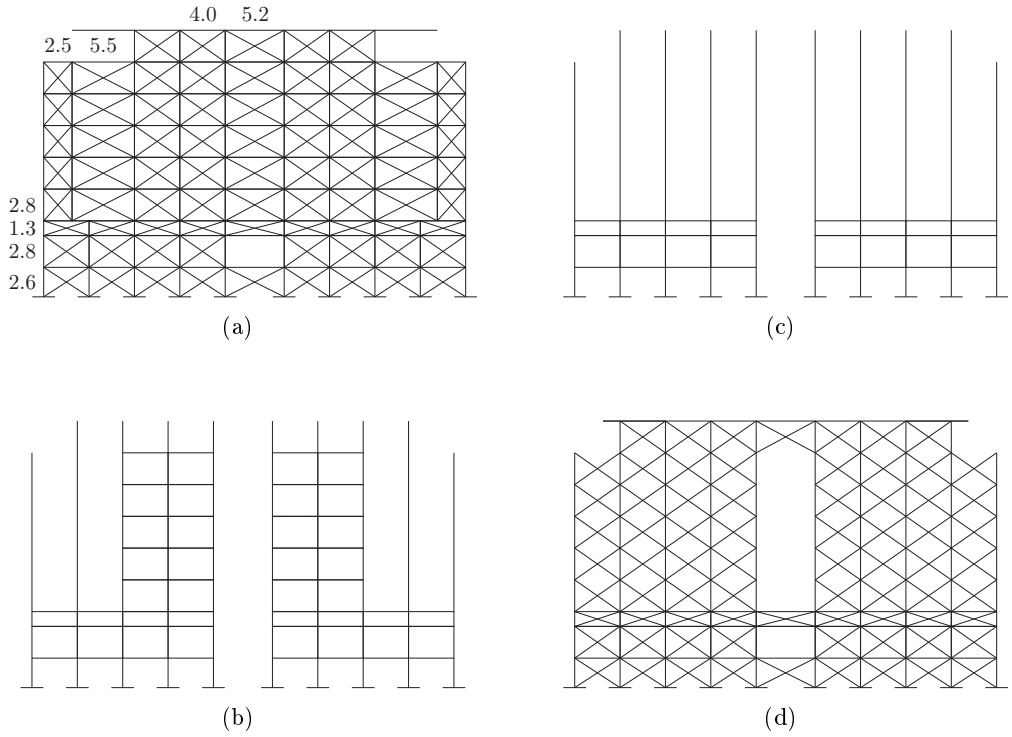

Figure B.1: Location of the longitudinal infill panels. Measures in meters. (a) Main façade. (b) Middle frame [1]. (c) Middle frame [2]. (d) Main back façade.

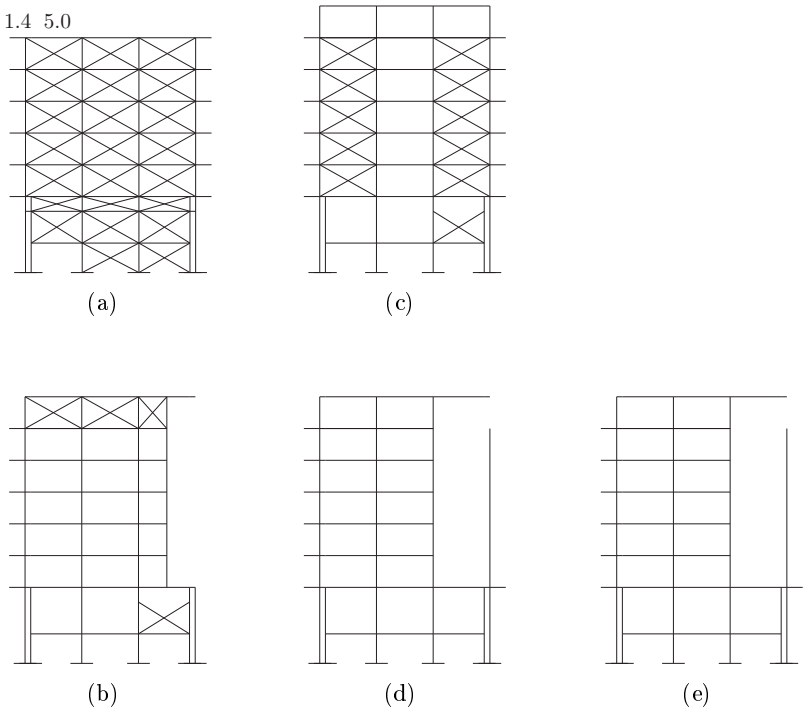

Figure B.2: Location of the transversal infill panels. Measures in meters. Four frames which are repeated once in the inverse order. (a) Lateral façade (x2). (b) Middle frame [1] (x2). (c) Middle frame [2] (x2). (d) Middle frame [3], near to half the width of the building (x2).

B.1.2 Parnaso Building

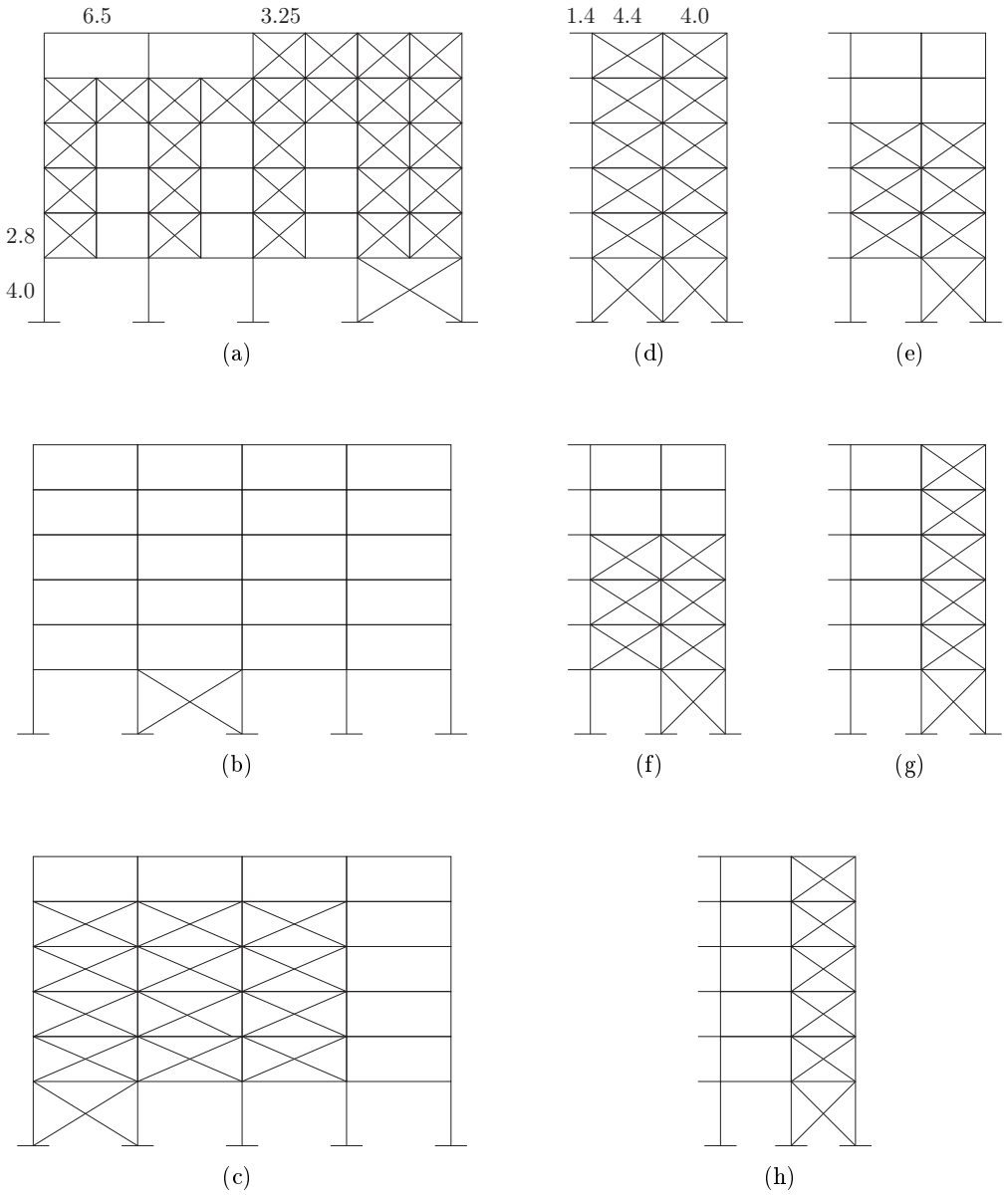

Figure B.3: Location of the infill panels. Measures in meters. (a) Main façade. (b) Middle longitudinal frame. (c) Back main façade. (d) Transversal façade, far from stairs. (e) Middle frame [1] (f) Middle frame [2] (g) Middle frame [3] (h) Transversal façade, next to the stairs block.

B.2 Empirical Results for Callibration of Natural Frequencies

B.2.1 Costa Cabral Data

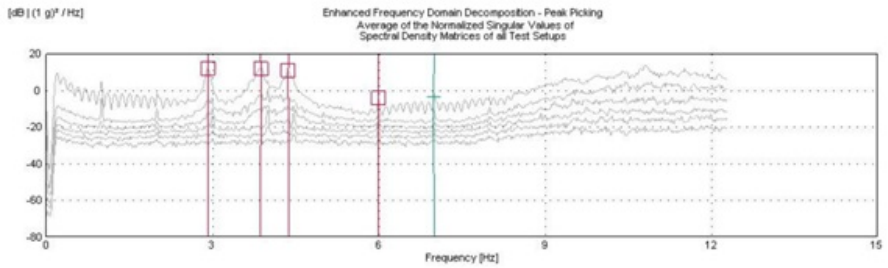

Figure B.4: Identification of natural frequencies of Costa Cabral [Milheiro 2008].

B.2.2 Parnaso Data

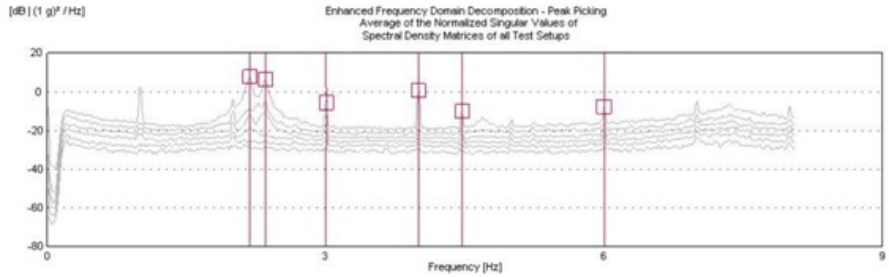

Figure B.5: Identification of natural frequencies of Parnaso [Milheiro 2008].

B.3 Print of Final Modelling

B.3.1 Costa Cabral Building

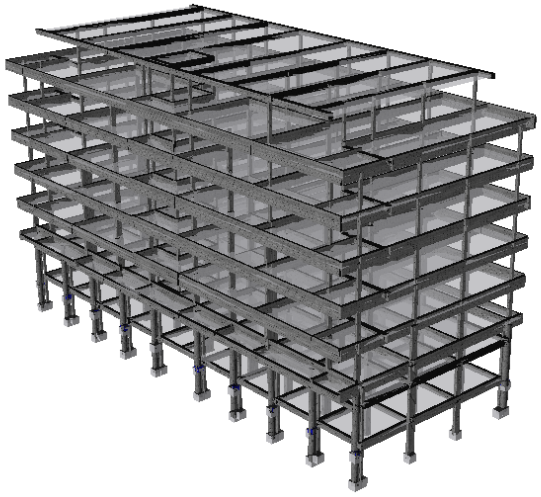

(a)

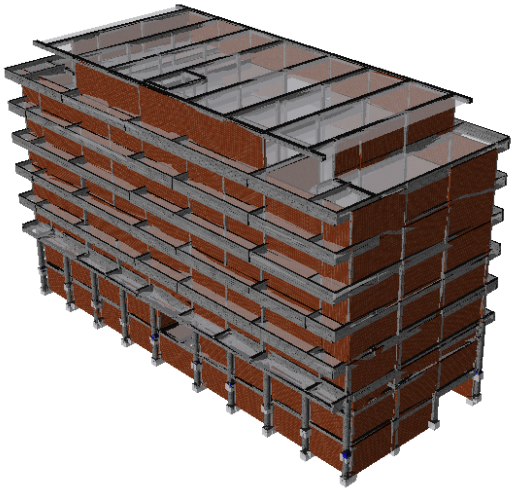

(b)

Figure B.6: Model of building Costa Cabral on SeismoStruct (a) without infill panels and (b) with infill panels.

B.3.2 Parnaso Building

(a)

(b)

Figure B.7: Model of building Parnaso on SeismoStruct for (a) without infill panels and (b) with infill panels.

Appendix C

Global Assessment Support

C.1 Costa Cabral Group

C.1.1 Displacements (For a Return Period of 475 years - Incomplete Earthquake)

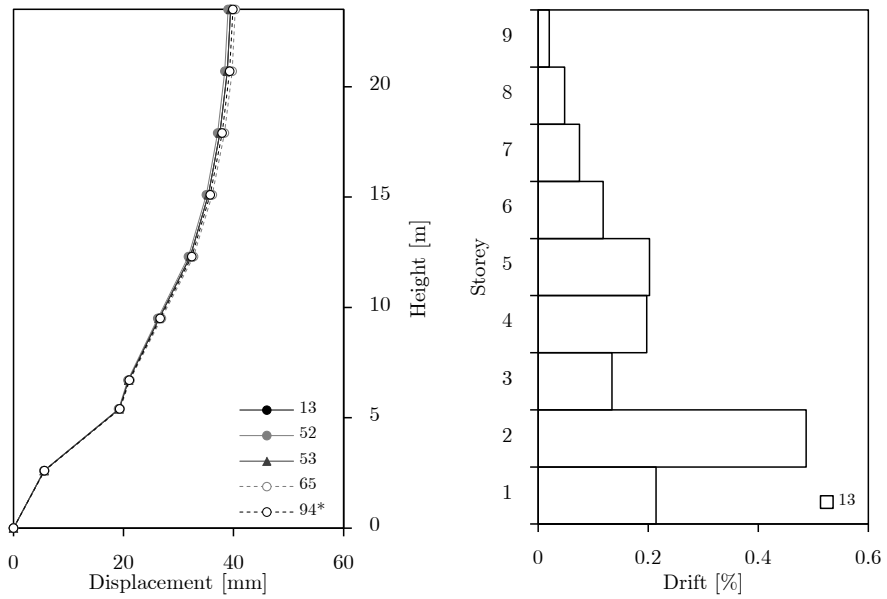

Figure C.1: Longitudinal earthquake and longitudinal response with infill panels. (a) Displacement. (b) Drift progression.

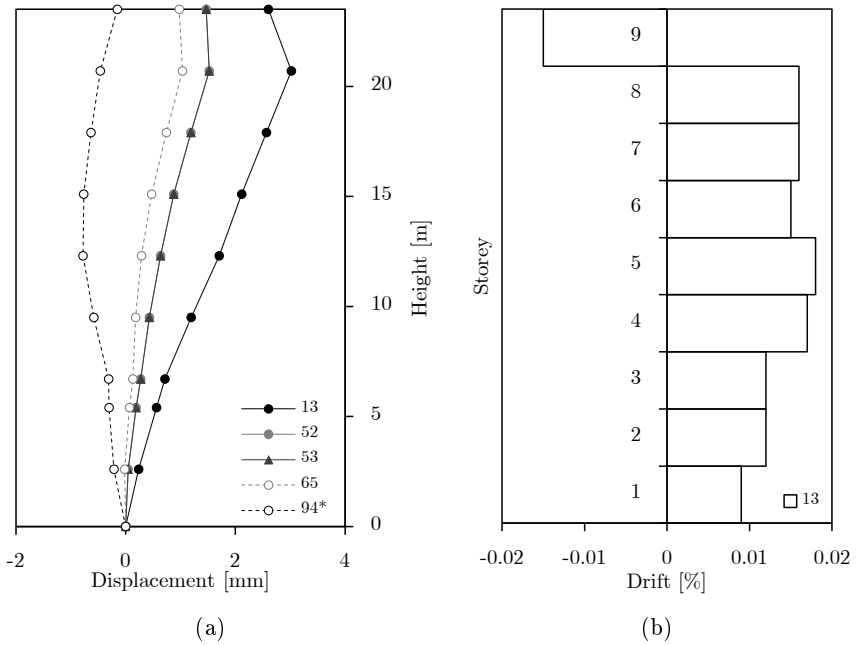

Figure C.2: Longitudinal earthquake and transversal response with infill panels. (a) Displacement. (b) Drift progression.

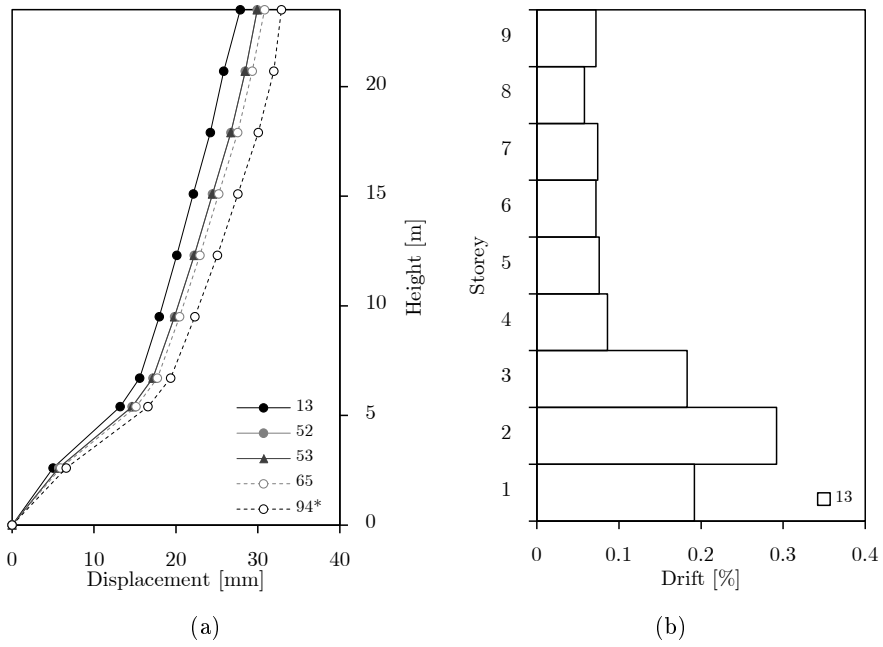

Figure C.3: Transversal earthquake and transversal response with infill panels. (a) Displacement. (b) Drift progression.

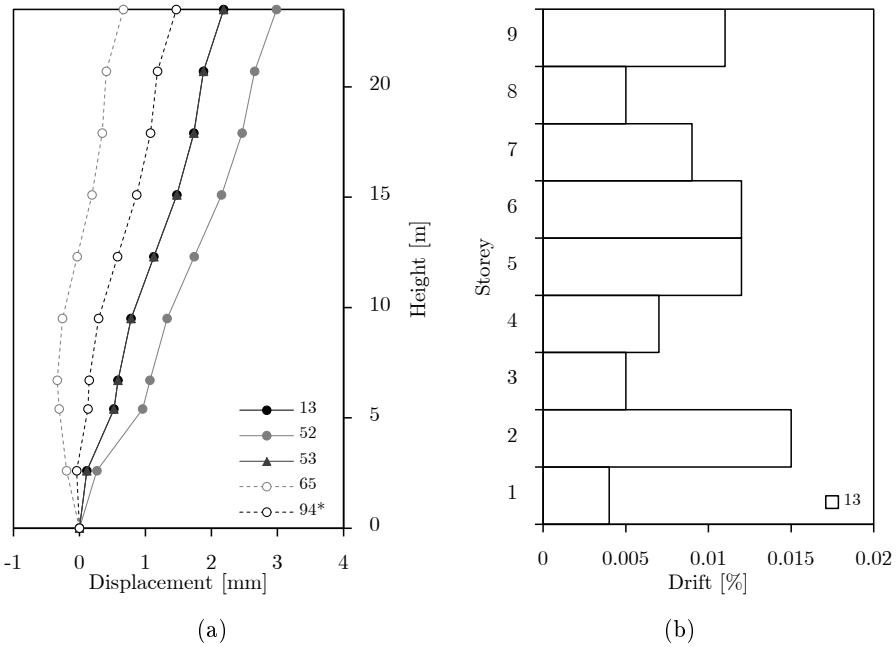

Figure C.4: Transversal earthquake and longitudinal response with infill panels. (a) Displacement. (b) Drift progression.

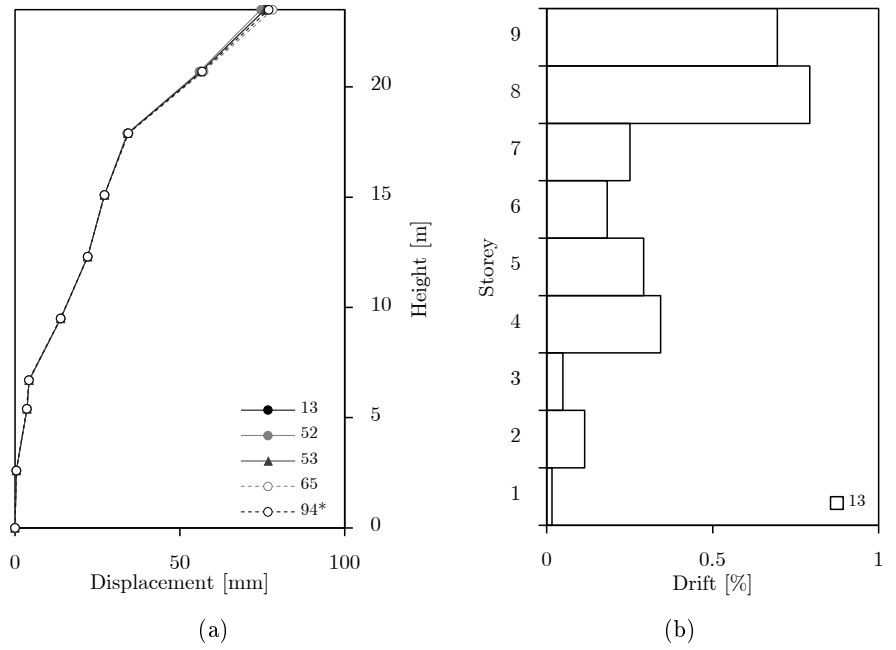

Figure C.5: Longitudinal earthquake and longitudinal response without infill panels. (a) Displacement. (b) Drift progression.

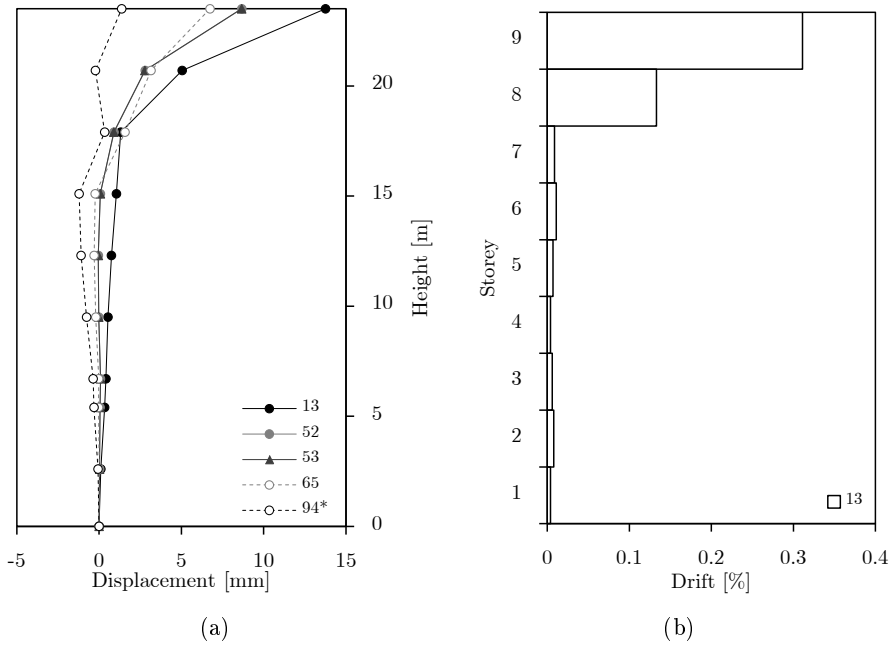

Figure C.6: Longitudinal earthquake and transversal response without infill panels. (a) Displacement. (b) Drift progression.

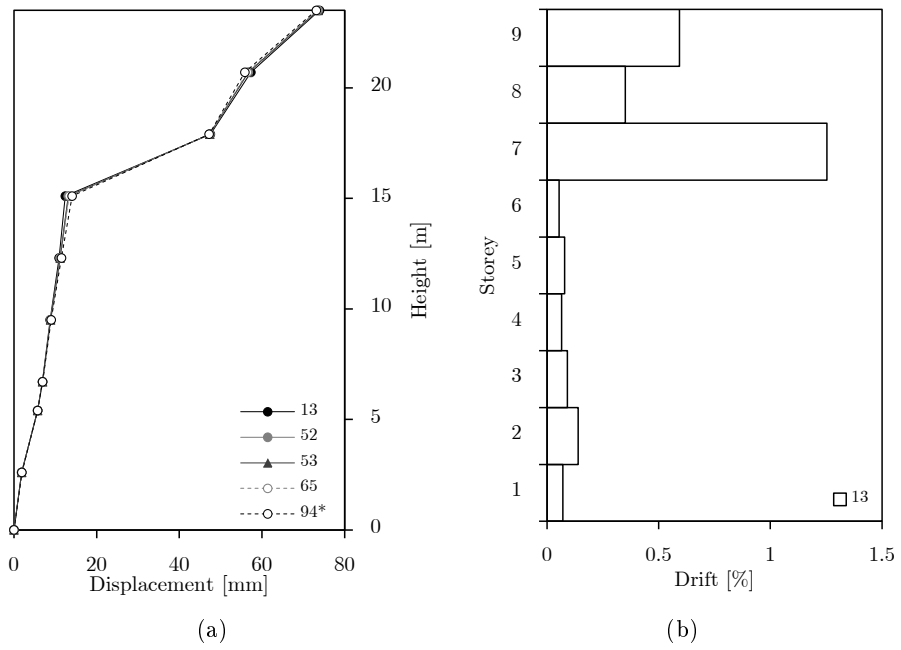

Figure C.7: Transversal earthquake and transversal response without infill panels. (a) Displacement. (b) Drift progression.

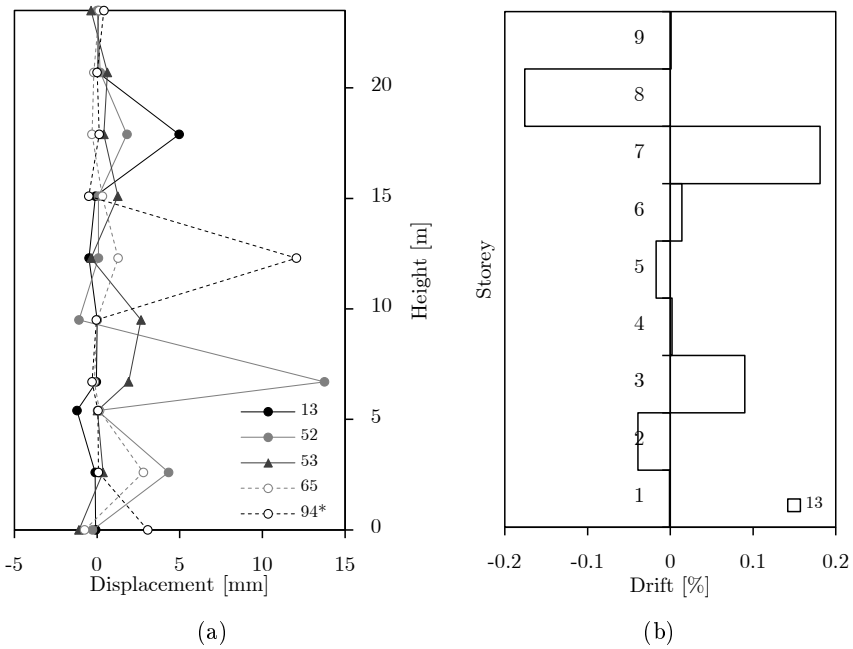

Figure C.8: Transversal earthquake and longitudinal response without infill panels. (a) Displacement. (b) Drift progression.

C.1.2 Shear Progression

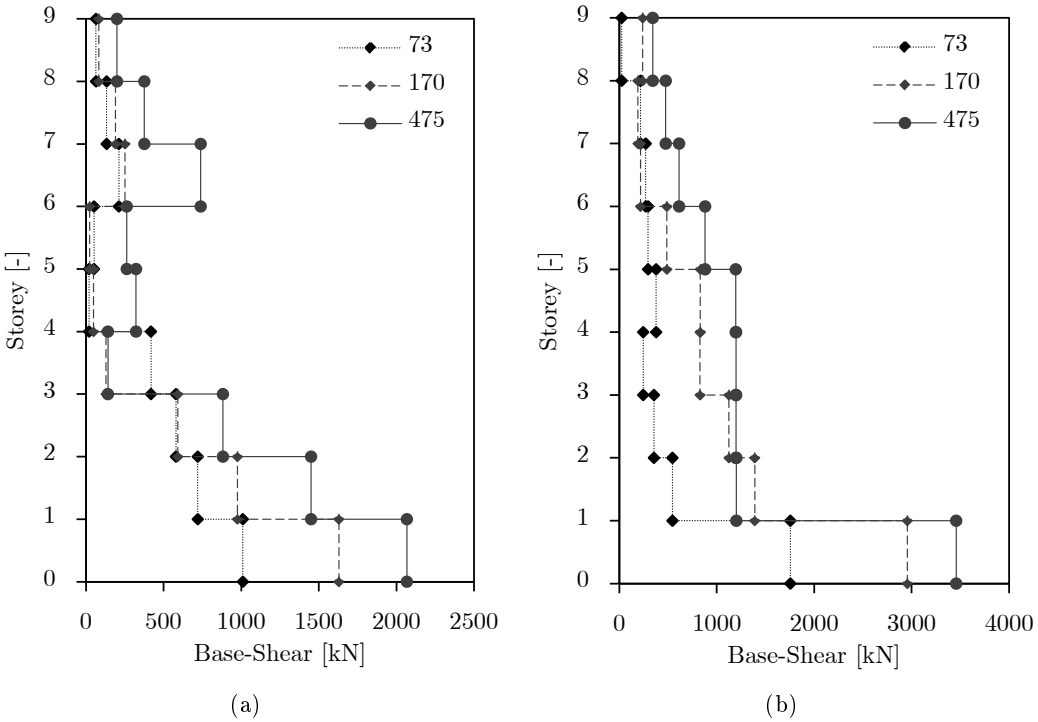

Figure C.9: Total shear on each storey, for the moment in which is attained the maximum base-shear for (a) longitudinal earthquake and demand and (b) transversal earthquake and demand.

C.1.3 Shear-Drift

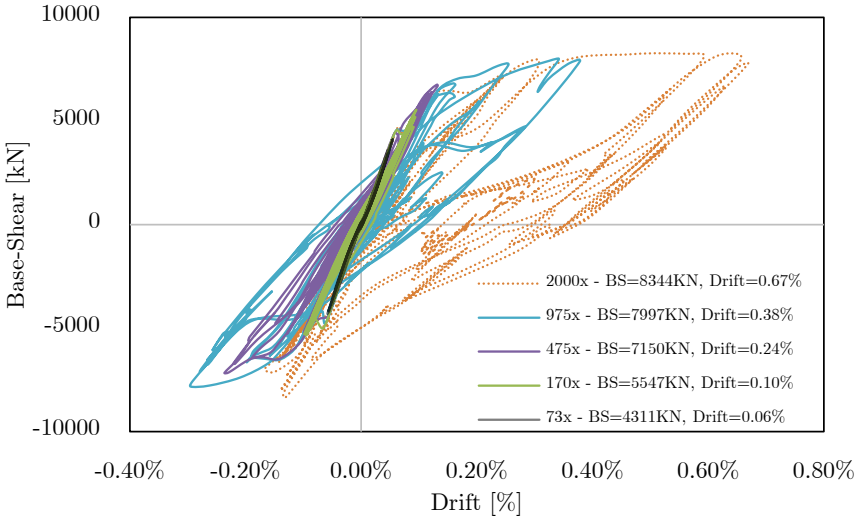

(a)

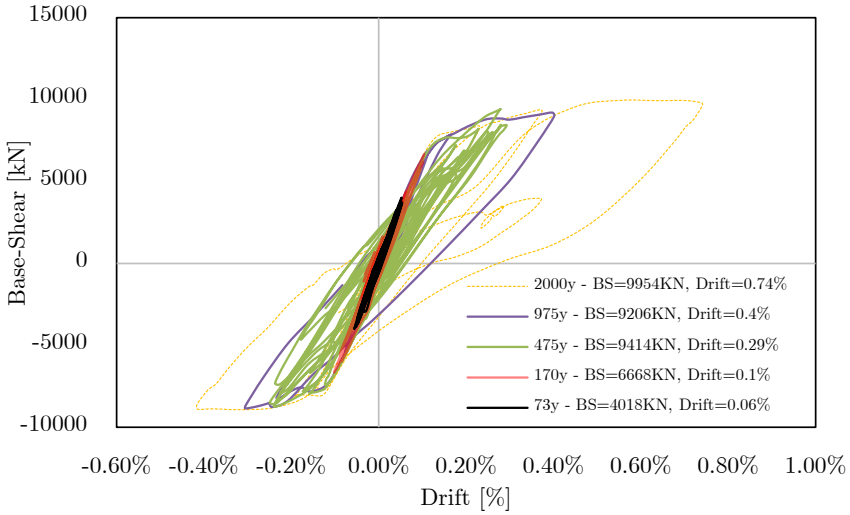

(b)

Figure C.10: Base-Shear-Drift for Costa Cabral with infill panels for (a) longitudinal earthquake and response and (b) transversal earthquake and response.

C.1.4 Shear-Drift by Floor

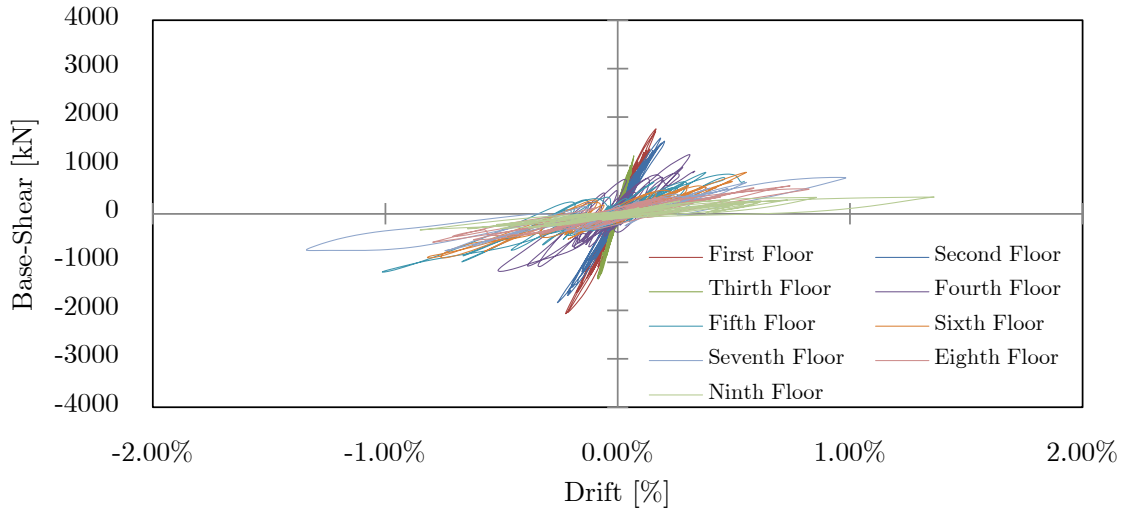

(a)

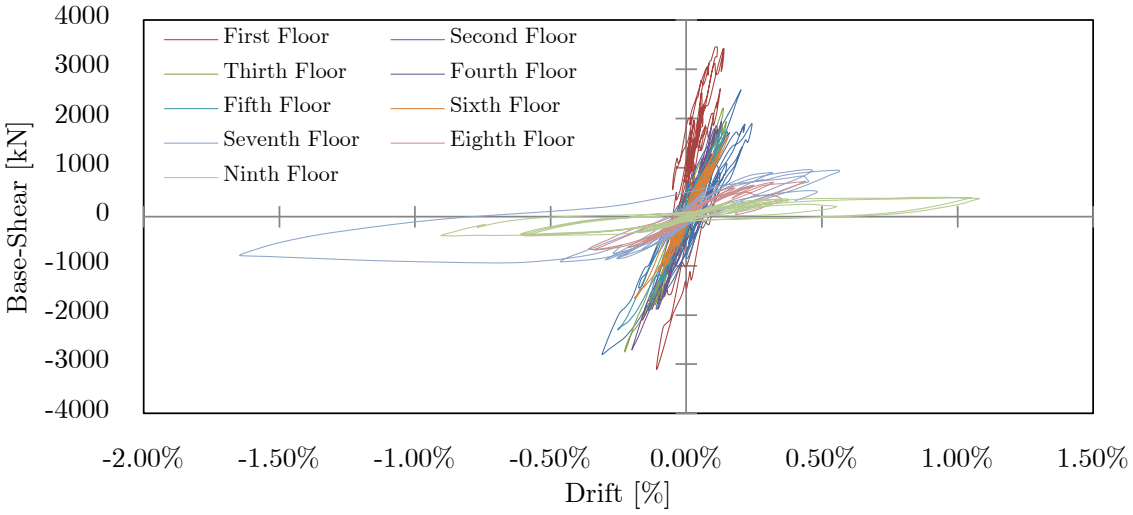

(b)

Figure C.11: Drift-Rotation progression by floor, on the centre column, for a return period of 475 years and for (a) longitudinal earthquake and (b) transversal earthquake.

C.2 Parnaso Group

C.2.1 Displacements (For a Return Period of 475 years)

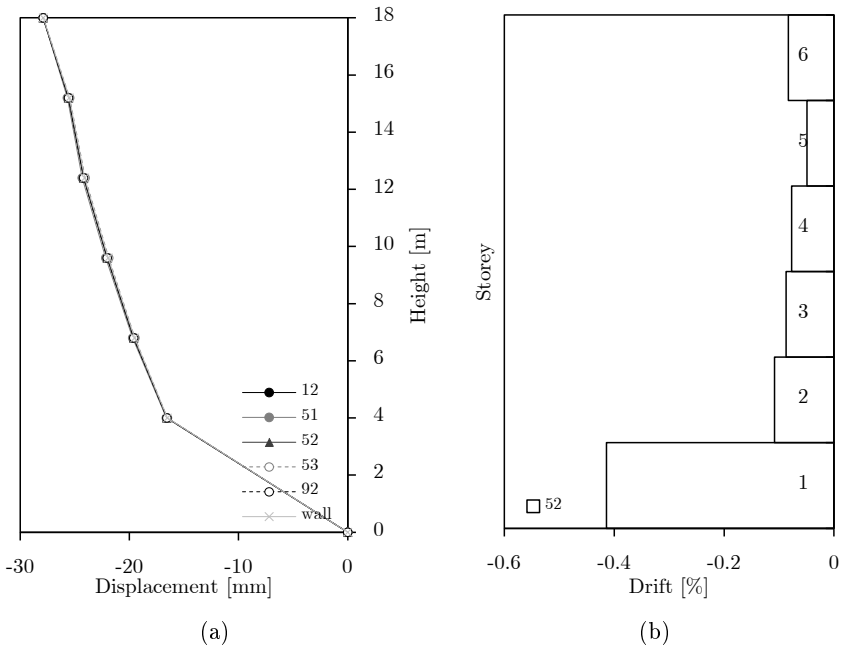

Figure C.12: Longitudinal earthquake and longitudinal response with infill panels. (a) Displacement. (b) Drift progression.

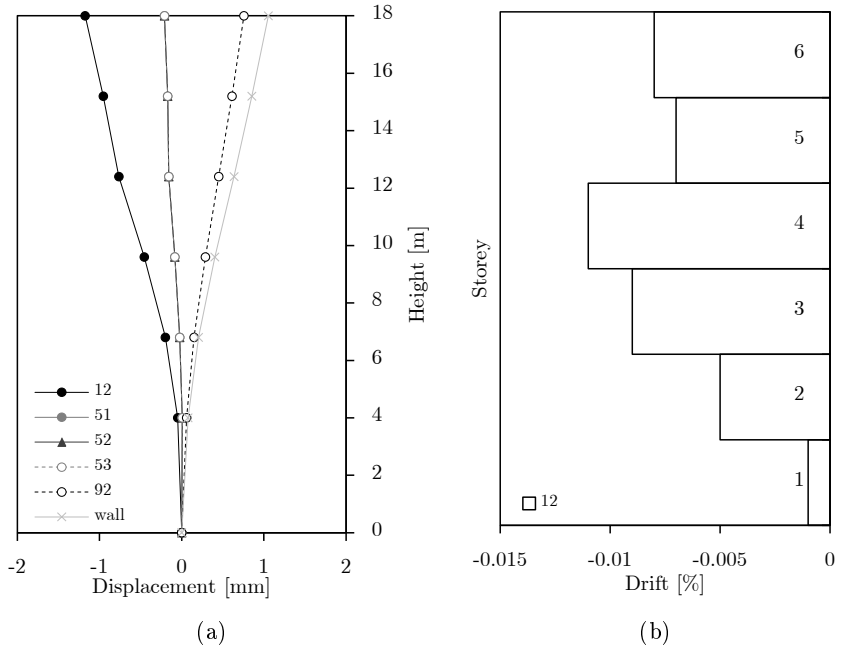

Figure C.13: Longitudinal earthquake and transversal response with infill panels. (a) Displacement. (b) Drift progression.

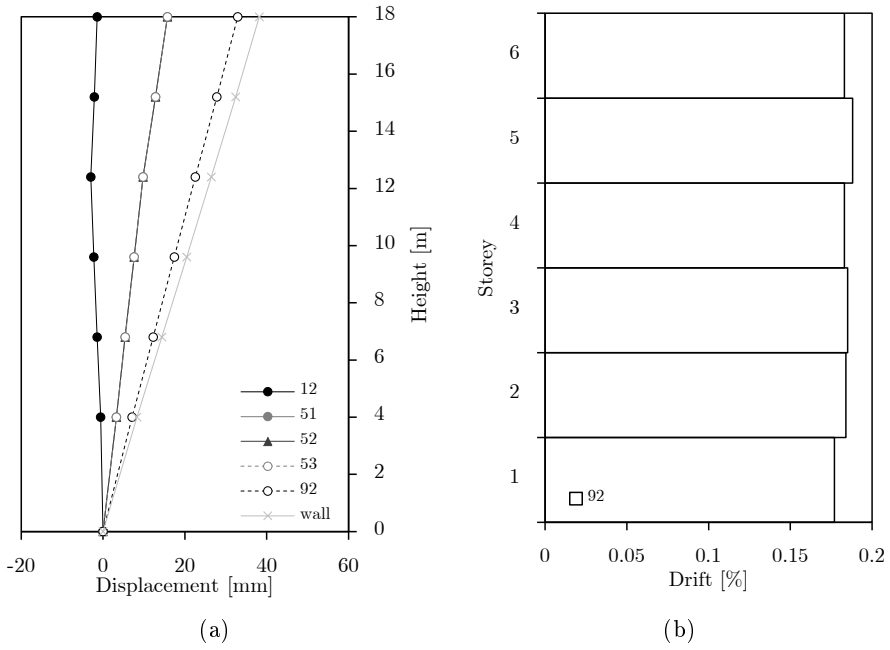

Figure C.14: Transversal earthquake and transversal response with infill panels. (a) Displacement. (b) Drift progression.

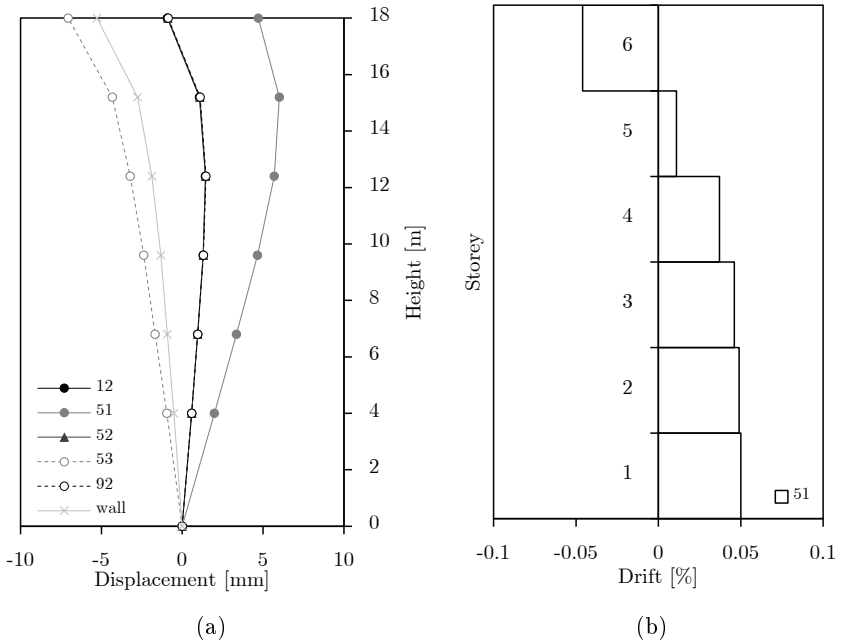

Figure C.15: Transversal earthquake and longitudinal response with infill panels. (a) Displacement. (b) Drift progression.

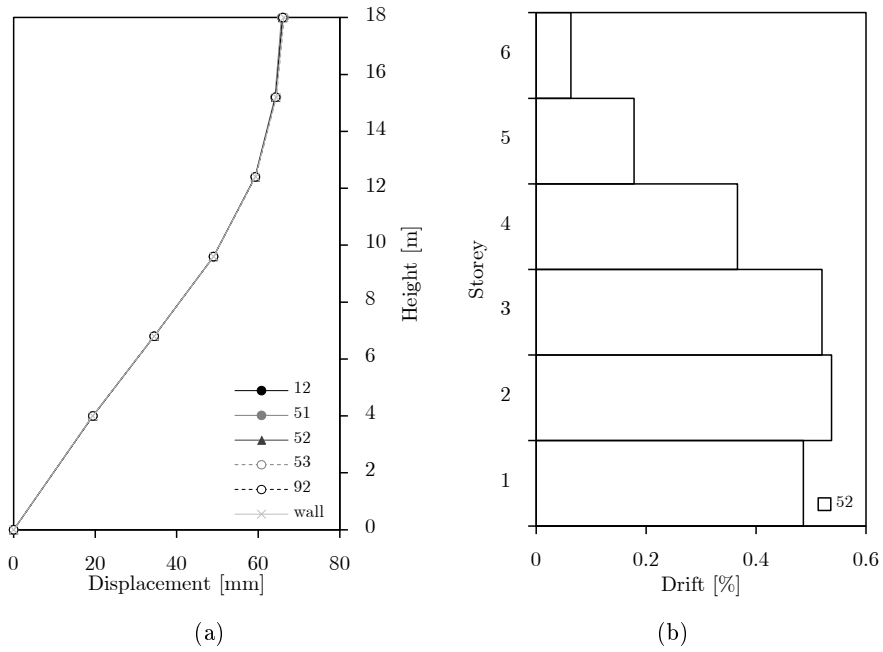

Figure C.16: Longitudinal earthquake and longitudinal response without infill panels. (a) Displacement. (b) Drift progression.

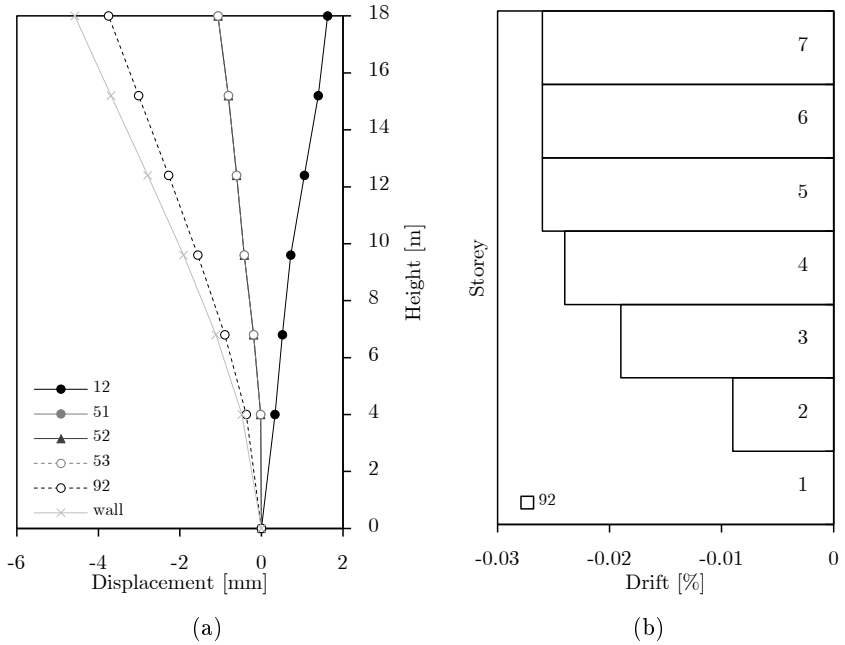

Figure C.17: Longitudinal earthquake and transversal response without infill panels. (a) Displacement. (b) Drift progression.

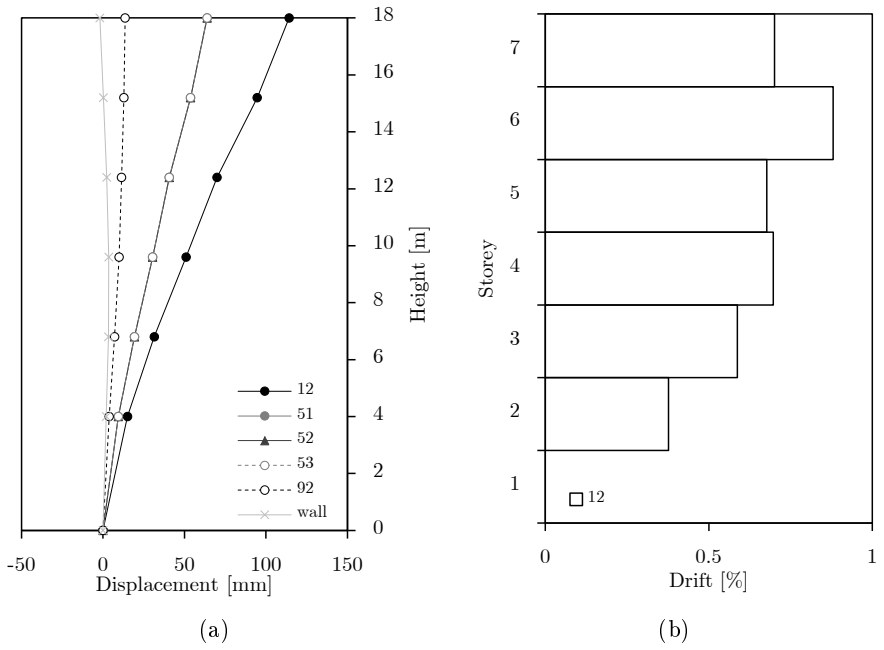

Figure C.18: Transversal earthquake and transversal response without infill panels. (a) Displacement. (b) Drift progression.

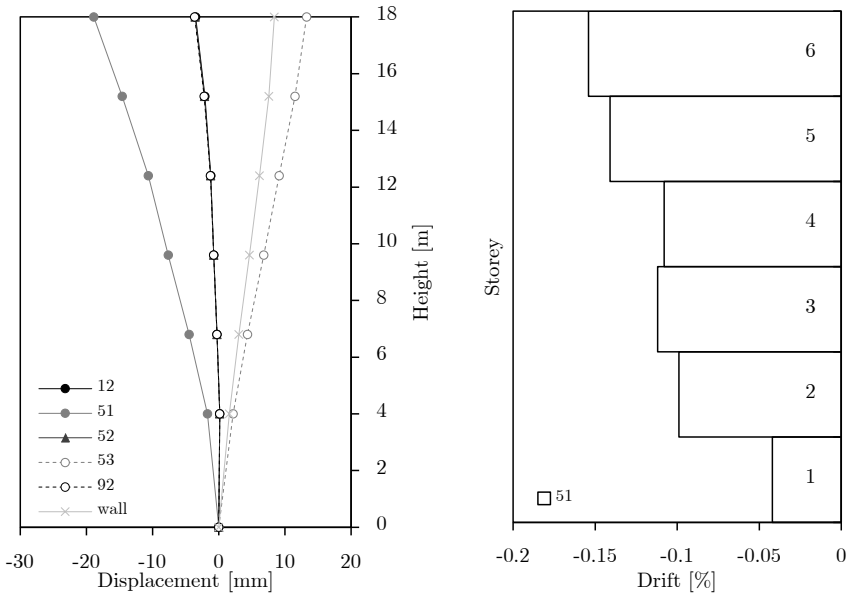

Figure C.19: Transversal earthquake and longitudinal response without infill panels. (a) Displacement. (b) Drift progression.

C.2.2 Variation of Axial Loads on Columns

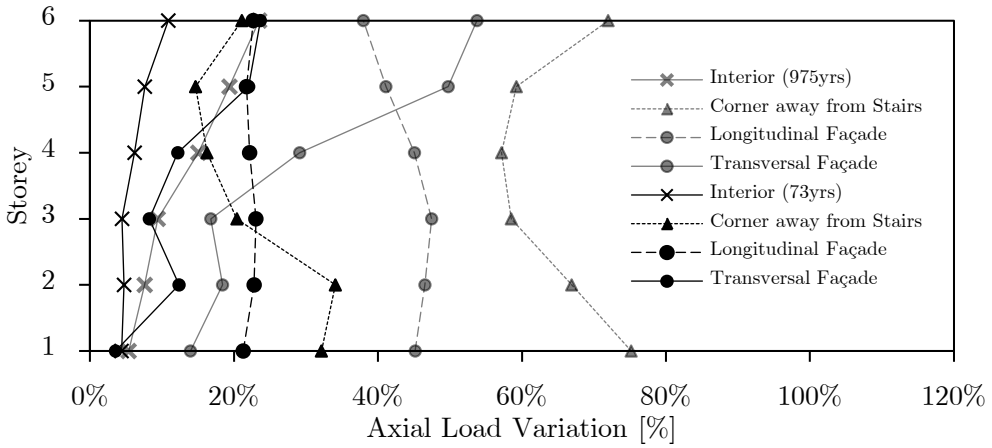

Figure C.20: Comparison between axial stress variation on columns for different places and longitudinal earthquakes with infill panels.

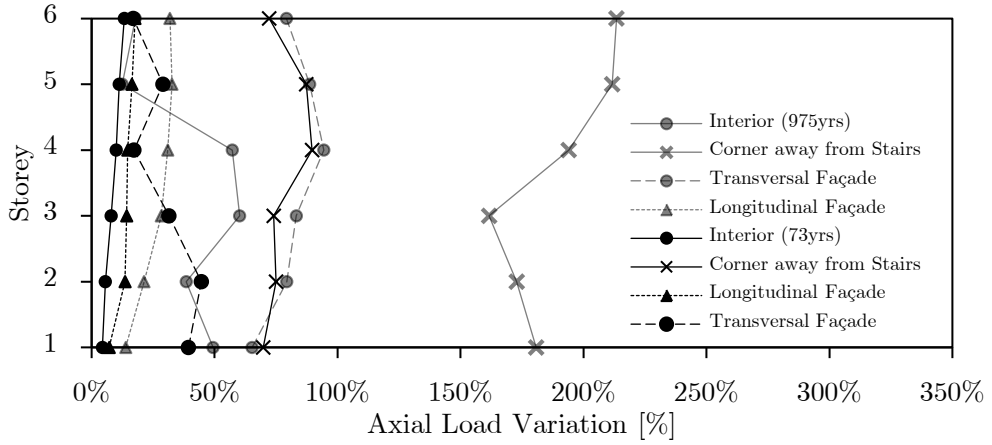

Figure C.21: Comparison between axial stress variation on columns for different places and transversal earthquakes with infill panels.

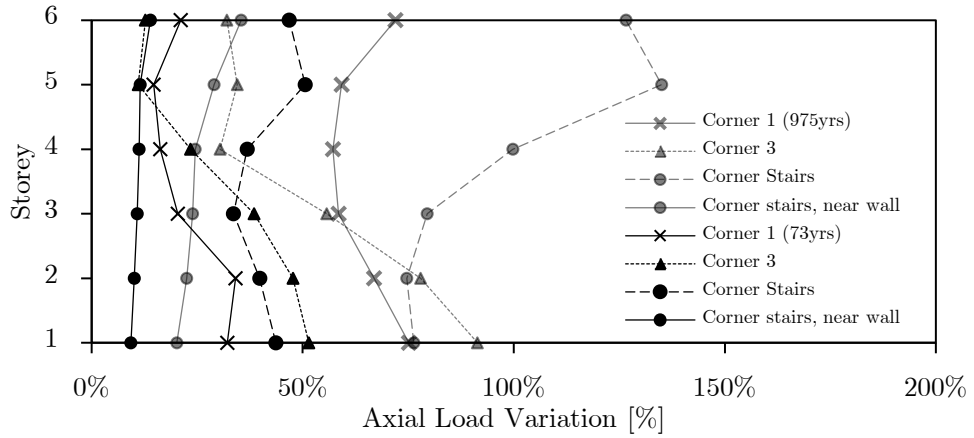

Figure C.22: Comparison between axial stress variation on corner columns and longitudinal earthquakes with infill panels.

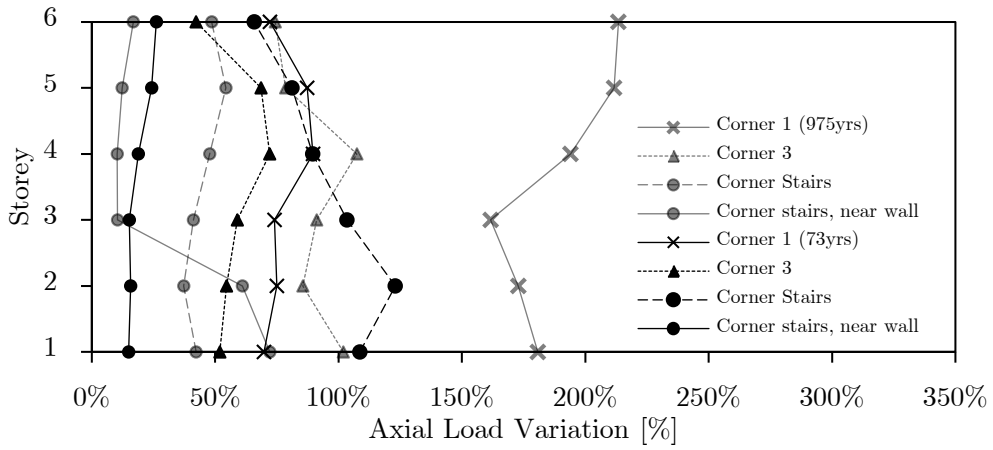

Figure C.23: Comparison between axial stress variation on corner columns and transversal earthquakes with infill panels.

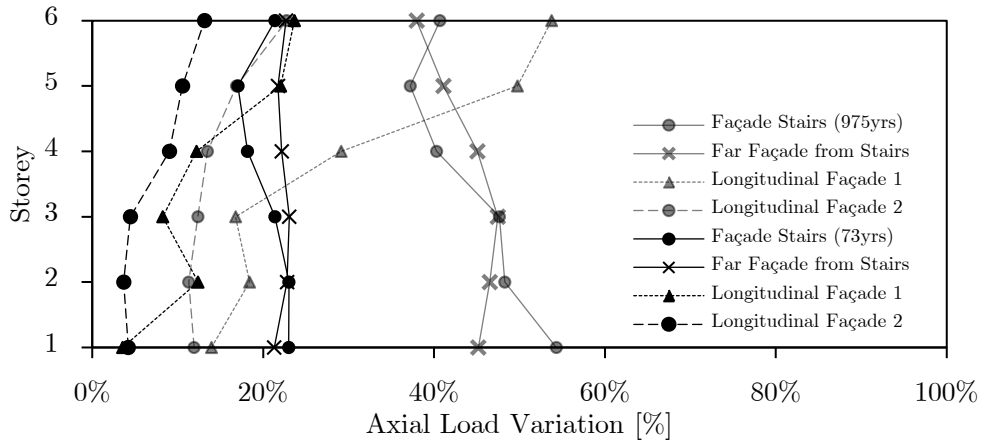

Figure C.24: Comparison between axial stress variation on façade columns and different earthquakes with infill panels.

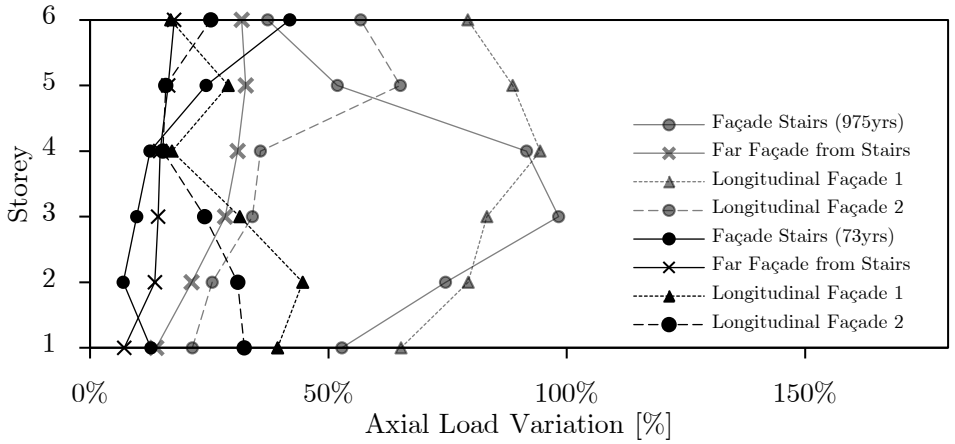

Figure C.25: Comparison between axial stress variation on façade columns and different earthquakes with infill panels.

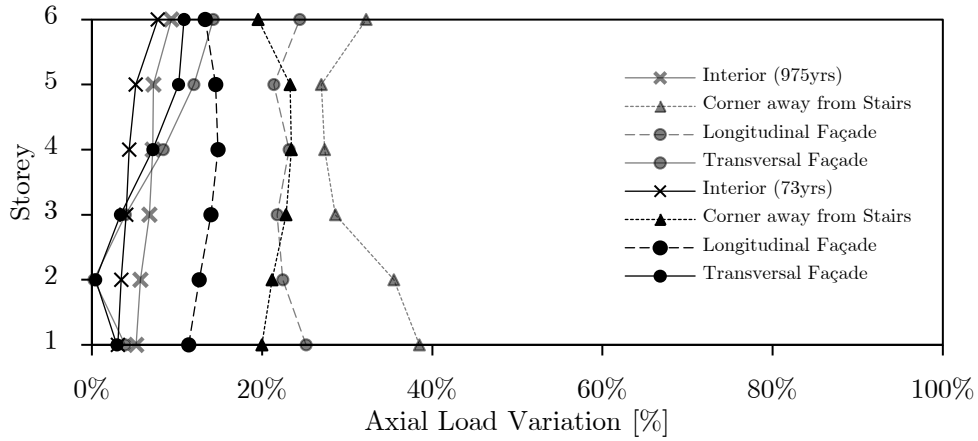

Figure C.26: Comparison between axial stress variation on columns for different places and longitudinal earthquakes without infill panels.

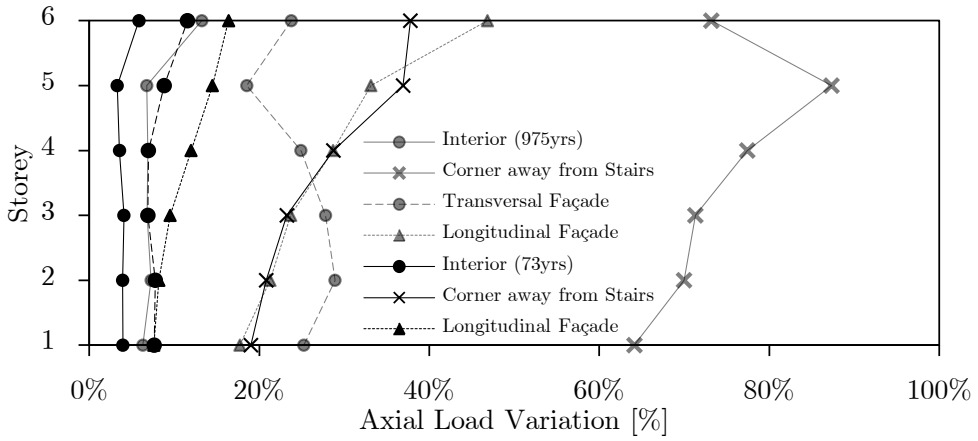

Figure C.27: Comparison between axial stress variation on columns for different places and transversal earthquakes without infill panels.

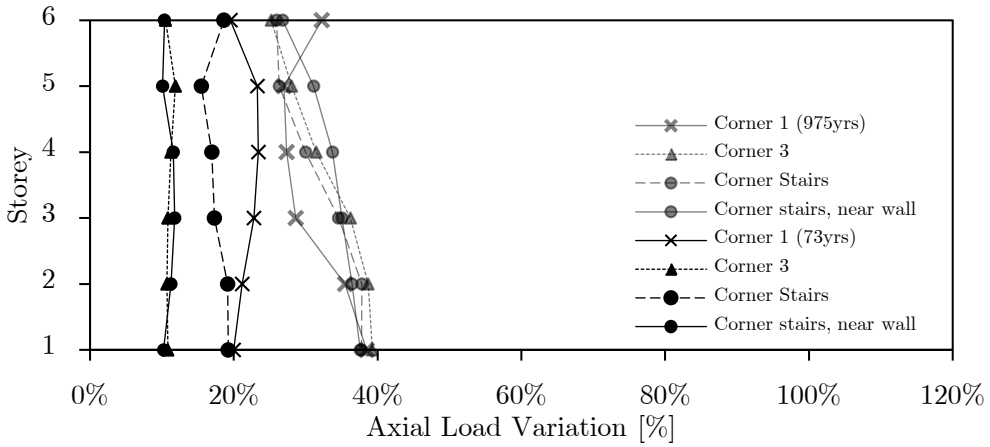

Figure C.28: Comparison between axial stress variation on corner columns and different earthquakes without infill panels.

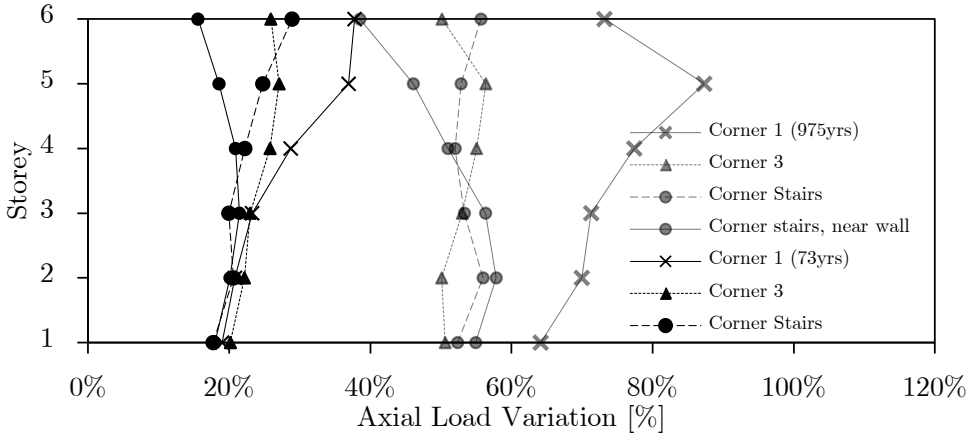

Figure C.29: Comparison between axial stress variation on corner columns and different earthquakes without infill panels.

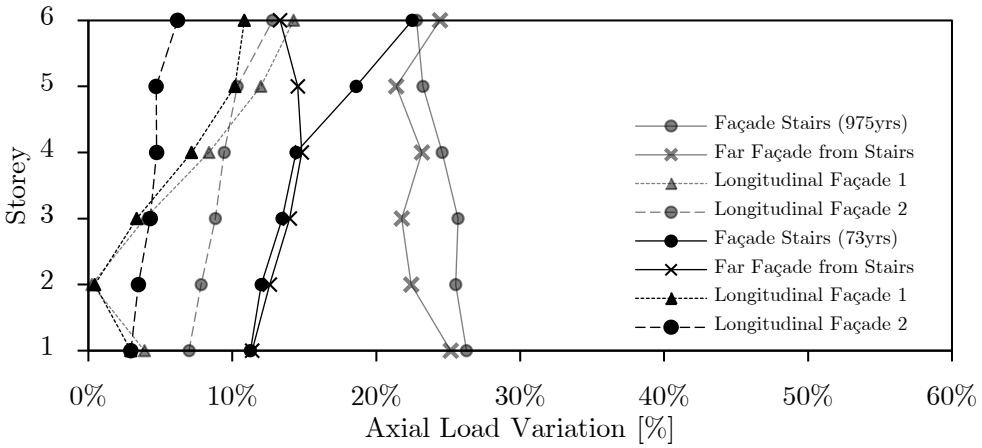

Figure C.30: Comparison between axial stress variation on façade columns and different earthquakes without infill panels.

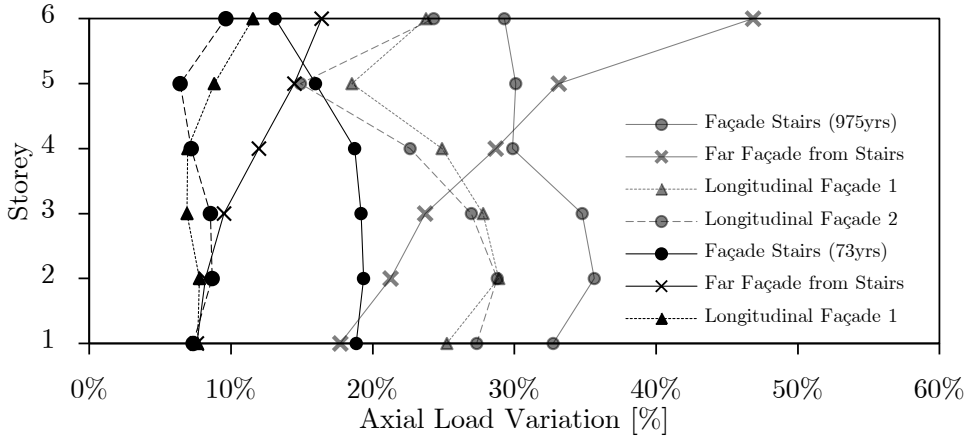

Figure C.31: Comparison between axial stress variation on façade columns and different earthquakes without infill panels.

C.2.3 Shear Progression

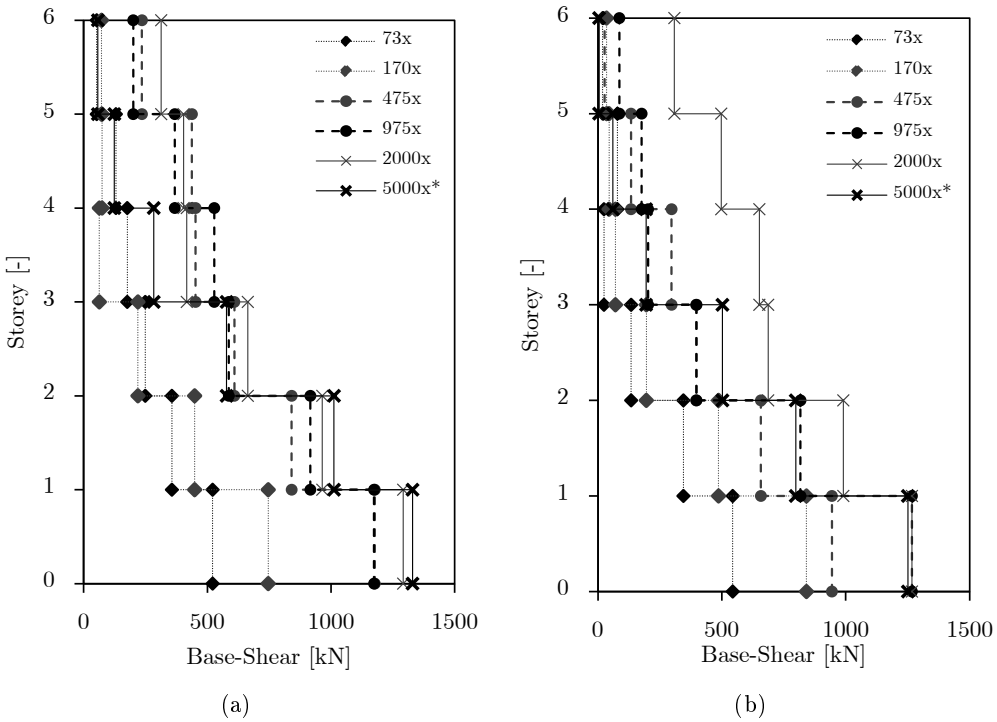

Figure C.32: Total shear on each storey, for the moment in which is attained the maximum base-shear for (a) longitudinal earthquake and demand and (b) transversal earthquake and demand.

C.2.4 Base-Shear-Drift

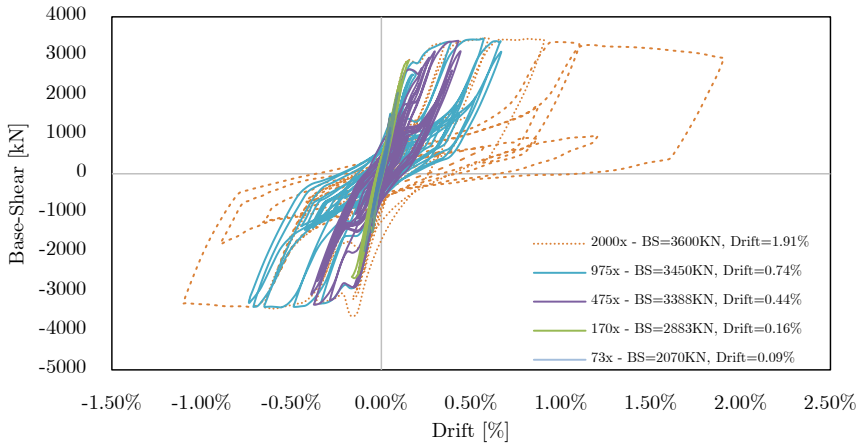

Figure C.33: Base-Shear-Drift for Parnaso with infill panels for longitudinal earthquake and response.

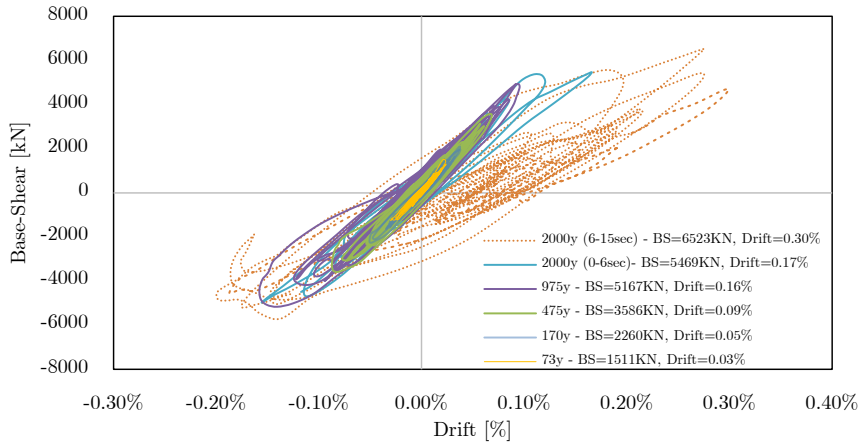

Figure C.34: Base-Shear-Drift for Parnaso with infill panels for transversal earthquake and response.

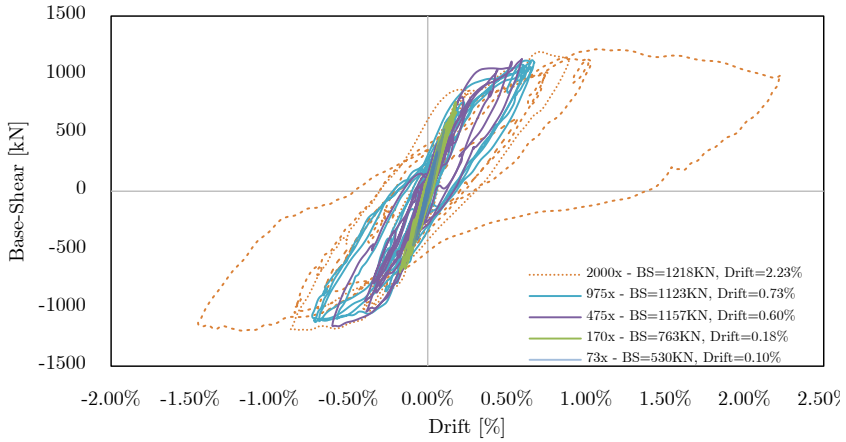

Figure C.35: Base-Shear-Drift for Parnaso without infill panels for longitudinal earthquake and response.

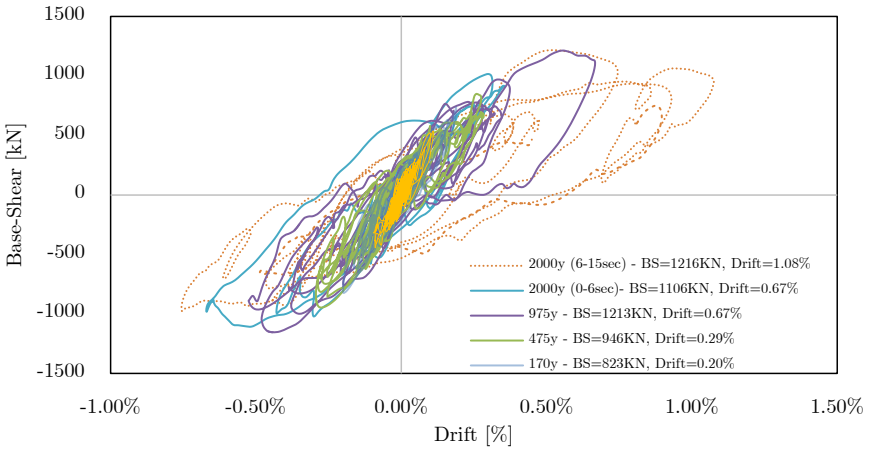

Figure C.36: Base-Shear-Drift for Parnaso without infill panels and transverse earthquake and response.

C.2.5 Comparison Between Framed and Infilled Structure

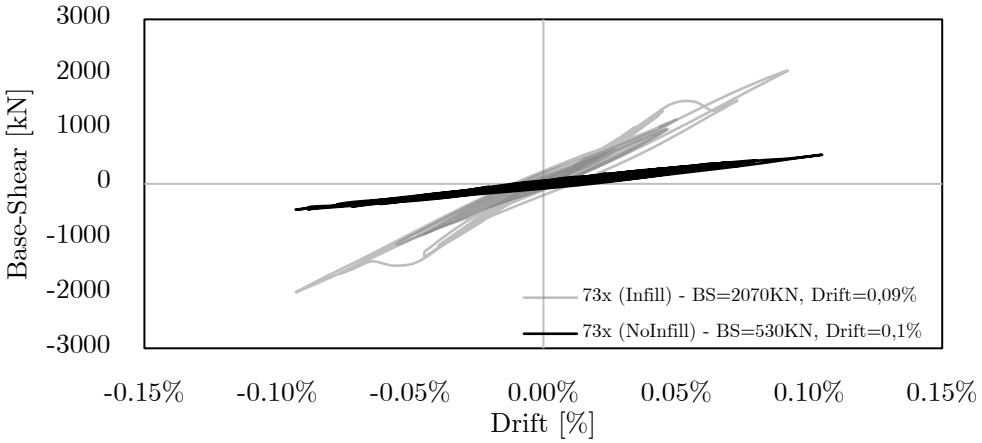

Figure C.37: Comparison of base-shear-drift with and without infill panels for longitudinal earthquake of 73 years of return period.

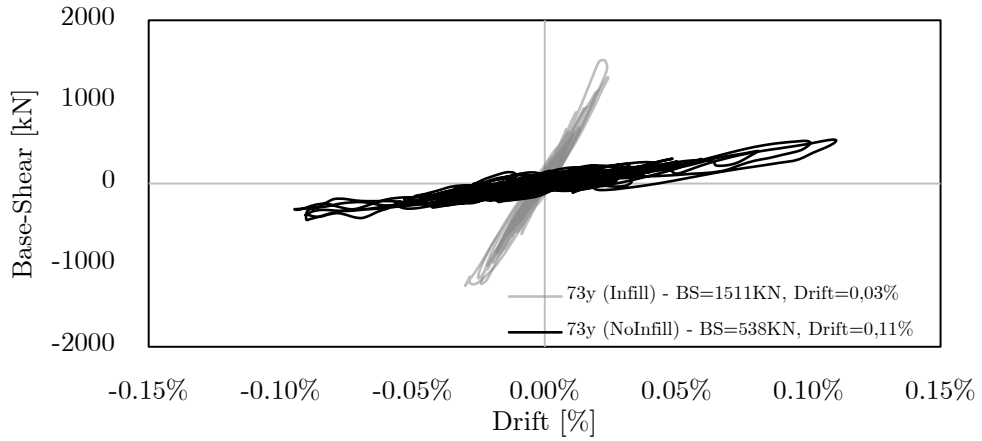

Figure C.38: Comparison of base-shear-drift with and without infill panels for transverse earthquake of 73 years of return period.

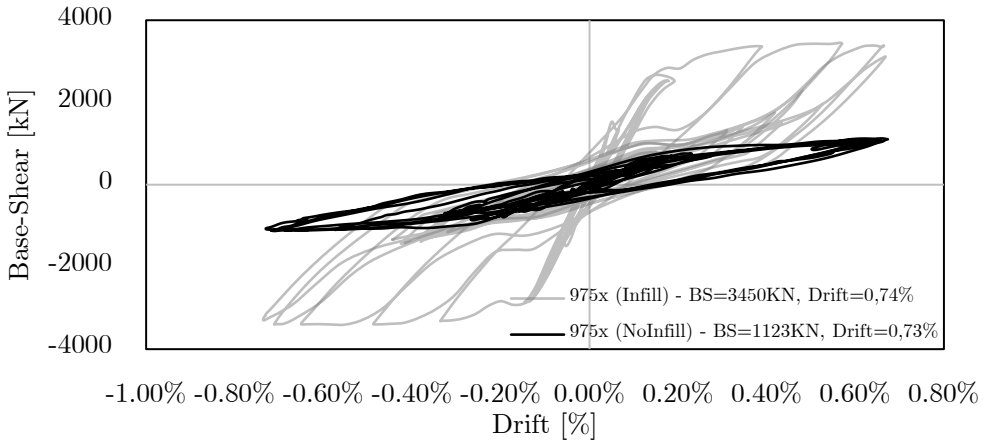

Figure C.39: Comparison of base-shear-drift with and without infill panels for longitudinal earthquake of 975 years of return period.

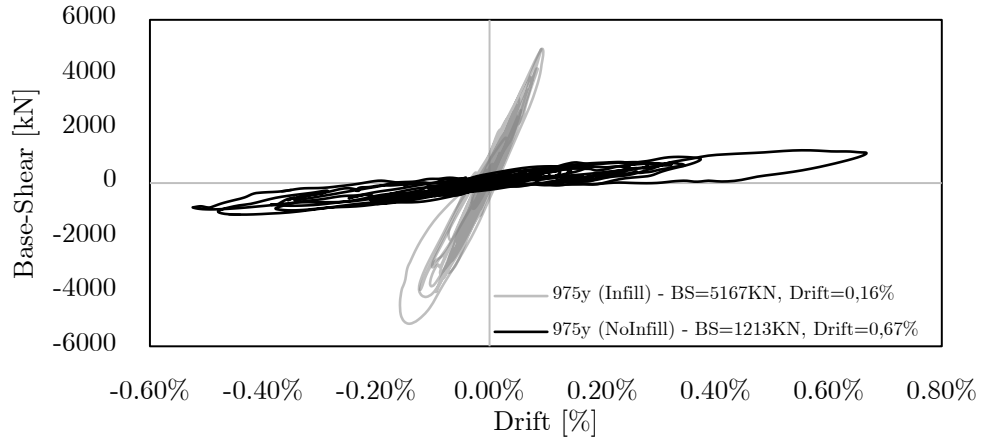

Figure C.40: Comparison of base-shear-drift with and without infill panels for transverse earthquake of 975 years of return period.

C.2.6 Shear-Drift by Floor

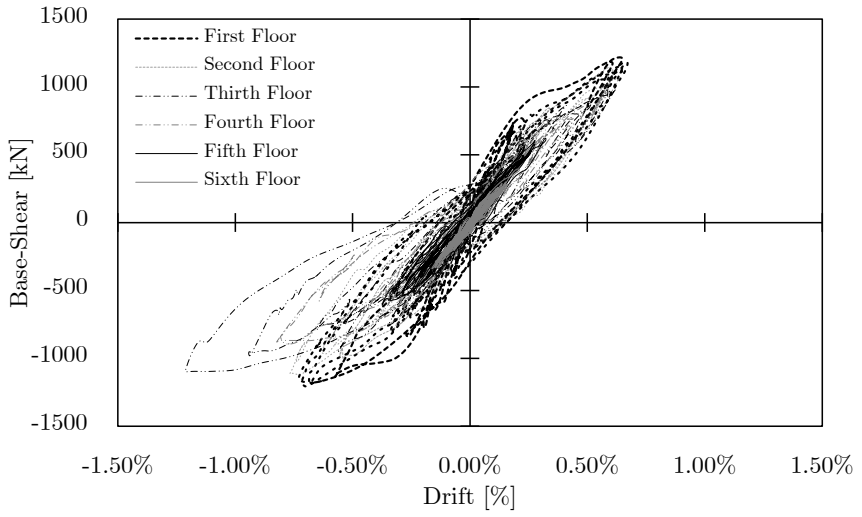

(a)

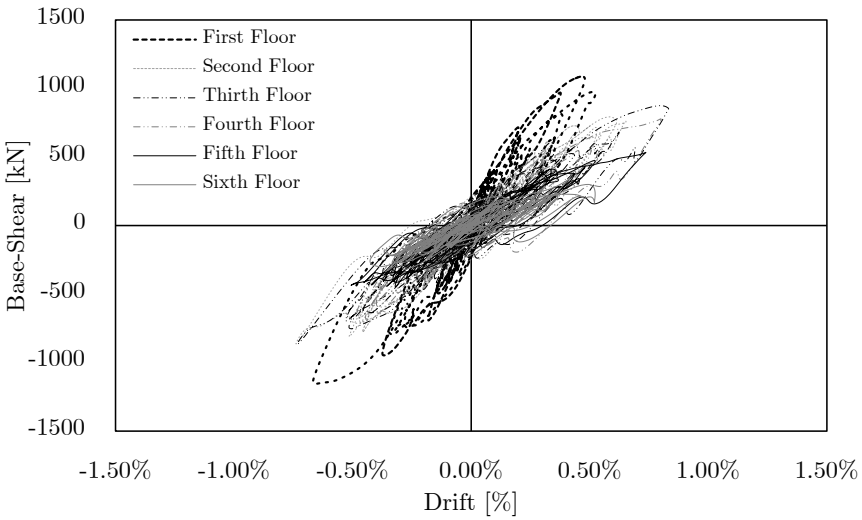

(b)

Figure C.41: Drift-Rotation progression by floor, on the centre column for a return period of 975 years for (a) longitudinal earthquake and (b) transversal earthquake.

C.2.7 Moment-Rotation

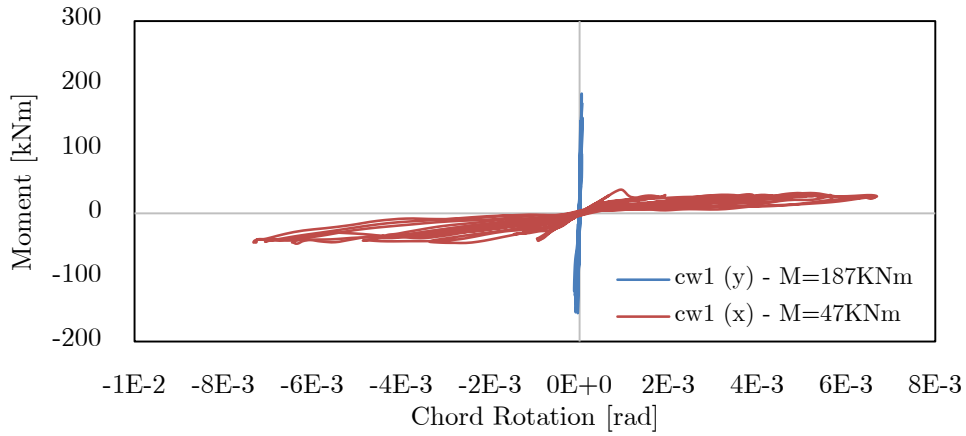

Figure C.42: Moment-Rotation for wall of Parnaso with infill panels for a longitudinal earthquake.

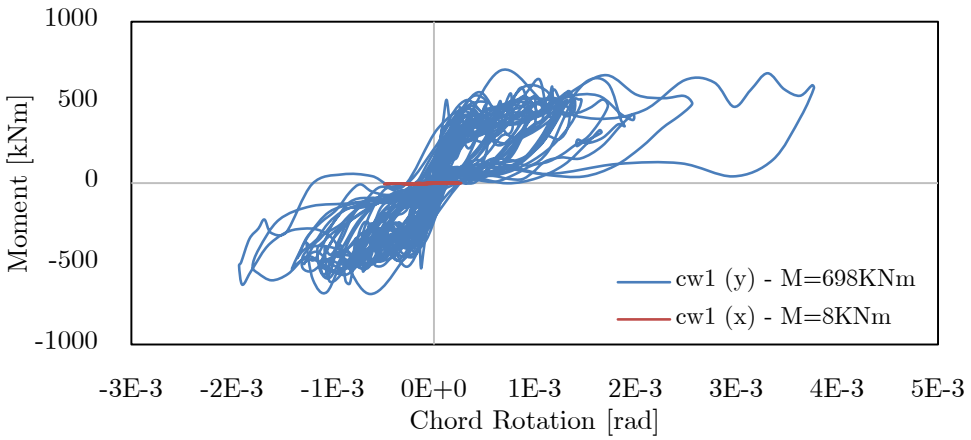

Figure C.43: Moment-Rotation for wall of Parnaso with infill panels for a transversal earthquake.

Appendix D

Local Assessment Support

D.1 Safety Level for Chord Rotation

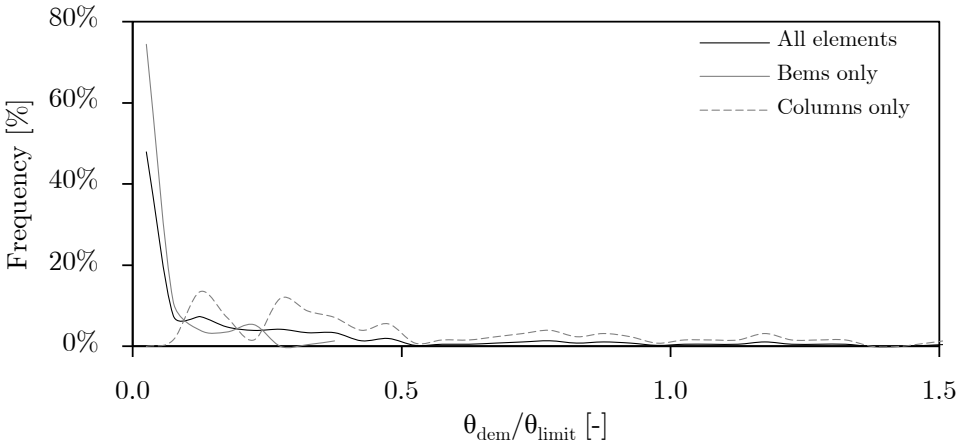

Figure D.1: Level of safety for all elements on a longitudinal earthquake.

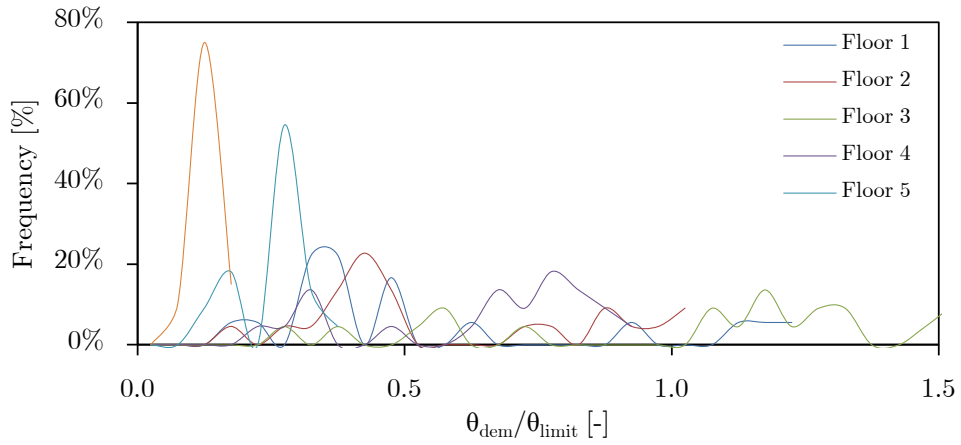

Figure D.2: Level of safety for columns in different storeys on a longitudinal earthquake.

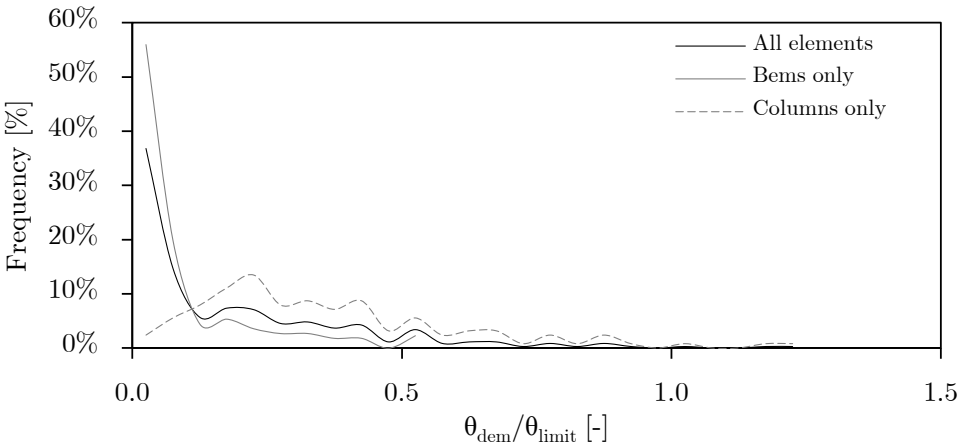

Figure D.3: Level of safety for all elements on a transversal earthquake.

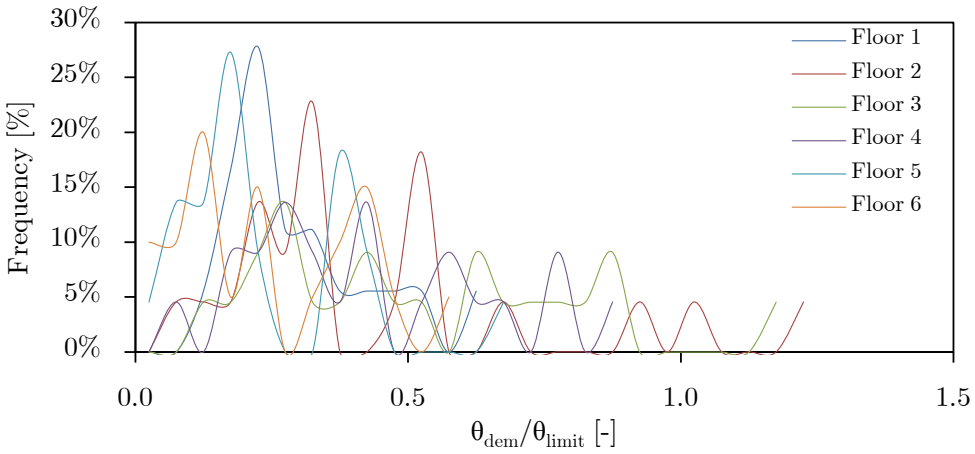

Figure D.4: Level of safety for columns in different storeys on a transversal earthquake.

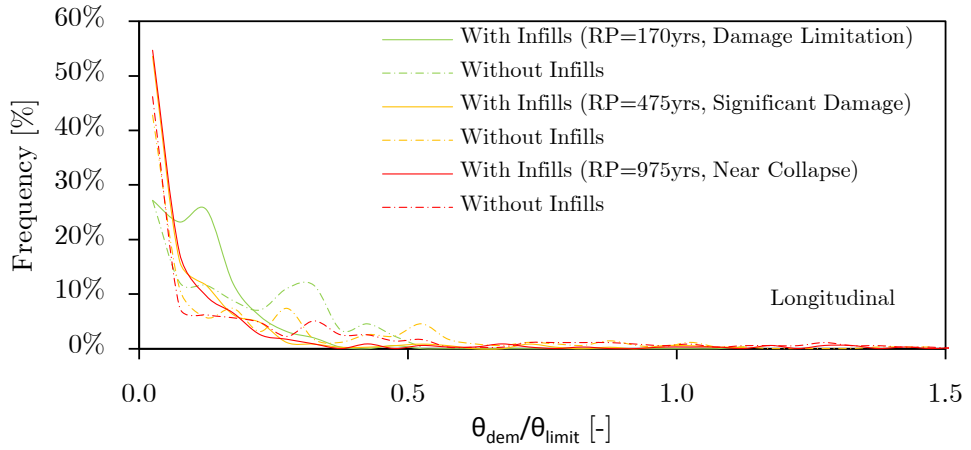

Figure D.5: Level of safety for elements on different earthquakes for its respective level of verification on a longitudinal earthquake.

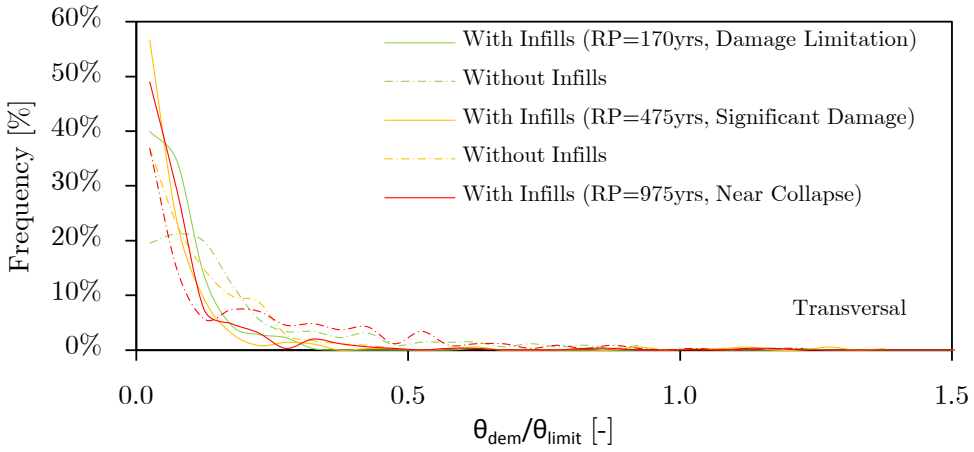

Figure D.6: Level of safety for elements on different earthquakes for its respective level of verification on a transversal earthquake.

D.2 Deformation With Slippage

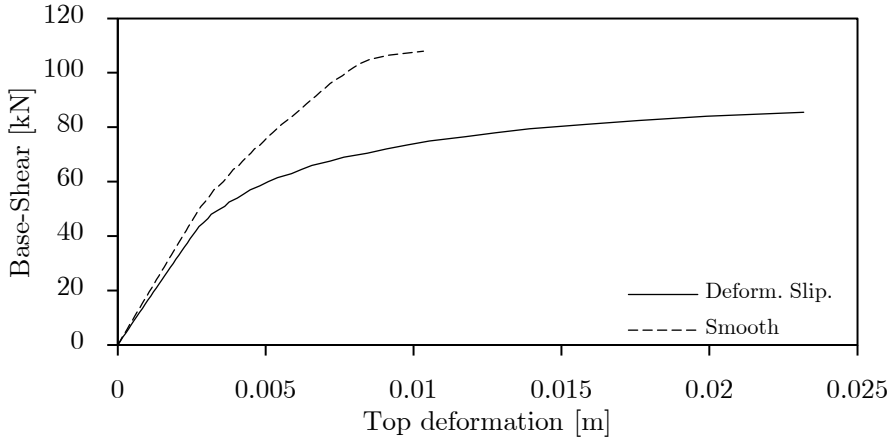

Figure D.7: Comparison between a model with half the length for plastic hinge and with reduction of the elastic modulus of steel, on base-shear-deformation, for the direction with reinforcement.

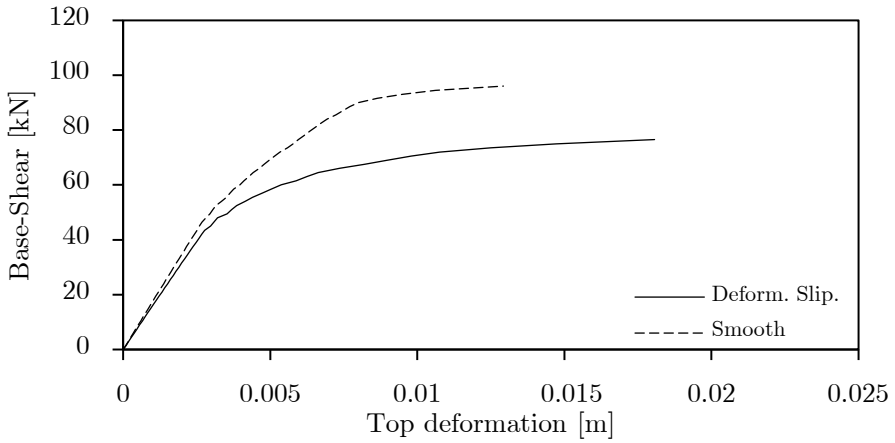

Figure D.8: Comparison between a model with half the length for plastic hinge and with reduction of the elastic modulus of steel, on base-shear-deformation, for the perpendicular direction of the reinforcement.

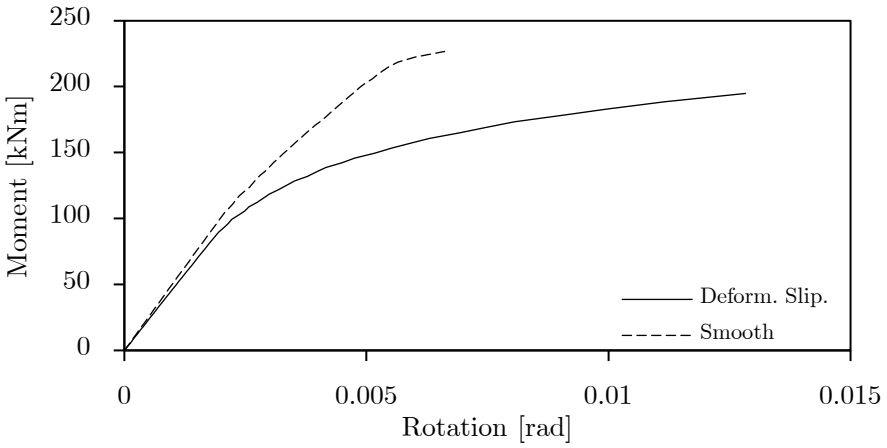

Figure D.9: Comparison between a model with half the length for plastic hinge and with reduction of the elastic modulus of steel, on moment-rotation, for the direction with reinforcement.

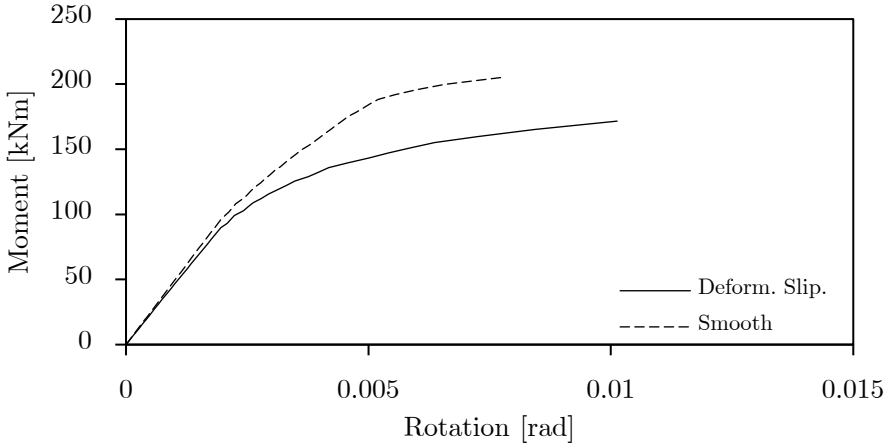

Figure D.10: Comparison between a model with half the length for plastic hinge and with reduction of the elastic modulus of steel, on moment-rotation, for the perpendicular direction of the reinforcement.

Appendix E

Nomenclature and Acronyms

E.1 Mander and Martinez Model

A_c	–	Area of the hoops
A_e	–	Effective area of confinement
A_{si}	–	Total transversal area
E_c	–	Modulus of elasticity of concrete
E_{sec}	–	Secant modulus of elasticity of concrete at peak stress
f'_{cc}	–	Compressive strength of confined concrete
f'_{co}	–	Compressive strength of unconfined concrete
f_{cr}	–	Strength on unloading
f_l	–	"Fluid" pressure outside the section
f_{new}	–	Degraded stress
f_{re}	–	Stress on reloading moment
f'_t	–	Tensile strength of concrete
f_{un}	–	Stress on unloading moment
k_1	–	Coefficients of calibration
k_2	–	Coefficients of calibration
k_e	–	Confinement factor
r	–	Factor to compute f_c
x	–	Factor to compute f_c
ε_{un}	–	Stain on unloading instant
ε_{35}	–	Strain for $0.35f'_c$
ε_a	–	"Common Strain"
ε_c	–	Longitudinal compressive strain of concrete
ε_{cc}	–	Maximum compressive strain for confined concrete
ε_{co}	–	Maximum compressive strain for unconfined concrete
ε_{cr}	–	Strain on unloading
ε_f	–	Strain of the "focal point"
ε_{new}	–	Strain for degraded stress
ε_{pl}	–	Residual/plastic strain

$\varepsilon_{\text{plcr}}$ – Inelastic strain corresponding to the upper limit of the intermediate strain range ε_{cr}
ε_{re} – Stain on reloading, returning point
ε_{ro} – Strain on reloading
ε_{un} – Strain on unloading
ρ_{cc} – Ratio of longitudinal reinforcement

E.2 Menegotto-Pinto Model

a_i – Parameters for calibration
b – Strain hardening ratio
E – Young Modulus
E_{s0} – Initial young modulus
E_{sp} – "Hardened" young modulus
R – Parameter describing the shape of the transient curve
R_0 – Initial shape of the transient curve
ε – Strain
ε^* – Iterated strain
ε_{max} – Maximum strain at the beginning of reversal
ε_{r} – Strain for intersection of two asymptotes
ε_{y} – Strain at yielding
ε_0 – Strain for intersection of two asymptotes which limits the steel stress-strain relationship
σ_0 – Strength for intersection of two asymptotes which limits the steel stress-strain relationship
σ_{r} – Strength for intersection of two asymptotes
σ^* – Iterated strength
σ_{shift} – Shift of yield stress after a load reversal
σ_{y} – Strength at yielding
ζ_{p} – Plastic excursion

E.3 Fixed-End Rotation

d' – Distance between top and bottom steel bars
u^{b} – Displacement of the bottom steel bars
u^{t} – Displacement of the top reinforced bars
θ_{FE} – Rotation at the fixed-end

E.4 Modelling and Assumptions

A_{m}	–	Area of strut
b_{w}	–	Equivalent width of the strut
d_{w}	–	Length of the of the strut
E_{sm}	–	Young modulus of the steel
f_{ck}	–	Characteristic compressive strength of the concrete
f_{cm}	–	Average compressive strength of the the concrete
f_{ct}	–	Tensile strength of the concrete
f_{l}	–	Strain at maximum stress
f_{n}	–	Normal stress at bed joint
$G_{\mathrm{k},j}$	–	Dead Loads (permanent)
h_{beam}	–	Height of the beam
h_{column}	–	Height of the column
h_{w}	–	Height of the wall
h_{w}	–	Vertical separation between struts
I_{c}	–	Inertia of the concrete section
k	–	Stiffness
L	–	Length of the element
l_{p}	–	Length of the plastic hinge
m	–	Mass
$Q_{\mathrm{k},i}$	–	Live Loads (variable)
$q_n(t)$	–	Modal coordinates
R_0	–	Transition curve of initial shape
t_{w}	–	Thickness of the panels
w_{n}	–	Natural frequency of vibration
$x_{\mathrm{o}i}$	–	Horizontal offsets
$y_{\mathrm{o}i}$	–	Vertical offsets
z	–	Contact length of the panel with deformed frame
ε_{u}	–	Ultimate strain
$\varepsilon_{\mathrm{ult}}$	–	Fracture/buckling strain
ε_{c}	–	Strain at peak stress of the concrete
λ	–	Dimensionless relative stiffness parameter
μ	–	Strain hardening parameter
ϕ_n	–	Deflected shape
$\psi_{\mathrm{E},i}$	–	Coefficient for seismic combinations
$\psi_{2,i}$	–	Coefficient for live combinations
φ	–	Coefficient according building typology
θ	–	Angle of the strut

E.5 Implemented Earthquakes

a_i	–	Acceleration
c	–	Damping
$[C]$	–	Damping matrix
k	–	Stiffness
$[K]$	–	Stiffness matrix
m	–	Mass
$[M]$	–	Mass matrix
u_0	–	Initial displacement
u_i	–	Displacement
$\vec{u}(t)$	–	Displacement (vector)
$\dot{\vec{u}}(t)$	–	Velocity (vector)
$\ddot{\vec{u}}(t)$	–	Acceleration (vector)
$\ddot{\vec{u}}_{\mathrm{g}}(t)$	–	Ground acceleration (vector)
$\ddot{u}_{\mathrm{g}}(t)$	–	Ground acceleration
v_0	–	Initial velocity
v_i	–	Velocity
w_{n}	–	Natural frequency of vibration
Δt	–	Time step
$\vec{\jmath}$	–	Identity vector
τ	–	Dummy time variable
ζ	–	Damping ratio

E.6 Local Assessments

A_{c}	–	Column cross-section area
A_{g}	–	Horizontal section area of the joint core
A'_{s}	–	Cross-sectional area of longitudinal compressive reinforcement steel
A_{s}	–	Cross-sectional area of longitudinal tensile reinforcement steel
A_{s1}	–	Area of the beam top reinforcement
A_{s2}	–	Area of the beam bottom reinforcement
A_{sw}	–	Cross-sectional area of stirrup
b	–	Width
b_{c}	–	Width of the column
b_{j}	–	Effective joint width
b_{w}	–	Width of the beam
c	–	Concrete cover
d'	–	Depth to the compression reinforcement

d	–	Effective depth of section (for tension reinforcement)
d_{bl}	–	Diameter of tension reinforcement
E_{c}	–	Young modulus of the concrete
E_{s}	–	Young modulus of the steel
f_{c}	–	Compressive strength of concrete
f_{c}	–	Concrete compressive strength
f_{cd}	–	Design value for compressive strength of concrete
f_{ck}	–	Characteristic value for compressive strength of concrete
f_{cm}	–	Average concrete compressive strength
f_{s}	–	Steel strength (of the bottom bars)
f'_{s}	–	Steel strength (of the top bars)
f_{sy}	–	Strength at yielding of steel
f_{yd}	–	Design value for yielding of steel
f_{ylm}	–	Average strength at yielding for longitudinal bars
f_{yw}	–	Strength at yielding for transversal bars
f_{ywm}	–	Average strength at yielding for transversal bars
h	–	Depth of the member
h_{c}	–	Height of the columns joint
h_{jc}	–	Distance between extreme layers of column reinforcement
L	–	Length of the element
L_{pl}	–	Length of the plastic hinge
L_{v}	–	Shear span at member end
l_0	–	Lapped bars length
M	–	Moment stress
M_{R}	–	Moment capacity
N_{E}	–	Axial force (positive for compression)
V	–	Shear stress
V_{C}	–	Shear contribution of concrete
V_{jhd}	–	Shear acting on joints
V_{N}	–	Shear contribution of axial load
V_{n}	–	Shear on the upper column plus the shear transmitted by the reinforcement bars of the beams
$V_{\mathrm{R,max}}$	–	Shear resistance as determined by crushing in the diagonal compression strut
V_{R}	–	Shear strength
V_{W}	–	Contribution of transverse reinforcement to shear resistance
w'	–	Mechanical reinforcement ratio of compression reinforcement
w	–	Mechanical reinforcement ratio of tension reinforcement
x	–	Compression zone depth
x_{dem}	–	Depth of neutral axis (demand)
x_{y}	–	Depth of neutral at yielding
y	–	Equivalent depth of neutral axis (simplification)
z	–	Length of section internal lever arm

α	–	Confinement effectiveness
α_{v}	–	Parameter regarding shear cracking
Δ	–	Deflection of the element
$\varepsilon_{\mathrm{c,max}}$	–	Maximum concrete strain (recommended)
ε_{c}	–	Concrete strain
$\varepsilon_{\mathrm{c2}}$	–	Extension when attained maximum strength on concrete
$\varepsilon_{\mathrm{sy}}$	–	Strain of steel at yielding
η	–	Reduction factor for shear joint strength
γ_{Rd}	–	Safety factor
γ_{c}	–	Safety factor
γ_{el}	–	Safety factor
γ_{s}	–	Safety factor
$\mu_{\Delta}^{\mathrm{pl}}$	–	Ratio of the plastic of the chord-rotation normalized to the chord-rotation at yielding
ϕ_{u}	–	Ultimate curvature
$\phi_{\mathrm{y,comp}}$	–	Curvature at yielding (compressive)
$\phi_{\mathrm{y,tens}}$	–	Curvature at yielding (tensile)
ϕ_{y}	–	Curvature at yielding
ρ_{sx}	–	Volumetric ratio of confinement reinforcement
ρ_{tot}	–	Total longitudinal reinforcement ratio
σ_{c}	–	Concrete compressive strength
σ_{nt}	–	Stress in the joint core
θ	–	Strut inclination angle in shear design
θ_{u}	–	Ultimate chord rotation capacity
θ_{um}	–	Ultimate chord rotation capacity (alternative)
θ_{y}	–	Chord rotation at yielding
υ_{d}	–	Normalised axial force in the column above the joint

E.7 Acronyms

CF	–	Confidence Factor
DL	–	Damage Limitation
EC2	–	Eurocode 2
EC8	–	Eurocode 8
EC8-1	–	Eurocode 8 part 1
EC8-3	–	Eurocode 8 part 3
EFDD	–	Enhanced Frequency Domain Decomposition
FRP	–	Fibre-Reinforced Plastic
LS	–	Limit State
MDoF	–	Multi Degree of Freedom
NC	–	Near Collapse
NTC08	–	*Norme Tecniche per le Costruzioni* (Italian building code)

PGA	–	Peak Ground Acceleration
RC	–	Reinforced Concrete
RP	–	Return Period
RSA	–	*Regulamento de Segurança e Acções* (Portuguese building code)
SD	–	Significant Damage
SDoF	–	Single Degree of Freedom

Intentionally blank page.

Bibliography

[Abrams 1913] D. A. Abrams. *Tests of bond between concrete and steel.* Technical report, University of Illinois Bulletin Vol. XI, Bulletin N. 71, University of Illinois, Urbana Champaign, USA, December, 1913.

[Alsiwat and Saatcioglu 1992] J. M. Alsiwat and M. Saatcioglu. Reinforcement anchorage slip under monotonic loading. *ASCE Journal of Structural Engineering*, **118**(9):2421–2438, 1992.

[ARTeMIS 2008] ARTeMIS. ARTeMIS modal - Software for operational modal analysis. http://www.svibs.com/ (consulted in 2013), 2008.

[Bach 1911] C. G. Bach. *Versuche mit eisenbeton-balken zur ermittlung der beziehungen zwischen formänderungswinkel und biegungsmoment.* Technical report, Deutcher Ausschuß für Eisenbeton, Heft 9-10, Berlin, Germany, 1911.

[Banon 1980] H. Banon. *Prediction of seismic damage in reinforced concrete frames.* PhD Thesis in Civil Engineering, Department of Civil Engineering, Massachusetts Institute of Technology, Cambridge, Massachusetts, USA, 1980.

[Blakeley and Park 1973] R. W. G. Blakeley and R. Park. Prestressed concrete sections with cyclic flexure. *ASCE Journal of Structural Division*, **99**(ST8):1717–1742, 1973.

[Carter and Stafford-Smith 1969] C. Carter and B. Stafford-Smith. Structural behaviour of masonry infilled frames subjected to racking loads. *Proceedings of Designing, Engineering, and Construction with Masonry Products, Houston, USA*, pp. 226–233, 1969.

[Carvalho *et al.* 1999] E. C. Carvalho, E. Coelho and A. Campos-Costa. *Preparation of the full-scale tests on reinforced concrete frames. Characteristics of the test specimens, materials and testing conditions.* Technical report, Innovative Seismic Design Concepts for New and Existing Structures, European TMR Network, LNEC, Lisbon, Portugal, 1999.

[CEN 2001] CEN. *Eurocode 0: Basis of structural design.* European Committee for Standardization, Brussels, Belgium, 2001.

[CEN 2003] CEN. *Eurocode 8: Design of structures for earthquake resistance – Part 1: General rules, seismic actions and rules for buildings.* European Committee for Standardization, Brussels, Belgium, 2003.

[CEN 2004] CEN. *Eurocode 2: Design of concrete structures – Part 1-1: General rules and rules for buildings.* European Committee for Standardization, Brussels, Belgium, 2004.

[CEN 2005] CEN. *Eurocode 8: Design of structures for earthquake resistance – Part 1-3: Strengthening and repair of buildings.* European Committee for Standardization, Brussels, Belgium, 2005.

[CEN 2009] CEN. Corrigenda to EN 1998-3. Document CEN/TC250/SC8/N437A. European Committee for Standardization, Brussels, Belgium, 2009.

[Chang and Mander 1994] G. Chang and J. Mander. *Seismic energy based fatigue damage analysis of bridge columns: Part I - Evaluation of seismic capacity.* Technical report, NCEER 94-0006, National Center for Earthquake Engineering Research, Buffalo, New York, USA, 1994.

[Cho and Pincheira 2006] J.-Y. Cho and J. A. Pincheira. Inelastic analysis of reinforced concrete columns with short lap splices subjected to reversed cyclic loads. *ACI Structural Journal*, **103**(2):280–290, 2006.

[Chopra 2006] A. K. Chopra. *Dynamics of structures - Theory and applications to earthquake engineering.* Pearson Prentice Hall, New Jersey, USA, second edition, 2006.

[Ciampi *et al.* 1981] V. Ciampi, R. Eligehausen, V. V. Bertero and E. P. Popov. *Analytical model for deformed bar bond under generalized excitations.* In IABSE Colloquium, Advanced Mechanics of Reinforced Concrete, Delft, Netherlands, June 2-5, 1981.

[Cofie and Krawinkler 1985] N. G. Cofie and H. Krawinkler. Uniaxial cyclic stress-strain behavior of structural steel. *ASCE Journal of Structural Engineering*, **111**(9):1105–1120, 1985.

[Crisafulli 1997] F. J. Crisafulli. *Seismic behaviour of reinforced concrete structures with masonry infills.* PhD Thesis in Civil Engineering, University of Canterbury, Christchurch, New Zealand, 1997.

[Dafalias and Popov 1976] Y. F. Dafalias and E. P. Popov. Plastic internal variables formalism of cyclic plasticity. *ASCE Journal of Structural Engineering*, **43**(4):645–651, 1976.

[DM 2008] DM. *Decreto ministeriale. Approvazione delle nuove norme tecniche per le costruzioni.* Gazzetta Ufficiale N. 29, 4/2/2008, 2008.

[Doudoumis and Mitsopoulou 1986] I. N. Doudoumis and E. N. Mitsopoulou. Non-linear analysis of multistorey infilled frames for unilateral contact conditions. *Proceedings on the 8th European Conference on Earthquake Engineering, Lisbon, Portugal*, 1986.

[Draganić *et al.* 2010] H. Draganić, M. Hadzima-Nyarko and D. Morić. Comparison of RC frames periods with the empiric expressions given in Eurocode 8. *Technical Gazette*, **17**(1):93–100, 2010.

[Eligehausen *et al.* 1983] R. Eligehausen, E. P. Popov and V. V. Bertero. *Local bond stress-slip relationships of deformed bars under generalized excitations.* Technical report, UCB/EERC 83/23, Earthquake Engineering Research Center, University of California, USA, 1983.

[Elnashai and Izzuddin 1993] A. S. Elnashai and B. A. Izzuddin. Modeling of material non-linearities in steel structures subjected to transient dynamic loading. *Earthquake Engineering and Structural Dynamics*, **22**:509–532, 1993.

[Fabbrocino *et al.* 2004] G. Fabbrocino, G. M. Verderame, G. Manfredi and E. A. Cosenza. Structural models of critical regions in old-type rc frames with smooth rebars. *Engineering Structures*, **26**(14):2137–2148, 2004.

[Fabbrocino *et al.* 2005] G. Fabbrocino, G. M. Verderame and G. Manfredi. Experimental behaviour of anchored smooth rebars in old type reinforced concrete buildings. *Engineering Structures*, **27**(10):1575–1585, 2005.

[Fang *et al.* 2006] C. Fang, K. Gylltoft, K. Lundgren and M. Plos. Effect of corrosion on bond in reinforced concrete under cyclic loading. *Cement and Concrete Research*, **36**(3):548–555, 2006.

[Fardis 2009] M. N. Fardis. *Seismic design, assessment and retrofitting of concrete buildings - based on Eurocode 8.* Springer, New York, USA, eighth edition, 2009.

[Feldman and Bartlett 2005] L. R. Feldman and F. M. Bartlett. Bond strength variability in pullout specimens with plain reinforcement. *ACI Structural Journal*, **102**(6):860–867, 2005.

[Feldman and Bartlett 2007] L. R. Feldman and F. M. Bartlett. Bond stresses along plain steel reinforcing bars in pullout specimens. *ACI Structural Journal*, **104**(6):685–692, 2007.

[FEMA356 2000] FEMA356. *Prestandard and commentary for the seismic rehabilitation of buildings.* Federal Emergency Management Agency, Washington, USA, 2000.

[Fernandes 2012] C. Fernandes. *Cyclic behavior of RC elements with plain reinforcing bars.* PhD Thesis in Civil Engineering, University of Aveiro, Aveiro, Portugal, 2012.

[Fernandes *et al.* 2010] C. Fernandes, J. Melo, H. Rodrigues, H. Varum, A. Costa and A. Arêde. *Análise do comportamento cíclico de uma viga de betão armado com armadura lisa.* In SÍSMICA 2010 - 8th National Conference on Seismology and Earthquake Engineering, University of Aveiro, Aveiro, Portugal, October 20-23, 2010.

[Fernandes *et al.* 2011a] C. Fernandes, J. Melo, H. Varum and A. Costa. Comparative analysis of the cyclic behaviour of beam-column joints with plain and deformed reinforcing bars. *Ibracon Structures and Materials*, **4**(1):147–172, 2011.

[Fernandes *et al.* 2011b] C. Fernandes, J. Melo, H. Varum and A. Costa. Cyclic behavior of a two-span RC beam built with plain reinforcing bars. *Periodica Polytechnica Civil Engineering*, **55**(1):21–29, 2011.

[Fernandes *et al.* 2012] C. Fernandes, J. Melo, H. Varum and A. Costa. *Experimental and numerical analysis of the cyclic behaviour of RC beam-column connections with plain reinforcing bars.* In 15th World Conference on Earthquake Engineering, Lisbon, Portugal, September 24-28, 2012.

[FIB 2000] FIB. *Bond of reinforcement in concrete.* Technical report, International Federation for Structural Concrete, State-of-art, Bulletin N. 10, 2000.

[Filippou *et al.* 1983] F. C. Filippou, E. P. Popov and V. V. Bertero. *Effects of bond deterioration on hysteretic behavior of reinforced concrete joints.* Technical report, UCB/EERC-83/19, Earthquake Engineering Research Center, University of California, USA, August 1983.

[Fishburn 1947] C. C. Fishburn. Strength and slip under load of bent-bar anchorages and straight embedments in haydite concrete. *ACI Journal Proceedings*, **44**(12):289–306, 1947.

[Fonseca 2005] J. Fonseca. *Forma e estrutura no bloco de habitação, património moderno em Portugal.* Marter's Thesis in Architecture, Faculty of Architecture of University of Oporto, Oporto, Portugal, 2005.

[Freitas 2008] R. Freitas. *Estudo numérico do impacto da nova acção sísmica prevista no Eurocódigo 8 para o comportamento de edifícios na região norte de Portugal.* Master's Thesis in Civil Engineering, University of Oporto, Oporto, Portugal, 2008.

[Hawkins *et al.* 1982] N. M. Hawkins, I. J. Lin and F. L. Jeang. *Local bond strength of concrete for cyclic reversed actions.* Proceedings, Bond in concrete, Applied Science Publishers, London, UK, 1982.

[Holmes 1961] M. Holmes. Steel frames with brickwork and concrete infilling. *Proceedings of the Institution of Civil Engineers*, **19**:473–478, 1961.

[Kankam 1997] C. K. Kankam. Relationship of bond stress, steel stress, and slip in reinforced concrete. *ASCE Journal of Structural Engineering*, **123**(1):79–85, 1997.

[Karsan and Jirsa 1969] I. D. Karsan and J. O. Jirsa. Behavior of concrete under compressive loadings. *ASCE Journal of Structural Division*, **95**(12):2543–2563, 1969.

[Klingner and Bertero 1976] R. E. Klingner and V. V. Bertero. *Infilled frames in earthquake resistant construction.* Technical report, Report 76–32, University of California, Berkeley, USA, 1976.

[Kwak *et al.* 2004] H.-G. Kwak, S.-P. Kim and J.-E. Kim. Nonlinear dynamic analysis of RC frames using cyclic moment-curvature relation. *Structural Engineering and Mechanics*, **17**(3-4):357–378, 2004.

[Lehman and Moehle 2000] D. E. Lehman and J. P. Moehle. *Seismic performance of well-confined concrete bridge columns.* Technical report, PEER-1998/01, Pacific Earthquake Engineering Research Center, University of California, USA, 2000.

[Liauw and Lee 1977] T. C. Liauw and S. W. Lee. On the behaviour and the analysis of multi-storey infilled frames subjected to lateral loading. *Proceedings of the Institution of Civil Engineers*, **63**(2):641–656, 1977.

[Lowes *et al.* 2003] L. N. Lowes, N. Mitra and A. Altoontash. *A beam-column joint model for simulating the earthquake response of reinforced concrete frames.* Technical report, Pacific Earthquake Engineering Research Center, University of California, USA, 2003.

[Lowes *et al.* 2004] L. N. Lowes, J. P. Moehle and S. Govindjee. A concrete-steel bond model for use in finite element modeling of reinforced concrete structures. *ACI Structural Journal*, **101**(4):501–511, 2004.

[Ma *et al.* 1976] S. Y. M. Ma, V. V. Bertero and E. P. Popov. *Experimental and analytical studies on the behavior of reinforced concrete rectangular and T-beams.* Technical report, UCE/EERC, 1976.

[Mander *et al.* 1988] J. B. Mander, M. J. N. Priestley and R. Park. Theoretical stress-strain model for confined concrete. *ASCE Journal of Structural Engineering*, **114**(8):1804–1826, 1988.

[Manfredi and Pecce 1998] G. Manfredi and M. Pecce. A refined R.C. beam element including bond-slip relationship for the analysis of continuous beams. *Computers & Structures*, **69**(1):53–62, 1998.

[Martins *et al.* 2003] F. F. Martins, A. F. Costa and J. A. Sousa. Túnel 4 (Porto) – Análise tridimensional por elementos finitos. *Sociedade Portuguesa de Geotecnia*, **99**:65–80, 2003.

[Martínez-Rueda and Elnashai 1997] J. E. Martínez-Rueda and A. S. Elnashai. Confined concrete model under cyclic load. *Materials and Structures*, **30**(3):139–147, 1997.

[Melo *et al.* 2010] J. Melo, C. Fernandes, H. Varum, H. Rodrigues, A. Costa and A. Arêde. Numerical modelling of the cyclic behaviour of RC elements built with plain reinforcing bars. *Engineering Structures*, **33**(2):273–286, 2010.

[Melo *et al.* 2012a] J. Melo, H. Varum, T. Rosseto and A. Costa. *Cyclic response of RC beam-column joints reinforced with plain bars: An experimental testing campaign.* In 15th World Conference on Earthquake Engineering, Lisbon, Portugal, September 24-28, 2012.

[Melo *et al.* 2012b] J. Melo, H. Varum, T. Rosseto and A. Costa. *Experimental response of RC columns built with plain bars under unidirectional cyclic loading.* In 15th World Conference on Earthquake Engineering, Lisbon, Portugal, September 24-28, 2012.

[Menegotto and Pinto 1973] M. Menegotto and P. E. Pinto. *Method of analysis for cyclically loaded RC plane frames including changes in geometry and non-elastic behaviour of elements under combined normal force and bending.* Symposium on the Resistance and Ultimate Deformability of Structures Acted, Lisbon, Portugal, 1973.

[Milheiro 2008] J. Milheiro. *Estudo numérico da influência de painéis de enchimento de alvenaria de tijolo no comportamento sísmico de estruturas porticadas existentes de betão armado.* Marter's Thesis in Civil Engineering, University of Oporto, Oporto, Portugal, 2008.

[Morita and Kaku 1974] S. Morita and T. Kaku. *Local bond stress-slip under repeated loading.* In Theme IV, Rilem Symposium, Prague, Czech Republic, 1974.

[Paulay and Priestley 1992] T. Paulay and M. J. N. Priestley. *Seismic design of reinforced concrete and masonry buildings.* Wiley-Interscience, New York, USA, first edition, 1992.

[Penelis and Kappos 1997] G. G. Penelis and A. J. Kappos. *Earthquake-resistant concrete structures.* Technical report, E & Fn Spon (Chapman & Hall), 1997.

[Polyakov 1956] S. V. Polyakov. *Masonry in framed buildings.* Gosudalst-Vennoe'stvo Literature po Straitel' stuv i Arkitecture, Moscow, Russia, Tranlation by G.L. Cairns, Building Research Station, Watford, England, 1956.

[Popov and Petersson 1978] E. P. Popov and H. Petersson. Cyclic metal plasticity: Experiments and theory. *ASCE Journal of Structural Engineering*, **104**(6):1371–1388, 1978.

[Popovic 1973] S. Popovic. A numerical approach to the complete stress-strain curve of concrete. *Cement and Concrete Research*, **3**(5):583–599, 1973.

[Ramberg and Osgood 1943] W. Ramberg and W. R. Osgood. *Description of stress-strain curve by three parameters.* Technical report, National Advisory Committee for Aeronautics, 1943.

[REBA 1967] REBA. *Regulamento de estruturas de betão armado.* Decreto-Lei N. 47723, Imprensa Nacional, Casa da Moeda, Lisbon, Portugal, 1967.

[REBAP 1984] REBAP. *Regulamento de estruturas de betão armado e pré-esforçado.* Decreto-Lei N. 349-C/83, Imprensa Nacional, Casa da Moeda, Lisbon, Portugal, 1984.

[Rehm 1961] G. Rehm. *Über die grundlagen des verbundes zwischen stahl und beton.* Technical report, Deutscher Ausschuss für Stahlbeton 138, Ernst & Sohn, Berlin, Germany, 1961.

[Ricci 2010] P. Ricci. *Seismic vulnerability of existing RC buildings.* PhD Thesis in Seismic Risk, University of Naples Federico II, Naples, Italy, 2010.

[RSA 1983] RSA. *Regulamento de segurança e acções para estruturas de edifícios e pontes.* Decreto-Lei N. 235/83, Imprensa Nacional, Casa da Moeda, Lisbon, Portugal, 1983.

[RSCCS 1958] RSCCS. *Regulamento de segurança das construções contra os sismos.* Decreto-Lei N. 41658, Imprensa Nacional, Casa da Moeda, Lisbon, Portugal, 1958.

[RSEP 1961] RSEP. *Regulamento de solicitações em edifícios e pontes.* Decreto-Lei N. 44041, Imprensa Nacional, Casa da Moeda, Lisbon, Portugal, 1961.

[Saatcioglu *et al.* 1992] M. Saatcioglu, J. M. Alsiwat and G. Ozcebe. Hysteretic behavior of anchorage slip in R/C members. *ASCE Journal of Structural Engineering*, **118**(9):2439–2458, 1992.

[Saliger 1913] R. Saliger. *Schubwiderstand und verbund in eisenbetonbalken auf grund von versuch und erfahrung.* Julius Springer, Berlin, Germany, 1913.

[Santhanam 1979] T. K. Santhanam. Model for mild steel in inelastic frame analysis. *ASCE Journal of Structural Engineering*, **105**(1):199–220, 1979.

[SEAOC 2005] SEAOC. *Performance based seismic engineering of buildings. Part 2: Conceptual framework.* Vision 2000 Committee, Structural Engineers Association of California, Sacramento, California, USA, 2005.

[SeismoSoft 2012] SeismoSoft. SeismoStruct (Version 100) – A computer programme for static and dynamic nonlinear analysis of framed structures. Help documentation of the program, http://www.seismosoft.com/, 2012.

[Sezen 2002] H. Sezen. *Seismic behavior and modeling of reinforced concrete building columns.* PhD Thesis in Civil and Environmental Engineering, University of California-Berkeley, Berkeley, California, USA, 2002.

[Sezen and Setzler 2008] H. Sezen and E. J. Setzler. Reinforcement slip in reinforced concrete columns. *ACI Structural Journal*, **105**(3):280–289, 2008.

[Smyrou 2006] E. Smyrou. *Implementation and verification of a masonry panel model for nonlinear dynamic analysis of infilled RC frames.* Master's Thesis in Earthquake Engineering, Rose School, Pavia, Italy, 2006.

[Soroushian and Choi 1991] P. Soroushian and K. B. Choi. Analytical evaluation of straight bar anchorage design in exterior joints. *ACI Structural Journal*, **88**(2):161–168, 1991.

[Stafford-Smith 1966] B. Stafford-Smith. Behaviour of square infilled frames. *ASCE Journal of Structural Division*, **92**(ST1):381–403, 1966.

[Stoker and Sozen 1970] M. F. Stoker and M. A. Sozen. *Investigation of prestressed reinforced concrete for highway bridges. Part V: Bond characteristics of prestressing strand.* Technical report, Bulletin 503, College of Engineering, University of Illinois, Urbana Champaign, USA, 1970.

[Tassios 1979] T. P. Tassios. *Properties of bond between concrete and steel under load cycles idealizing seismic actions.* In AICAP-CEB Symposium on Structural Concrete Under Seismic Actions, Rome, Italy, 1979.

[Taucer *et al.* 1991] F. F. Taucer, E. Spacone and F. C. Filippou. *A fiber beam-column element for seismic response analysis of reinforced concrete structures.* Technical report, Report UCB/EERC-91/17, Earthquake Engineering Research Center, University of California, Berkeley, USA, 1991.

[Thiruvengadam 1985] H. Thiruvengadam. On the natural frequencies of infilled frames. *Journal of Earthquake Engineering and Structural Dynamics*, **13**:507–526, 1985.

[Tseng and Lee 1983] N. T. Tseng and G. C. Lee. Simple plasticity model of two-surface type. *ASCE Journal of Structural Engineering*, **109**(3):795–810, 1983.

[Varum 2003] H. Varum. *Seismic assessment, strengthening and repair of existing buildings*. PhD Thesis in Civil Engineering, University of Aveiro, Aveiro, Portugal, 2003.

[Verderame *et al.* 2008a] G. M. Verderame, G. Fabbrocino and G. Manfredi. Seismic response of RC columns with smooth reinforcement. Part 1: Monotonic tests. *Engineering Structures*, **30**(9):2277–2288, 2008.

[Verderame *et al.* 2008b] G. M. Verderame, G. Fabbrocino and G. Manfredi. Seismic response of RC columns with smooth reinforcement. Part 2: Cyclic tests. *Engineering Structures*, **30**(9):2289–2300, 2008.

[Verderame *et al.* 2008c] G. M. Verderame, P. Ricci, G. Manfredi and E. A. Cosenza. *La capacità deformativa di elementi in C. A. con barre lisce: Modellazione monotona e ciclica*. In Reluis2Rm08 Conference, Valutazione e riduzione della vulnerabilità sismica di edifici esistenti in c.a. Rome, Italy, May 29-30, 2008.

[Verderame *et al.* 2009a] G. M. Verderame, P. Ricci, G. De Carlo and G. Manfredi. Cyclic bond behaviour of plain bars. Part 1: Experimental investigation. *Construction and Building Materials*, **23**(12):3499–3511, 2009.

[Verderame *et al.* 2009b] G. M. Verderame, P. Ricci, G. De Carlo and G. Manfredi. Cyclic bond behaviour of plain bars. Part 2: Analytical investigation. *Construction and Building Materials*, **23**(12):3512–3522, 2009.

[Verderame *et al.* 2010] G. M. Verderame, P. Ricci, G. Manfredi and E. Cozenza. Ultimate chord rotation of RC columns with smooth bars: Some considerations about EC8 prescriptions. *Bulletin of Earthquake Engineering*, **8**(6):1351–1373, 2010.

[Viwathanatepa *et al.* 1979] S. Viwathanatepa, E. P. Popov and V. V. Bertero. *Effects of generalized loadings on bond of reinforcing bars embedded in confined concrete blocks*. Technical report, Earthquake Engineering Research Center, University of California, Berkeley 79/22, Earthquake Engineering Research Center, University of California, Berkeley, USA, 1979.

[Yankelevsky and Reinhardt 1987] D. Z. Yankelevsky and H. W. Reinhardt. Model for cyclic compressive behavior of concrete. *Journal of Structural Engineering and Mechanics*, **113**(2):228–240, 1987.

[Yassin 1994] M. H. M. Yassin. *Nonlinear analysis of prestressed concrete structures under monotonic and cyclic loads*. PhD Thesis in Structural Engineering, University of California, Berkeley, California, USA, 1994.

[Yu 2006] W. Yu. *Inelastic modeling of reinforcing bars and blind analysis of the benchmark tests on beam-column joints under cyclic loading*. PhD Thesis in Earthquake Engineering, Rose School, Pavia, Italy, 2006.

[Zhao and Sritharan 2007] J. Zhao and S. Sritharan. Modeling of strain penetration effects in fiber-based analysis of reinforced concrete structures. *ACI Structural Journal*, **104**(2):133–141, 2007.